FLUTTER ANALYSIS OF FIXED AND ROTARY WINGS

A THESIS SUBMITTED TO
THE GRADUATE SCHOOL OF NATURAL AND APPLIED SCIENCES
OF
MIDDLE EAST TECHNICAL UNIVERSITY

BY

ORHUN ÇİÇEK

IN PARTIAL FULFILLMENT OF THE REQUIREMENTS
FOR
THE DEGREE OF MASTER OF SCIENCE
IN
AEROSPACE ENGINEERING

JULY 2019

Approval of the thesis:

FLUTTER ANALYSIS OF FIXED AND ROTARY WINGS

submitted by **ORHUN ÇİÇEK** in partial fulfillment of the requirements for the degree of **Master of Science in Aerospace Engineering Department, Middle East Technical University** by,

Prof. Dr. Halil Kalıpçılar
Dean, Graduate School of **Natural and Applied Sciences**   _____

Prof. Dr. İsmail Hakkı Tuncer
Head of Department, **Aerospace Engineering**   _____

Prof. Dr. Altan Kayran
Supervisor, **Aerospace Engineering, METU**   _____

Examining Committee Members:

Assoc. Prof. Dr. Melin Şahin
Aerospace Engineering, METU   _____

Prof. Dr. Altan Kayran
Aerospace Engineering, METU   _____

Assoc. Prof. Dr. Nilay Sezer Uzol
Aerospace Engineering, METU   _____

Assist. Prof. Dr. Mustafa Perçin
Aerospace Engineering, METU   _____

Assist. Prof. Dr. Touraj Farsadi
Aerospace Engineering, Adana Science and Tech. Uni.   _____

Date: 05.07.2019

I hereby declare that all information in this document has been obtained and presented in accordance with academic rules and ethical conduct. I also declare that, as required by these rules and conduct, I have fully cited and referenced all material and results that are not original to this work.

Name, Surname: Orhun Çiçek

Signature:

ABSTRACT

FLUTTER ANALYSIS OF FIXED AND ROTARY WINGS

Çiçek, Orhun
Master of Science, Aerospace Engineering
Supervisor: Prof. Dr. Altan Kayran

July 2019, 112 pages

Flutter is a critical stability problem that needs to be considered for the design of fixed and rotary wings. Although flutter susceptibility is addressed during the test phases of the most of the aircraft, an analytical model is required for the determination of flutter boundaries and most importantly for supplying feedback to the design procedure in order to have a structure that is free from flutter.

In this thesis, several flutter analysis methodologies are investigated for both fixed and rotary wing structures. For the analytical models, a theoretical background is given for Theodorsen, Loewy, Wagner unsteady aerodynamic theories and Pitt-Peters and Peters-He inflow theories. In addition, derivation of the simple beam theory is explained with the expansion methods of Rayleigh-Ritz and Galerkin. Three different solution types; k-method, modified k-method and p-method are studied based on the aerodynamic theory implemented. The flutter analysis results are verified and compared with the results given in the literature. The fixed wing analyses are validated with Goland's fixed wing results, rotary wing analyses are validated both with helicopter blade and wind turbine blade analyses results. Case studies are performed to investigate the effects of the shear center and center of gravity locations and the forward velocity of the helicopter on the flutter analysis results.

v

ÖZ

SABİT VE DÖNER KANATLARIN ÇIRPINMA KARARSIZLIĞI ANALİZİ

Çiçek, Orhun
Yüksek Lisans, Havacılık ve Uzay Mühendisliği
Tez Danışmanı: Prof. Dr. Altan Kayran

Temmuz 2019, 112 sayfa

Çırpınma kararsızlığı sabit ve döner kanatların tasarımı açısından kritik bir öneme sahiptir. Pek çok hava aracının testleri esnasında çırpınma kararsızlığının incelenmesine karşın, kararsızlık sınırlarının belirlenebilmesi ve en önemlisi tasarım sürecine geribildirim sağlanabilmesi açısından analitik bir modele ihtiyaç duyulmaktadır.

Bu tezin kapsamı içerisinde sabit ve döner kanatlı yapılar için çırpınma kararsızlığı analizi metodları incelendi. Oluşturulan analitik modeller için kullanılan Theodorsen, Loewy, Wagner zamana bağlı aerodinamik teorileri ve Pitt-Peters ve Peter-He indüklenmiş akış teorileri incelendi. Bunlara ilaveten yapısal modellerin oluşumu için kullanılan basit kiriş teorisi, genişleme metotları Rayleigh-Ritz ve Galerkin metotları ile birlikte kullanıldı. Seçilen aerodinamik teorinin yapısına göre kullanılacak olan üç farklı çözüm yöntemi olan k-metodu, modifiye k-metodu ve p-metodu incelendi. Çözüm sonuçları literatürde bulunan sonuçlar ile karşılaştırıldı ve doğrulandı. Sabit kanal çırpınma karasızlığı analizleri Goland'ın sabit kanat analizleri ile, döner kanat çırpınma kararsızlığı analizleri ise hem helikopter kanadı hem de rüzgar türbünü kanadı analizleri ile doğrulandı. Elastik eksen ve ağırlık merkezinin lokasyonlarının

ve helikopterin ileri hızının çırpınma kararsızlığı üzerine etkisini incelemek amacıyla örnek problem çözümleri gerçekleştirildi.

Anahtar Kelimeler: Çırpınma Kararsızlığı, Zamana Bağlı Aerodinamik Akış, Dinamik İndüklenmiş Akış, Rayleigh-Ritz Metodu

To my wife

ACKNOWLEDGEMENTS

TABLE OF CONTENTS

LIST OF TABLES

TABLES

LIST OF FIGURES

FIGURES

LIST OF SYMBOLS

Latin Symbols

a	Dimensionless Elastic Axis Distance Parameter
AC	Aerodynamic Center
AR	Aspect Ratio
b	Half Chord Length
$B_1(t), B_2(t)$	Aerodynamic Lag States
c	Chord Length
$C(k)$	Lift Deficiency Function
C_L	Roll Moment Coefficient
$C_{L\phi}$	Lift Curve Slope
C_M	Pitch Moment Coefficient
C_T	Thrust Coefficient
CG	Center of Gravity
e	Dimensionless Center of Gravity Distance Parameter
EA	Elastic Axis
EI	Bending Stiffness per Unit Length
$F(k)$	Real Part of the Lift Deficiency Function
$G(k)$	Imaginary Part of the Lift Deficiency Function
GJ	Torsional Stiffness per Unit Length
h	Bending Degree of Freedom
$H_0(k)$	Hankel Function of the First Kind of Order Zero
$H_1(k)$	Hankel Function of the First Kind of Order One
I_θ	Polar Mass Moment of Inertia
I_{zz}	Bending Second Moment of Inertia
J	Torsional Constant
$J_0(k)$	Bessel Function of the First Kind of Order Zero
$J_1(k)$	Bessel Function of the First Kind of Order One
k	Reduced Frequency
k_m	Mass Radius of Gyration of the Blade Cross Section
$\bar{L}^c, \bar{L}^s$	Elements of Influence Coefficient Matrix
L_h	Lift of the Cross Section
m	Mass Per Length
M_θ	Pitching Moment of a Cross Section
N_s	Total State Number
Q	Number of Blades
r	Blade Radial Coordinate

R	Radius of the Blade
S	Inflow Format Vector
U	Free Stream Velocity
U_{inflow}	Inflow Velocity
V	Total Velocity of the Blade
$V_{inplane}$	Tangential Velocity of the Blade
W	Bending Shape Function
$W(k, h, m)$	Weighting Factor of Loewy
x_{cg}	Distance between Elastic Axis and Center of Gravity

Greek Symbols

α	Effective Disk Angle of Attack
α_j^r, β_j^r	Induced Flow States
θ	Torsional Degree of Freedom
λ	Induced Flow
λ_0	Mean Induced Flow
λ_s	Sin Coefficient of Induced Flow
λ_c	Cos Coefficient of Induced Flow
λ_f	Freestream Inflow
λ_m	Mean Induced Flow
μ	Advance Ratio
ξ_j	Spatial Function
ρ	Air Density
τ	Nondimensional Time
τ_n^{mc}, τ_n^{ms}	Pressure Coefficients
ϕ_j^r	Induced Flow Shape Function
$\phi(\tau)$	Wagner Function
χ	Wake Skew Angle
ψ	Azimuth Angle
ω	Natural Frequency
Θ	Torsional Shape Function
Ω	Rotational Speed

CHAPTER 1

INTRODUCTION

Flutter is one of the most dangerous aeroelastic instabilities. There are several types of flutter such as whirl, stall and classical. This thesis study focuses only on classical flutter. Other types of flutter instabilities are out of the scope of this thesis. It should be noted that the term flutter refers to the classical flutter from this point on.

Flutter is a self-excited instability caused by the coupling of pitching and flapping modes of an elastic blade. It results from the energy transfer between the airstream and the elastic modes. Flutter speed is theoretically the highest speed that an aircraft can fly safely. At this speed, the aircraft experiences limit cycle oscillations (constant amplitude harmonic oscillations). Beyond the flutter speed, the system is unstable (divergent oscillations) and catastrophic failure of the structure is inevitable.

Flutter is a complex phenomenon because it includes two different kinds of disciplines; aerodynamics and structural dynamics together. In normal operating conditions, airflow contributes additional damping to the system. At the flutter phase, airstream transfers more energy to the structure than it extracts. This results in growing oscillations. Aerodynamic and structural coupling is the main mechanism of flutter. Fluctuations of the pitching motion affect the lift on the blade. Then, the lift results in flapping motion and in return, the flapping motion creates an excitation for the pitching motion again [1]. When the lift and the vertical motions of the blade are in the same direction, there is an energy transfer to the system. If the direction of the vertical motion changes, energy is extracted from the system (aerodynamic damping). Flutter susceptibility arises once the energy is transferred to the structure.

Flutter free aircraft design is possible in theory. If the blade is designed in such a way that the elastic axis (EA), the aerodynamic center (AC) and the center of gravity (CG)

are coincident at the quarter chord of the airfoil, elastic modes of the blade are decoupled and flutter susceptibility vanishes. However, keeping EA, CG and AC at the same point increases the weight of the blade dramatically and in return the power need of the aircraft increases. Therefore, this type of modeling is not practical to substantiate.

Flutter analysis does not require blade-to-blade or rotor-body couplings. These couplings have little effect on the results. Since flutter is a complex phenomenon itself, single blade flutter solution is simple, understandable and computationally faster compared to whole rotor [2]. This general approach is applied for the flutter analysis study performed in this thesis.

Solution domain is another important aspect of the analysis. Albeit the time domain solution is useful for the observation of the responses of the structure, it does not supply any modal information. For the identification of the frequencies and damping of the modes around flutter point, frequency domain solution approaches are implemented in this thesis.

There are three types of solution methodologies for the flutter analysis; k, modified k and p method solutions. The k method is built on assumption of a simple harmonic motion for both aerodynamic and resultant motions. Therefore, k method is valid only at the flutter point, where normally there exists no damping in the system. The k method requires no iteration for every reduced frequency, k which is calculated as $k = b\omega/U$. Here b is the half chord length, ω is the frequency of the motion and U is the free stream velocity. In the k method, artificial structural damping is added into the governing equations of the system proportional with the displacement. General methodology of k method is schematically given in Figure 1.1. In the beginning, mass, stiffness and aerodynamic matrices are constructed to obtain an eigenvalue problem solution. The eigenvalue problem solution gives frequency and damping values of each mode for a selected reduced frequency. The solution is repeated for a range of

selected reduced frequency values in order to determine where damping becomes zero. This point defines the flutter boundary.
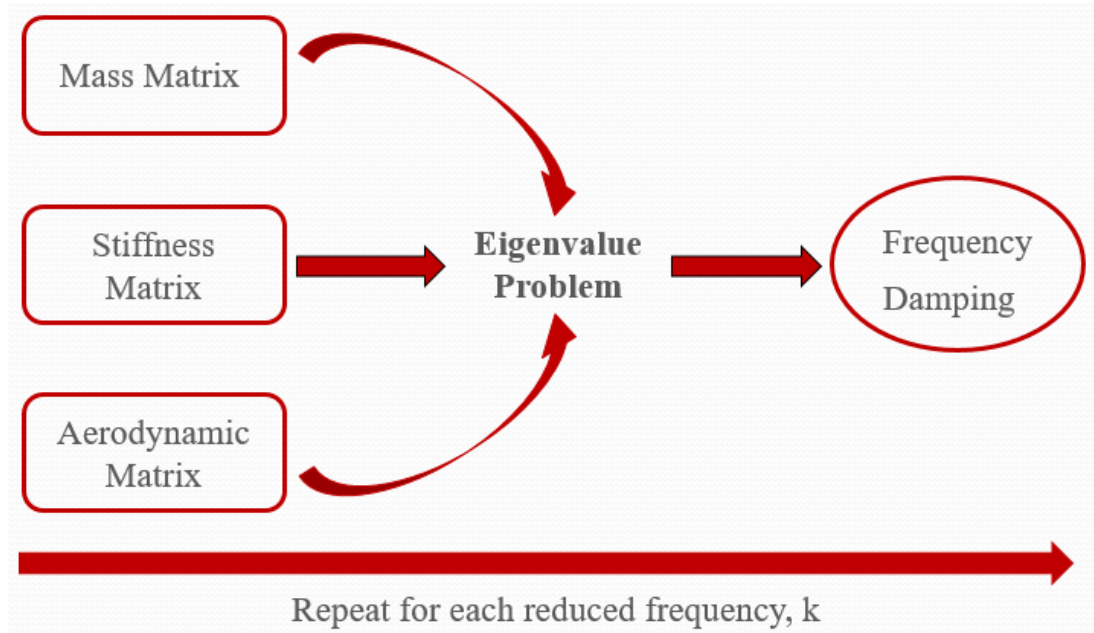
Figure 1.1. The k Method Solution Procedure

There is also a modified k method developed in this thesis which can be categorized as a k type solution also. The modified k method also assumes simple harmonic motion for the aerodynamic motions. Unlike the k method solution based on Theodorsen's unsteady aerodynamic theory, this modified k method requires iterative solution in each solution step which is developed for rotary wing flutter analysis based on Loewy's unsteady aerodynamic method. This is because each radial station of the rotary wing experiences different airspeeds and this makes the reduced frequency variable along the span of the blade. In order to overcome this situation, at the beginning of the solution, initial frequency (ω) value is assumed for one of the modes. Free vibration analysis result is a good start as an initial guess. Reduced frequency value is calculated for each radial station with $k = b\omega/U$ formulation. Here $U = \Omega r$ for rotary wings, where Ω is the rotational velocity and r is the radial position. After the flutter determinant solution is performed, a new ω value is calculated from the roots of the solution and compared with the initial estimation. If the difference

3

between two frequencies is within the desired tolerance limit, then the solution is continued with the next solution step (solution for a different Ω value). If the desired tolerance is not satisfied, then the initially estimated frequency is replaced with the new calculated frequency and the eigenvalue problem solution is repeated. This procedure is repeated until the desired convergence criteria is satisfied. This whole procedure is summarized schematically in Figure 1.2.
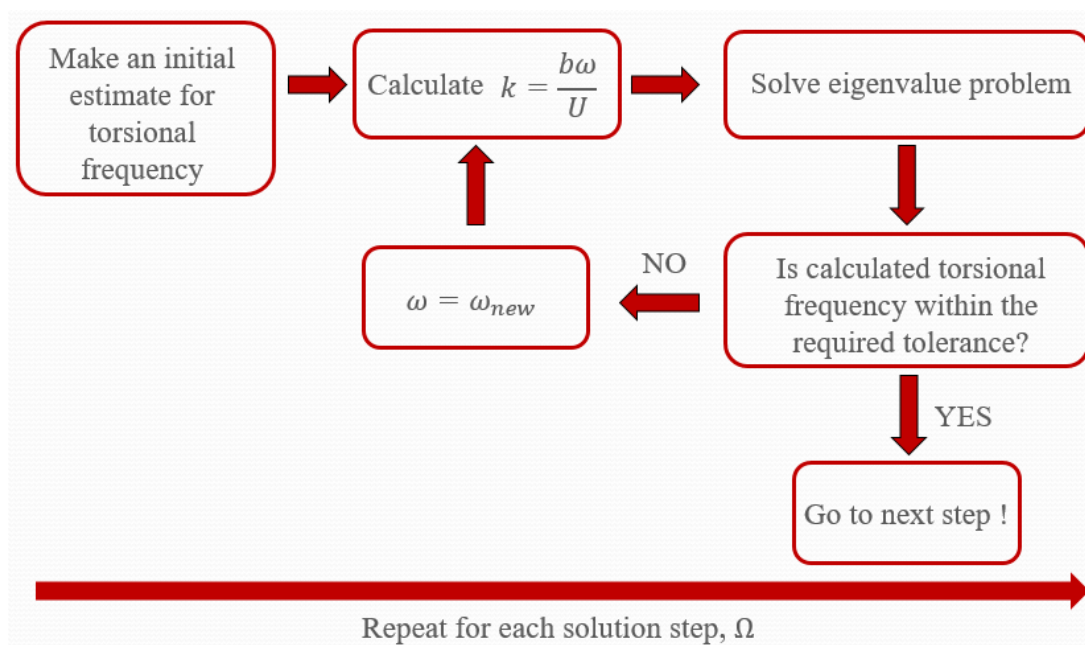
Figure 1.2. The Modified k Method Solution Procedure

The p method solution assumes general p type $(p = a + i\omega)$ solution for both structural and aerodynamic motions. In the p method, mass, damping and stiffness matrices are constructed to solve for flutter determinant. The frequency and damping characteristics of each root are obtained from the roots of the flutter determinant solution. This procedure is repeated for each required solution step. The results obtained from p type analysis are correct at every solution point unlike the k and modified k methods because of general p type motion assumption. The p method solution methodology is schematically shown in Figure 1.3.
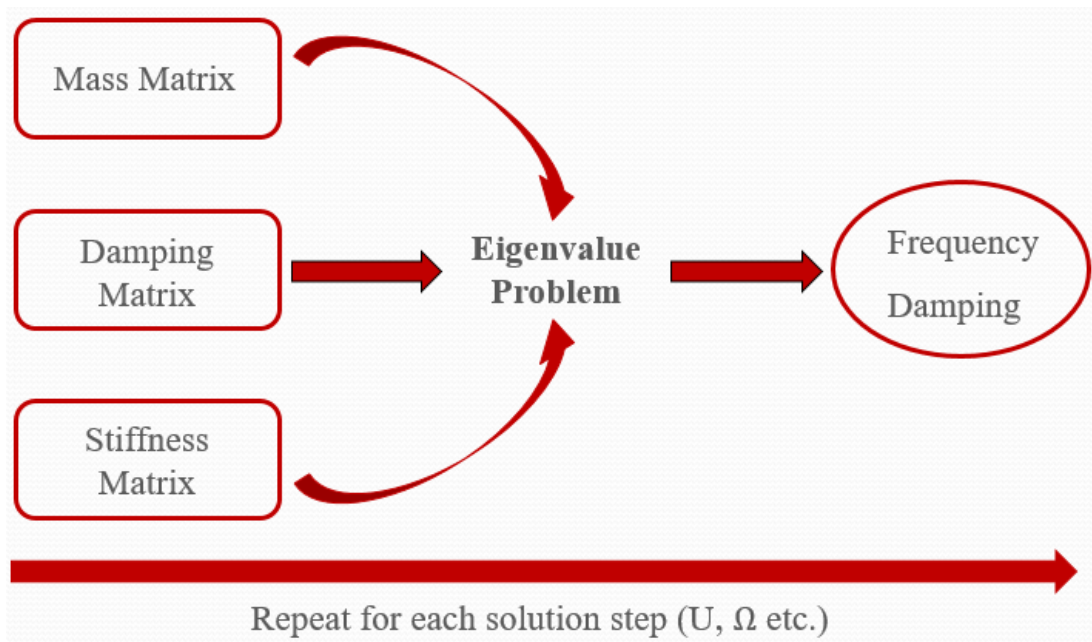
Figure 1.3. The p Method Solution Procedure

1.1. Literature Survey

In the history of flutter analysis, several types of solution methods have been studied. The studies focused on both fixed and rotary blade problems. Patil, Yurkovich and Hodges [3] stated that there are differences in p and k methods of flutter speed calculations. They claimed that k method flutter solution catches the correct order of magnitude, but gives a wrong flutter mode solution. They also suggested that it is more useful to solve the flutter problem as a function of flight speed rather than the reduced velocity. Denegri and Cutchins [4] compared the V-g method analytical flutter analysis with the conducted test results. The tests were performed with the random atmospheric excitation while the aircraft is flying in a trimmed condition. In the case of insufficient turbulence excitations, the aircraft was excited by the flaperon controls starting from high frequency excitation and sweeping the frequency content to low frequency excitations. The analysis and test results compared within 10% error. Viswanathan [5] studied on different types of flutter solution methods such as k, p-k and p methods on helicopter rotors. The p-k method is chosen to be the most suitable type of analysis due to its ability to evaluate damping of the system at subcritical flight

5

speeds where the k method gives incorrect results. The p-k method is compared with the p type method based on unsteady aerodynamics and reasonable results are obtained. Irani and Sazesh [6] studied a new type of flutter method and compared well with the conventional methods such as k, p-k and p type analysis. They introduced a new random force into the governing equations apart from the lift and the moment. This force added the Gaussian white noise effect to the system. The results were examined in terms of spectral density rather than the classical frequency domain approach. The spectral density variation was observed with the increasing flight velocity. The maximum response represented the flutter velocity.

Hodges and Ormiston [2] studied a two dimensional model using quasi-steady aerodynamics. They used a correction factor to catch the three dimensional effects. The induced flow was based on simple momentum theory. Therefore, the model was not capable of evaluating shed wakes for low induced flows. They investigated the effect of the precone angle to be destabilizing for the flutter analysis results. Pierce and White [7] conducted flutter analysis based on compressible unsteady aerodynamics with low induced flow on the rotor. The rotor was modeled as a nonuniform rotating beam with elastic bending and torsional degrees of freedom. They correlated their results with the results of Brooks and Baker [8] and concluded that when the effects of lower wakes are neglected, the flutter analysis leads to non-conservative results. Dinyavari and Friedmann [9] derived time domain representations of Theodorsen and Loewy's theories with arbitrary motion by using the Pade approximants of the circulatory lift coefficient. They used second order Pade approximant of Jones [10] which provided accurate and efficient solutions. Shipman [11] declared that inclusion of wakes and decay functions to the lift deficiency function has a significant effect at low reduced frequencies. He suggested that this effect lowers the calculated flutter speed in a noticeable manner. Haddadpour and Firouz-Abadi [12] compared flutter instability of quasi-steady and unsteady aerodynamics based models for fixed wings in subsonic incompressible flight

6

conditions. They concluded that the quasi steady models give inaccurate and more conservative results with respect to the unsteady models.

Loewy [13] extended Theodorsen's theory by including shed wakes to be applicable for rotary wings in hover. Hammond [14] compared flutter results for a two degree of freedom system using Theodorsen and Loewy theories. The analysis with the Loewy theory resulted in lower flutter speeds for the same system. This showed that the rotor wake generates destabilizing effect on the system. Therefore, application of Theodorsen's unsteady aerodynamics to rotary wing analysis is not reliable and will result in non-conservative results. Shipman and Wood [15] developed a method for determining rotor blade flutter in forward flight including the wake effects. They improved Loewy's model to include forward flight effects. They assumed that oscillations begin to build up at the onset of flutter until reaching a critical azimuth position and then decay after that azimuth. They worked on a compound helicopter model that allows variation of the rotor speed during the flight. They presented a chart of safe rotor tip speeds according to which the pilot can decrease rotational speed of the rotor beyond specific forward flight speeds to avoid flutter occurrence.

Gates, Piziali and DuWaldt [16] developed an analytical model with unsteady aerodynamics for a rotor in translational flight. The velocity of the rotor blade varied for each azimuthal position. There were some regions on the retreating blade side where the tangential velocity of the blade was negative. The authors included reverse flow effect to their model with a correction factor. This correction factor subtracts the lift due to normal flow and adds terms resulting from the reversed flow. They also correlated their analysis results with experimental results of a model rotor in translational flight. Stammers [17] developed a method for the solution of the flutter analysis for forward flight conditions where periodic coefficients enter in the equations. He used quasi steady aerodynamics and observed that forward flight has a stabilizing effect on the flutter results.

Politakis, Haans and van Bussel [1] studied the trailing edge flap effects on 10MW+ capacity wind turbine blades having rotor diameter around 170 meters. They observed that trailing edge flap deflections of 20 Hz and angles around 13 degrees have a stabilizing effect on flutter modes of the blades.

Tuzcu and Nguyen [18] investigated effects of maneuvers on the flutter stability with a comprehensive mathematical model including elastic degrees of freedom of blade, fuselage, horizontal and vertical stabilizers. The aerodynamic model used in the model is unsteady having circulatory and noncirculatory portions. They observed that maneuvers have a variable influence depending on the climb angle, turn radius and as well as the flight altitude and the blade parameters. They concluded that climbing flight has a stabilizing effect on flutter, while descending flight decreases the stability. The effects of maneuvers on the stability get larger with the increasing altitude.

Nibbelink [19] studied flutter analysis on both fixed wings and rotary wings at the stopped rotor configuration with the generalized dynamic inflow theory of Peters and He. He derived linear structural equations with torsional and bending degrees of freedom from Lagrange equations and expanded them with the Galerkin method to be applicable for three dimensional solutions. He compared both fixed and rotary wing flutter solutions with the widely accepted unsteady aerodynamic theories of Theodorsen and Loewy respectively. The first comparison is made in terms of steady and unsteady parts of the sectional lift distributions. It is observed that the lift distributions match well, frequency and damping values of the systems with varying location of the center of gravity are compared. For the fixed wing, the induced flow based results not only shows no divergence, but also they converge very near to the quasi-steady results based on Theodorsen's theory. For rotary wings, Loewy's theory approximates a constant reduced frequency for the whole wing while dynamic inflow theory avoids this approximation by using the p-type aerodynamics solution. This affects the frequency content of the solution. In addition, dynamic inflow theory shows better damping characteristics than the Loewy's theory.

Rauchenstein [20] performed flutter analysis with uniform beam having average property values of a UH-60 blade. The structural equations are expanded with the Rayleigh's method to reflect the 3D effect. For the lifting equations, Theodorsen's unsteady aerodynamics theory was used. The lift deficiency function was calculated for a range of forward velocities (reduced frequencies). The results show that the UH-60 model remains stable within its forward speed range of 0 to 180 knots. If the center of gravity position of the blade is changed step by step, beyond the 70% chord location, the blade experiences flutter instability by the coupling of first bending and torsion modes.

Couch [21] developed structural and aerodynamic equations of motion for a rotor blade having a trailing edge flap. He used Lagrange's equations to derive the equations for the flutter analysis. He divided the rotor into several segments for application of lumped mass parameters for each section. This sectioning method helped the author to calculate reduced frequency for each segment of the rotor by including the radial variation of the velocity. He investigated two separate conditions in his dissertation. First, he increased the frequency of the flapping mode and observed that it gets more unstable when the flap frequency is increased to approach the torsional frequency. Second, he tried different lift deficiency functions such as Theodorsen, Loewy and finite wake. He observed that in the case of wakes being in phase (Theodorsen) gives always the most non-conservative result for flutter, in other words the highest flutter speed.

1.2. Objective of the Thesis

This thesis study is focused on the flutter analysis of fixed and rotary wings utilizing different unsteady aerodynamic models and solution methods accordingly. Although each method is explained in the literature, comparison of the methods with each other for the same case problem is not common.

Study aims to define the derivation of the structural models for fixed and rotary wings in detail from two dimensional bending-torsion Euler-Bernoulli beam theory. The

structural models are coupled with the unsteady aerodynamic theories of Theodorsen, Loewy, Wagner, Pitt-Peters and Peters-He. The Theodorsen and Loewy based flutter equations are solved with the k and modified k methods because the lift deficiency function is defined in terms of the reduced frequency k. The rest of the analytical flutter models are solved with the p-method. In this thesis, analytical solutions of the coupled equations of structural and aerodynamic models are performed with developed MATLAB codes.

The fixed wing flutter solution methodologies are compared with the Goland wing [22] flutter solutions given in the literature. The comparisons are made for Theodorsen, Wagner, Pitt-Peters and Peters-He based aerodynamic model solutions. With the correlated structural, aerodynamic equations and solution techniques, rotary wing flutter analysis are performed and the effect of aerodynamic theories on the rotary wing flutter analysis is investigated. The rotary wing flutter solution methodologies are validated with two separate models: for a helicopter blade model with the Couch's flutter results [21] and for a wind turbine blade model with the Farsadi's flutter results [38]. The validations are performed with Loewy, Wagner, Pitt-Peters and Peters-He based unsteady aerodynamic models for the rotary wings. The summary of the analysis methodologies are given in Table 1.1.

Table 1.1. *Summary of the Flutter Solution Methodologies*

Structural Model	Aerodynamic Model	Solution Type	Drawbacks	Assumptions
Fixed Wing	Theodorsen	k Method	Applicable Mostly for Fixed Wings	Simple Harmonic Motion, Constant and Infinite Wakes, Incompressible Flow
	Wagner	p Method	-	Incompressible Flow
	Pitt-Peters Inflow	p Method	Radially Linear Distribution, Azimuthally Only First Harmonics	Incompressible Flow, Infinite Number of Blades
	Peters-He Inflow	p Method	-	Incompressible Flow
Rotary Wing	Loewy	Modified k Method	Accurate for Low inflow Hover Conditions	Simple Harmonic Motion, Incompressible Flow
	Wagner	p Method	-	Incompressible Flow
	Pitt-Peters Inflow	p Method	Radially Linear Distribution, Azimuthally Only First Harmonics	Incompressible Flow, Infinite Number of Blades
	Peters-He Inflow	p Method	-	Incompressible Flow

1.3. Outline of the Thesis

In Chapter 1, a brief introduction about the flutter terminology is given. Studies of flutter analysis of fixed and rotary wings based on different types of aerodynamic models and solution methodologies from the literature are presented.

In Chapter 2, fundamental theoretical background of the thesis is explained. As a basis of the structural methodologies, Rayleigh-Ritz expansion method is described. In addition to the Rayleigh-Ritz method, the Galerkin method is also explained. The unsteady aerodynamic theories such as Theodorsen, Loewy, Wagner and dynamic

inflow theories which are used in the forthcoming flutter solution methodologies are discussed in detail.

In Chapter 3, fixed wing flutter analysis is discussed. Starting from the derivation of the fixed wing structural equations of motion, the chapter is focused on the solution methodologies of the flutter analysis based on various aerodynamic theories.

In Chapter 4, rotary wing flutter analysis is discussed. Starting from the derivation of the rotary wing structural equations of motion, the chapter is focused on the solution methodologies of the flutter analysis of rotary wings based on various aerodynamic theories.

In Chapter 5, structural equations of motion for both fixed and rotary wings are verified with Dymore [35] multibody dynamics code free vibration solutions. With the confidence of the verified structural equations, flutter analyses are performed for each given solution methodology in the theory parts. The results are compared with the results that are found from the literature for both fixed and rotary wings. Also additional case studies are performed to investigate the effect of critical parameters center of gravity and shear center position on rotary wing flutter analysis.

In Chapter 6, presented results and all of the effort that are explained in the dissertation are summarized and recommendations for the future work are shared.

CHAPTER 2

TECHNICAL BACKGROUND

2.1. Rayleigh-Ritz Method

Rayleigh-Ritz method provides an approximate analytical solution to 3D wing structural models by the implementation of assumed mode shapes. This approach is widely used in the literature for the solution of flutter problems because of its analytical simplicity and computational time benefits regarding conventional beam theories and finite element method. The Rayleigh-Ritz method can analyze structural configurations accurately [23]. The theory is based on the derivation of equations of motion of a system utilizing Lagrange equations with energy theories.

The Rayleigh-Ritz method is useful for representing the motion of a beam $h(x,t)$ in terms of spatial and time functions as shown in Eqn. (2-1). Here $\xi_j(t)$ is time dependent variable and $\phi_j(x)$ is the spatial function which is generated by assumed shape functions.

$$h(x,t) = \sum_{j=1}^{n} \xi_j(t)\phi_j(x) \qquad (2\text{-}1)$$

The assumed shape functions of $\phi_j(x)$ must be orthogonal to each other and all of the mode shapes must satisfy the geometrical boundary conditions in order to obtain correct modal behavior for the case of interest. By the help of n number of assumed mode shapes, the partial differential equation of the system is turned into n number of ordinary differential equations in time. The number n is increased until the convergence is obtained for the essential modes. In this dissertation, the mode shapes are selected as polynomials such as r, r^2, r^3 and so on. Here r is used for defining radial position of a beam along the span.

2.2. Galerkin Method

The methodology of the Galerkin approach is similar to the Rayleigh-Ritz method. Instead of the solution with energy methods of Lagrange equation, in the Galerkin method, the equations of motion of the system are derived from the Newtonian approach. After the equations are obtained, the variable of the equation $h(x, t)$ is separated to its variants as shown in Eqn. (2-1). Then, the equation is multiplied by the spatial function $\phi_j(x)$ and integrated over the span of the blade. The mode shapes selected for the Galerkin method must satisfy both geometrical and force boundary conditions. The selected mode shapes must also be linearly independent. In this thesis, the assumed mode shapes are selected from Duncan polynomials. In the literature, these polynomials are studied to give a good representative for the elastic mode shapes of the beams [24]. The first two mode shapes satisfying the cantilevered boundary condition for the fixed wing solution are given as,

For Bending Equation,

$$W_1 = \frac{1}{11}(15\bar{r}^2 - 5\bar{r}^4 + \bar{r}^6)$$
$$W_2 = 2.61\bar{r}^8 - 10.1\bar{r}^6 + 14\bar{r}^4 - 5.51\bar{r}^2$$

(2-2)

For Torsion Equation,

$$\Theta_1 = 0.5(3\bar{r} - \bar{r}^3)$$
$$\Theta_2 = \frac{1}{32}(290\bar{r}^3 - 153\bar{r}^5 - 105\bar{r})$$

(2-3)

In Eqns. (2-2) and (2-3) $\bar{r}$ represents normalized radial position over the blade span R. Mode shapes of the cantilever beam are shown in Figure 2.1 and Figure 2.2. Flapping mode shapes are normalized with vertical displacement of the blade tip and torsional mode shapes are normalized with the torsional deflection of the blade tip.
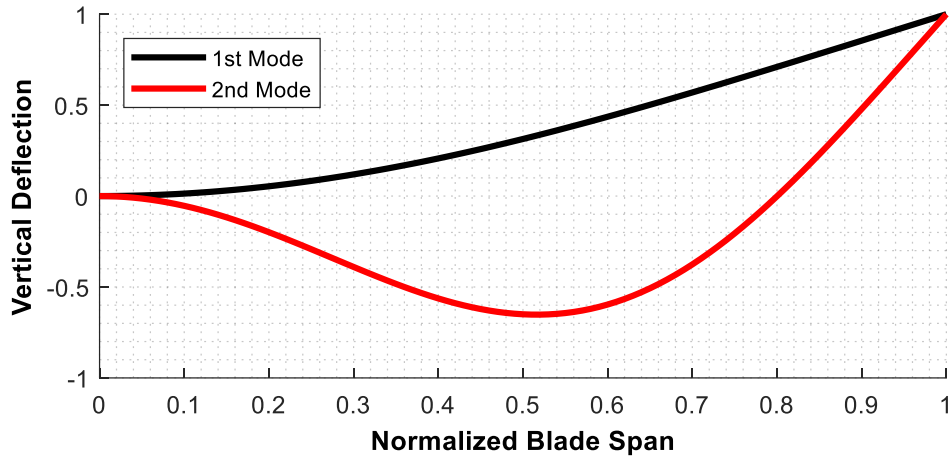
Figure 2.1. Fixed Wing Flapping Mode Shapes
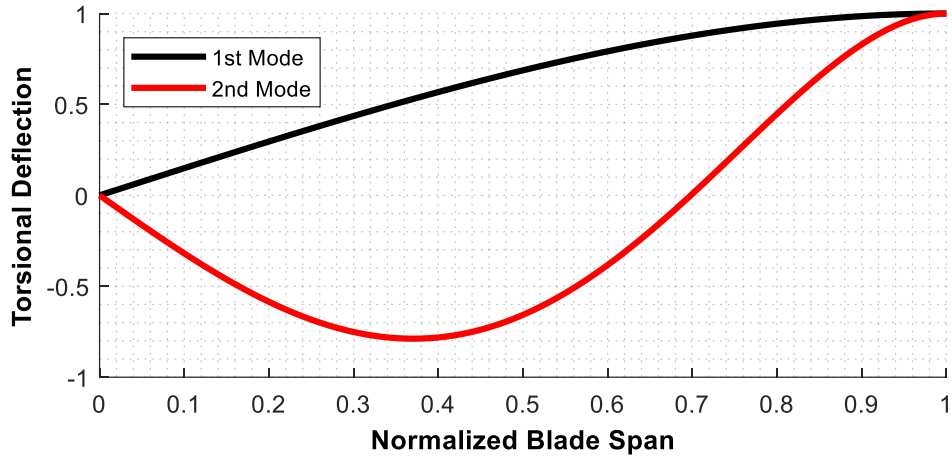
Figure 2.2. Fixed Wing Torsional Mode Shapes

For the rotating blade, the selected Duncan polynomials are shown below. Note that the flapping motion has a pinned boundary condition in these assumed mode shapes.

For Bending Equation,

$$W_1 = \bar{r}$$

$$W_2 = \frac{1}{16}(15\bar{r}^7 - 63\bar{r}^5 + 105\bar{r}^3 - 41\bar{r})$$

$$(2\text{-}4)$$

For Torsion Equation,

$$\Theta_1 = 0.5(3\bar{r} - \bar{r}^3)$$

$$\Theta_2 = \frac{1}{32}(290\bar{r}^3 - 153\bar{r}^5 - 105\bar{r})$$

(2-5)

Mode shapes of the rotating beam are shown in Figure 2.3 and Figure 2.4. Flapping mode shapes are normalized with vertical displacement of the blade tip and torsional mode shapes are normalized with the torsional deflection of the blade tip.
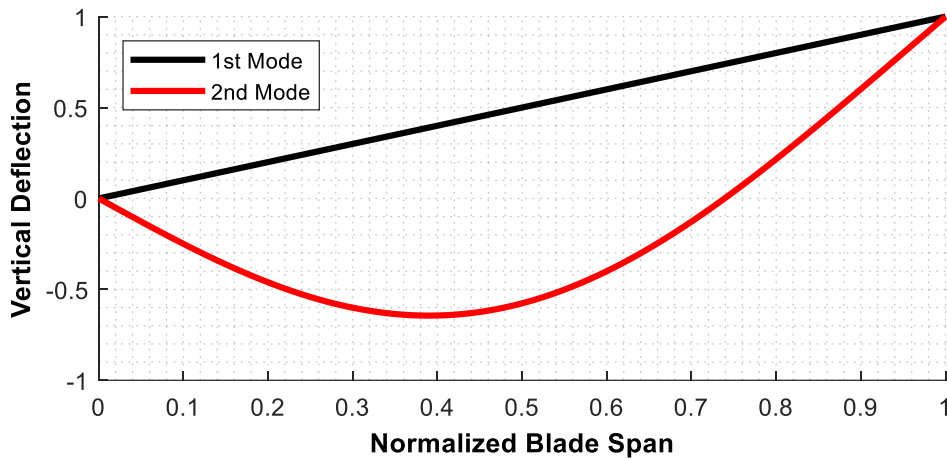
Figure 2.3. Rotary Wing Flapping Mode Shapes
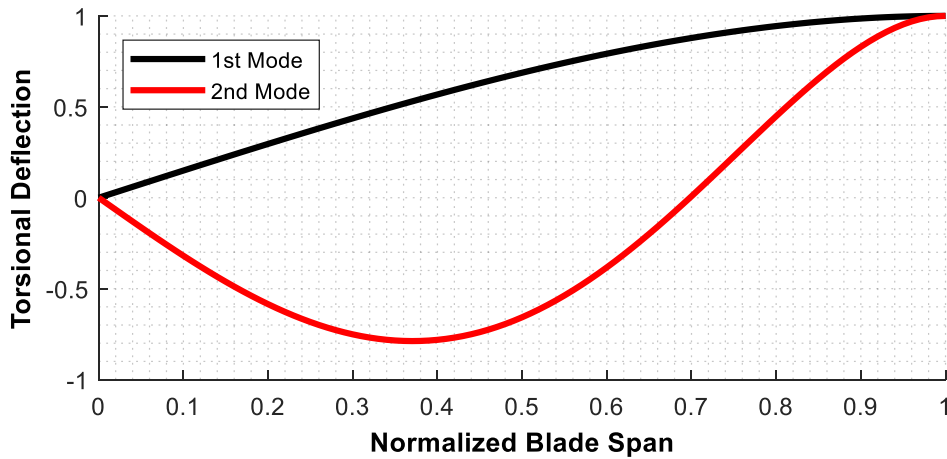
Figure 2.4. Rotary Wing Torsional Mode Shapes

2.3. Unsteady Aerodynamics

Flutter analysis requires dynamic motion to affect the aerodynamic surfaces through resultant forces and moments. This is called as unsteady effects of aerodynamics and results from changing circulation and wake upon the moving airfoil. Consideration of unsteady aerodynamics in the flutter analysis has a remarkable influence on the flutter results [25]. Therefore, analysis approaches listed in this thesis evaluate types of unsteady aerodynamic methods for two dimensional incompressible, inviscid and rigid airfoils under the assumption of the small amplitude of pitch and flap motions and fully attached flows. Additional effects of unsteady aerodynamics such as flow separation, stall, airfoil thickness and compressibility are beyond the scope of this thesis.

In the unsteady aerodynamics, lift and moment consist of circulatory and noncirculatory parts. Noncirculatory part includes apparent mass and inertia effects. The most important part is the circulatory part which consists of the motion history and the influence of the wake. Most of the unsteady aerodynamic theories used in the literature are less complicated and harmonic motion of the airfoil is assumed to derive the unsteady lift and moment. The details of the unsteady theories used in this thesis are given in the following sections.

2.3.1. Theodorsen's Theory

Theodorsen's unsteady aerodynamic theory [23] is based on the potential flow and Kutta condition. The theory assumes incompressible flow. Lift consists of both circulatory and noncirculatory parts, albeit the pitching moment which is defined with respect to the aerodynamic center contains only the noncirculatory part. Theodorsen's unsteady aerodynamic theory is based on simple spring restrained airfoil models. These models are called typical section models and can be represented as shown in Figure 2.5.

17
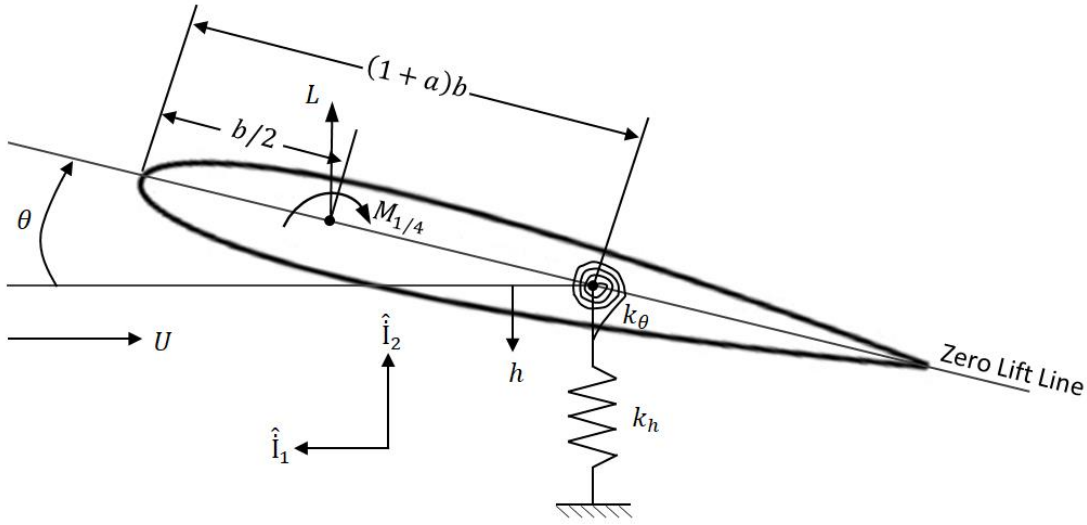
Figure 2.5. Typical Blade Section Model

The h and θ variables are vertical displacements due to bending and angular rotation due to pitching motions respectively. The term "a" is a dimensionless parameter which is used to define the location of the elastic axis and the "b" term is the half chord.

Lift and moment equations are given by [23],

$$L_h = 2\pi\rho U b C(k)\left[\dot{h} + U\theta + b\left(\frac{1}{2} - a\right)\dot{\theta}\right] + \pi\rho b^2(\ddot{h} + U\dot{\theta} - ba\ddot{\theta}) \qquad (2\text{-}6)$$

$$M_{1/4c} = -\pi\rho b^3\left[\frac{1}{2}\ddot{h} + U\dot{\theta} + b\left(\frac{1}{8} - \frac{a}{2}\right)\ddot{\theta}\right] \qquad (2\text{-}7)$$

Here ρ is the air density and U is the free stream velocity. In the lift and moment equations, the noncirculatory part depends mostly on apparent mass and inertia terms. The most important part is the circulatory part. In Eqn. (2-6) the lift curve slope is 2π. The term including $C(k)$ is the circulatory part of the equation. $C(k)$ is dependent on reduced frequency k which is defined as $k = b\omega/U$ where b is the half chord length, ω is the frequency of the motion and U is the free stream velocity.

Although it might be thought that the lift and moment equations are time domain equations due to the dots over h and θ, the presence of $C(k)$ is illogical in a time domain equation. Therefore, the theory is valid for only simple harmonic motion. The $C(k)$ function of Theodorsen is given by,

$$C(k) = F(k) + iG(k) = \frac{H_1^{(2)}(k)}{H_1^{(2)}(k) + iH_0^{(2)}(k)} \tag{2-8}$$

Where $H_n^{(2)}$ is the Hankel function of the second kind of order n. The variation of the real and imaginary part of Eqn. (2-8) with reduced frequency varying from zero to unity is given in Figure 2.6. Note that for steady motion, $C(k)$ is equal to unity ($k = 0$). As k approaches to infinity $C(k)$ approaches to $1/2$.
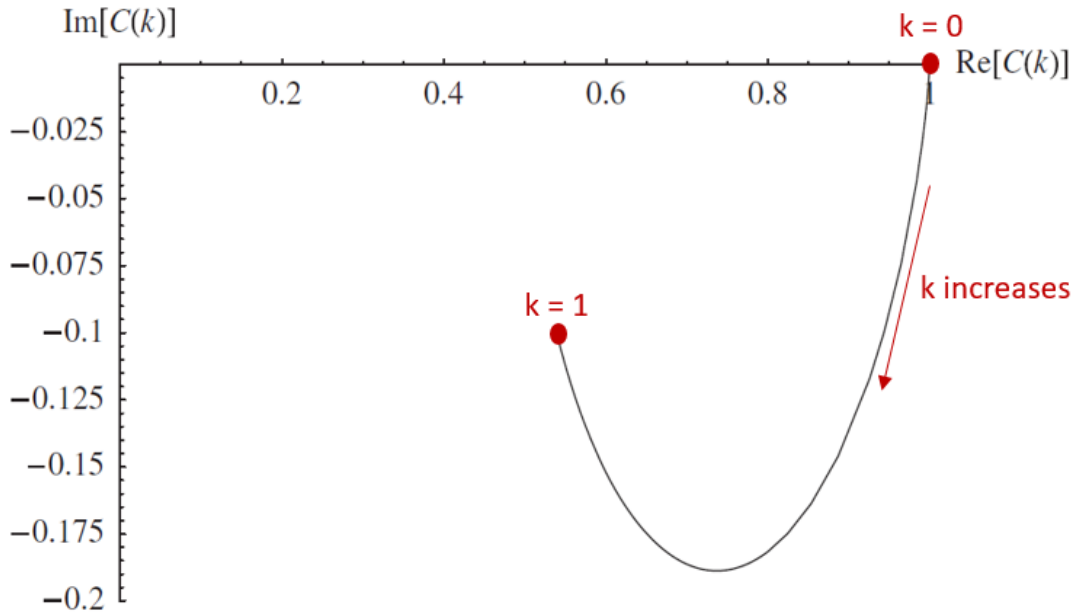
Figure 2.6. Real and Imaginary Parts of $C(k)$ Varying with Reduced Frequency [23]

Two-dimensional thin airfoil theory of Theodorsen is mostly applicable for fixed wings because the wake is assumed to be carried from downstream to infinity [9]. For the rotary wings, the shed vortices coming from the previous blade is not taken into account.

2.3.2. Loewy's Theory

Because Theodorsen unsteady aerodynamic theory assumes constant and infinite wakes, Loewy extended this theory to include the effects of the returning shed wakes [13]. Loewy used Biot-Savart law instead of potential theory to include layers of shed

vorticity. Since vorticity shed from the previous blade affects the lift and moment distribution of the oncoming blade, it must be taken into calculations for the rotating blades. The geometrical representation of the returning shed wakes is shown in Figure 2.7.

a) **High inflow**   b) **Low inflow**
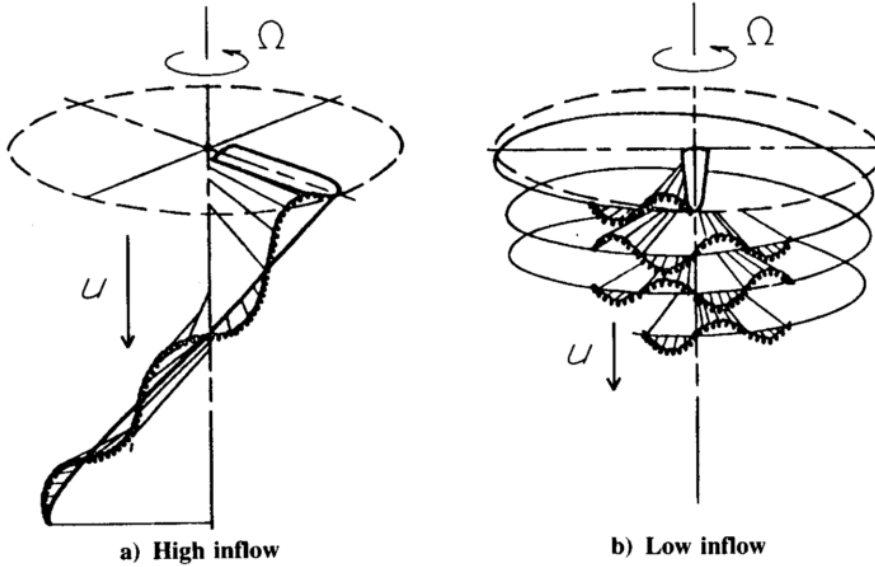
Figure 2.7. Returning Shed Wakes of Loewy's Model [13]

In Loewy's theory, the lift and moment equations of Theodorsen's theory are kept the same. The only change is applied to the lift deficiency function $C(k)$ which implicitly includes the shed wakes of induced flow. Lift deficiency function is written in the same format except a wake spacing function $W(k, h, m)$ is added to capture influences of shed wake. The lift deficiency function of Loewy is given by,

$$C(k, h, m) = \frac{H_1^{(2)}(k) + 2J_1(k)W(k, h, m)}{H_1^{(2)}(k) + iH_0^{(2)}(k) + 2[J_1(k) + iJ_0(k)]W(k, h, m)} \quad (2\text{-}9)$$

where,

$$W(k, h, m) = \left[e^{(kh+i2\pi m)} - 1\right]^{-1}, m = \frac{kr}{Qb} = \frac{\omega}{Q\Omega}, h = \frac{2\pi U_{inflow}}{\Omega bQ} \quad (2\text{-}10)$$

In the above equations, k is the reduced frequency, h is the inflow ratio and Q is the number of blades. J_n is the Bessel function of the first kind order n evaluated at reduced frequency k. In Eqn. (2-10) m is the frequency ratio. If m is not an integer value, that means there is a phasing between the wakes.

For large wake spacing ($h \rightarrow \infty$), the wake spacing function W approaches zero and the lift deficiency function of Loewy turns into Theodorsen's lift deficiency function. Although being derived for rotating blades, Loewy's unsteady aerodynamic theory has some limitations. It gives accurate results only for hover and low inflow conditions [21].

2.3.3. Wagner's Theory

Wagner function is an alternative, widely used aerodynamic theory for transient aerodynamics such as rapid maneuvers and gusts. Wagner function is used for modeling the effect of a step change of the incidence on the lift at the quarter chord of the airfoil by obtaining the downwash velocity at the ¾ chord. Aerodynamic force definition of the theory is given by [26]. The h and θ variables are vertical displacement due to bending and angular rotation due to pitching motions respectively.

$$
\begin{aligned}
L_h = \pi \rho b^2 \left(\ddot{h} + U\dot{\theta} - ba\ddot{\theta} \right) \\
+ 2\pi \rho U b \left\{ w_{0.75c}(0)\phi(\tau) \right. \\
\left. + \int_0^\tau \phi(\tau - \sigma) \frac{d}{d\sigma} \left(w_{0.75c}(t) \right) d\sigma \right\}
\end{aligned}
\tag{2-11}
$$

$$
M_{1/4c} = -\pi \rho b^3 \left[\frac{1}{2}\ddot{h} + U\dot{\theta} + b\left(\frac{1}{8} - \frac{a}{2}\right)\ddot{\theta} \right]
\tag{2-12}
$$

where the nondimensional time is $\tau = Ut/b$, U is the free stream velocity and the Wagner function ϕ is given by Eqn. (2-13).

$$
\phi = \frac{2}{\pi} \int_0^\infty \frac{F(k)}{k} \sin(k\tau)\, dk \approx \frac{\tau + 2}{\tau + 4}
\tag{2-13}
$$

21

In Eqn. (2-11), the downwash at the ¾ chord is given by Eqn. (2-14).

$$w_{0.75c}(t) = \dot{h} + U\theta + b\left(\frac{1}{2} - a\right)\dot{\theta} \qquad (2\text{-}14)$$

In order to take the 3D effects into account, the following corrections are applied on the lift curve slope [27],

$$2\pi \rightarrow C_{L\phi} = \frac{AR}{AR\sqrt{1 + \left(\frac{2}{AR}\right)^2} + 2} 2\pi \qquad (2\text{-}15)$$

$$\frac{1}{2}b \rightarrow \frac{b}{2}\left[\frac{C_{L\phi}}{\pi} - 1\right]$$

where AR is the aspect ratio of the wing, b is the half chord length and $C_{L\phi}$ is the lift curve slope. The correction should be applied only on the circulatory terms.

The integral term in the lift equation is handled by an approximate expression of the Wagner function given by [10],

$$\phi(s) = 1 - 0.165e^{-0.0455s} - 0.335e^{-0.3s} \qquad (2\text{-}16)$$

where s is defined as $s = \frac{Ut}{b}$. Here U is the free stream velocity, t is time and b is half chord length. With this new definition of s, approximate Wagner function takes the form,

$$\phi\left(\frac{U(t-\tau)}{b}\right) = 1 - C_1 e^{-\varepsilon_1\frac{U}{b}(t-\tau)} - C_2 e^{-\varepsilon_2\frac{U}{b}(t-\tau)} \qquad (2\text{-}17)$$

where,

$$C_1 = 0.165 \quad C_2 = 0.335 \quad \varepsilon_1 = 0.0455 \quad \varepsilon_2 = 0.3 \qquad (2\text{-}18)$$

Now, the integral term of the lift equation can be defined with the approximate Wagner function as,

$$\int_0^t \frac{dw_{0.75c}(\tau)}{d\tau} \phi \left[\frac{U}{b}(t-\tau) \right] d\tau$$

$$= \int_0^t \frac{dw_{0.75c}(\tau)}{d\tau} \left[1 - C_1 e^{-\varepsilon_1 \frac{U}{b}(t-\tau)} \right. \tag{2-19}$$

$$\left. - C_2 e^{-\varepsilon_2 \frac{U}{b}(t-\tau)} \right] d\tau$$

If we call the integral,

$$\int_0^t \frac{dw_{0.75c}(\tau)}{d\tau} e^{-\varepsilon_1 \frac{U}{b}(t-\tau)} = B_1(t) \tag{2-20}$$

and,

$$\int_0^t \frac{dw_{0.75c}(\tau)}{d\tau} e^{-\varepsilon_2 \frac{U}{b}(t-\tau)} = B_2(t) \tag{2-21}$$

The equation (2-19) is simplified to,

$$\int_0^t \frac{dw_{0.75c}(\tau)}{d\tau} \phi \left[\frac{U}{b}(t-\tau) \right] d\tau = w_{0.75c}(t) - C_1 B_1(t) - C_2 B_2(t) \tag{2-22}$$

where $B_1(t)$ and $B_2(t)$ are the aerodynamic lag states. These terms can be evaluated with the use of Leibniz integral rule. The details of the Leibniz integral rule derivation are not explained here. The equations take the final form of,

$$\dot{B}_1(t) + \varepsilon_1 \frac{U}{b} B_1(t) = \dot{w}_{0.75c}(t) \tag{2-23}$$

$$\dot{B}_2(t) + \varepsilon_2 \frac{U}{b} B_2(t) = \dot{w}_{0.75c}(t) \tag{2-24}$$

Equations (2-23) and (2-24) must be solved together with the governing equations of the system.

2.3.4. Dynamic Inflow Theories

Dynamic inflow theories include the effect of varying vorticity in time to the wake of the induced flow on the rotor plane. These wake induced velocities are essential for the evaluation of the unsteady aerodynamics and must be accounted for transient

motions especially. Although it is more accurate to represent a wake by a vortex model, analysis such as flutter requires finite-state model of the wake. Dynamic inflow model can be written in state-space form and used in the frequency domain for flutter analysis.

There are many dynamic inflow models in the literature. The most commonly used dynamic models are Pitt-Peters and Peters-He models. In this thesis, these two models are focused on.

2.3.4.1. Pitt-Peters Inflow

Pitt-Peters inflow theory developed in 1980 [28] is one of the most commonly used, simple and computationally practical induced flow theories in the literature. The theory is based on the actuator-disk theory. It consists of both unsteady and quasi-steady parts. The induced flow is defined with three parameters including mean (λ_0), lateral (λ_s) and longitudinal (λ_c) variations of the induced flow. The inflow definition is given in [29] as,

$$\lambda = \lambda_0 + \lambda_s r sin\psi + \lambda_c r cos\psi \qquad (2\text{-}25)$$

In Eqn. (2-25) radial variation of the flow is linear. The azimuthal variation is obtained by the first harmonics of the rotation. The general coordinate system of the induced flow is given in Figure 2.8.
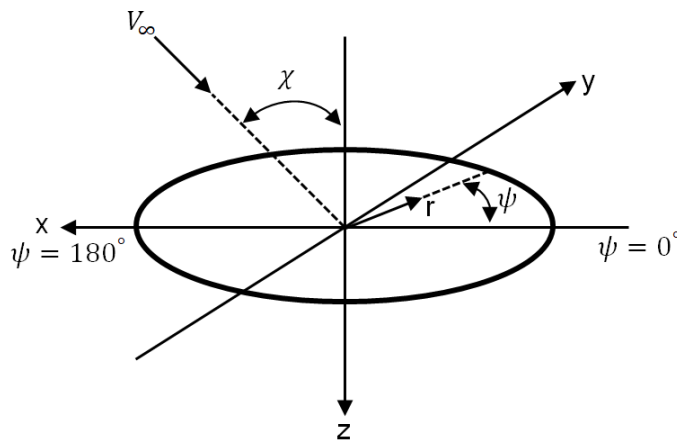
Figure 2.8. Coordinate System of the Induced Flow

The ψ angle is the azimuth angle of the rotor where $\psi = 0°$ is towards the aft of the helicopter. V_∞ is the free stream airflow, χ is the wake skew angle and r is the radial position.

As a result of linear variation, the induced velocity gets larger at the tip of the blade resulting in slower normal wind speed. This is one of the disadvantages of the theory. The variation of the inflow on the rotor blades is shown in Figure 2.9.
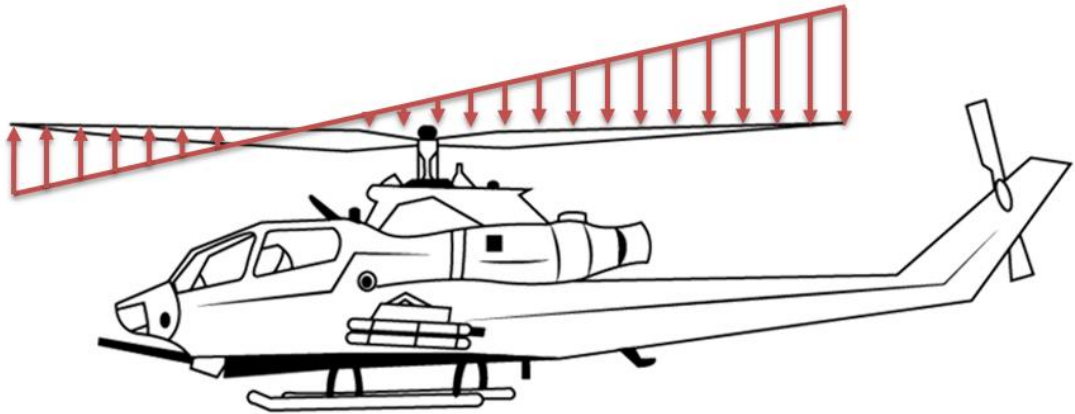
Figure 2.9. Variation of the Pitt-Peters Inflow on Rotor Blades

In Pitt-Peters inflow theory, the states are obtained by solution of a first order differential equation. This differential equation is given in [30] as,

$$[\tilde{M}]\begin{Bmatrix} \dot{\lambda}_0 \\ \dot{\lambda}_s \\ \dot{\lambda}_c \end{Bmatrix} + [V][L]^{-1}\begin{Bmatrix} \lambda_0 \\ \lambda_s \\ \lambda_c \end{Bmatrix} = \begin{Bmatrix} C_T \\ -C_L \\ -C_M \end{Bmatrix} \tag{2-26}$$

Here $[\tilde{M}]$ is the apparent mass matrix and it includes time delay effect due to unsteady wake. $[V]$ is the flow parameter matrix and $[L]$ is known as the influence coefficient matrix. These matrices are given in [31] as,

$$[\tilde{M}] = \begin{bmatrix} \dfrac{128}{75\pi} & 0 & 0 \\ 0 & \dfrac{16}{45\pi} & 0 \\ 0 & 0 & \dfrac{16}{45\pi} \end{bmatrix} \tag{2-27}$$

$$[L] = \begin{bmatrix} \dfrac{1}{2} & 0 & -\dfrac{15\pi}{64}\sqrt{\dfrac{1-sin\alpha}{1+sin\alpha}} \\[3mm] 0 & \dfrac{4}{1+sin\alpha} & 0 \\[3mm] \dfrac{15\pi}{64}\sqrt{\dfrac{1-sin\alpha}{1+sin\alpha}} & 0 & \dfrac{4sin\alpha}{1+sin\alpha} \end{bmatrix} \qquad (2\text{-}28)$$

$$[V] = \begin{bmatrix} V_T & 0 & 0 \\ 0 & V & 0 \\ 0 & 0 & V \end{bmatrix} \qquad (2\text{-}29)$$

where the terms α, V_T and V are defined as,

$$\alpha = \tan^{-1}\dfrac{|\lambda|}{\mu} \qquad (2\text{-}30)$$

$$V_T = \sqrt{\mu^2 + \lambda^2} \qquad (2\text{-}31)$$

$$V = \dfrac{\mu^2 + (\lambda + \lambda_0)\lambda}{V_T} \qquad (2\text{-}32)$$

$$\lambda = \lambda_0 + \lambda_f \qquad (2\text{-}33)$$

$$\mu = \dfrac{V_{inplane}}{\Omega R} \qquad (2\text{-}34)$$

In hover condition (axial flow) where $\alpha = 0$, the influence coefficient matrix turns into simple momentum theory.

In Eqn. (2-26) C_T, C_L and C_M are the instantaneous rotor thrust, roll moment and pitch moment respectively. In this theory, these force terms include only aerodynamic effects. Inertial effects are not taken into consideration. The theory relates the aerodynamic forces C_T, C_L and C_M to the induced flow distributions λ_0, λ_S and λ_C. Formulation of the aerodynamic forces is given by [29],

$$C_T = \dfrac{1}{\pi\rho\Omega^2 R^4}\int_0^{2\pi}\int_0^R Ldrd\psi \qquad (2\text{-}35)$$

$$C_L = -\dfrac{1}{\pi\rho\Omega^2 R^5}\int_0^{2\pi}\int_0^R Lrsin\psi drd\psi \qquad (2\text{-}36)$$

$$C_M = -\dfrac{1}{\pi\rho\Omega^2 R^5}\int_0^{2\pi}\int_0^R Lrcos\psi drd\psi \qquad (2\text{-}37)$$

In Eqns. (2-35), (2-36) and (2-37) *L* represents the sectional blade lift. The lift function can be obtained from any theory that includes inflow explicitly.

2.3.4.2. Peters-He Inflow

Peters-He dynamic inflow theory is obtained by solution of the potential flow equation in the elliptical domain. The theory assumes inviscid, incompressible flow and satisfies the continuity equation. The pressure distribution over the rotor disk is continuous however it is discontinuous across the disk. This fact comes from the actuator disk theory. In order to generate thrust, there has to be a pressure difference between the upper and lower sides of the rotor disk.

Peters-He induced flow is three dimensional with a skewed cylindrical wake [32]. The induced flow caused by the in-plane lift is not included. The model does not have any restriction for the lift theory. It implements 2D lift theory at every radial blade section and integrates them to reach the 3D inflow. The restrictions of the theory are mainly the usage of the cylindrical wake and assumption of the infinite number of blades for the disk.

The theory implicitly recovers Theodorsen, Loewy, Miller, Prandtl/Goldstein and simple dynamic inflow theories [33]. Peters-He inflow theory is validated with wind tunnel test data [34]. It is used in widely accepted production programs such as FLIGHTLAB, COPTER, CAMRAD, DYMORE, etc…

Since Pitt-Peters model does not compensate for higher harmonic demand, Peters-He model is derived as an extension of the Pitt-Peters model. Induced flow on the rotor plane is expanded radially by the Legendre functions of the first and second kind, while as azimuthally the flow is distributed by the Fourier series functions with theoretically infinite number of harmonics. The inflow formulation is given by Eqn. (2-38) [33].

$$\lambda_i(\bar{r}, \psi, \bar{t}) = \sum_{r=0}^{\infty} \sum_{j=r+1, r+3, \ldots}^{\infty} \phi_j^r(\bar{r}) \left[\alpha_j^r(\bar{t}) \cos(r\psi) + \beta_j^r(\bar{t}) \sin(r\psi) \right] \quad (2\text{-}38)$$

Here α_j^r and β_j^r are axial states of the induced flow. ϕ_j^r is the shape function defined by Eqn. (2-39) with factorial ratios for a given harmonic number r and polynomial order j.

$$\phi_j^r(\bar{r}) = \sqrt{(2j+1)H_j^r} \sum_{q=r,r+2,\dots}^{j-1} \bar{r}^q \frac{(-1)^{\frac{q-r}{2}}(j+q)!!}{(q-r)!!\,(q+r)!!\,(j-q-1)!!} \qquad (2\text{-}39)$$

$$H_j^r = \frac{(j+r-1)!!\,(j-r-1)!!}{(j+r)!!\,(j-r)!!} \qquad (2\text{-}40)$$

The double factorial definition is given by,

$$n!! = \begin{cases} n \cdot (n-2) \cdot (n-4) \cdots 3 \cdot 1 & (n = odd) \\ n \cdot (n-2) \cdot (n-4) \cdots 4 \cdot 2 & (n = even) \end{cases} \qquad (2\text{-}41)$$

Similar to the Pitt-Peters theory, the states are obtained by the solution of a first order differential equation given by,

$$\{\alpha_n^m\}^* + [\bar{L}^c]^{-1}[V_n^m]\{\alpha_n^m\} = \{\tau_n^{mc}\}$$
$$\{\beta_n^m\}^* + [\bar{L}^s]^{-1}[V_n^m]\{\beta_n^m\} = \{\tau_n^{ms}\}$$
$$(2\text{-}42)$$

The superscript $\{\}^*$ means differentiation with respect to time. The $\bar{L}^c$ and $\bar{L}^s$ terms are known as influence coefficient matrices. The closed form derivation of the theory gives these terms as follows,

$$[\bar{L}_{jn}^{0m}] = (X^m)[\Gamma_{jn}^{0m}] \qquad (2\text{-}43)$$
$$[\bar{L}_{jn}^{rm}]^c = [X^{|m-r|} + (-1)^l X^{|m+r|}][\Gamma_{jn}^{rm}] \qquad (2\text{-}44)$$
$$[\bar{L}_{jn}^{rm}]^c = [X^{|m-r|} + (-1)^l X^{|m+r|}][\Gamma_{jn}^{rm}] \qquad (2\text{-}45)$$

where $l = \min(r, m)$, $X = \tan|\chi/2|$, χ is wake skew angle and,

for $r + m$ even,

$$\Gamma_{jn}^{rm} = \frac{(-1)^{(n+j-2r)/2} 4\sqrt{(2n+1)(2j+1)}}{\pi(j+n)(j+n+2)[(j-n)^2 - 1]} \qquad (2\text{-}46)$$

for $r + m$ odd, $j = n \pm 1$,

$$\Gamma_{jn}^{rm} = \frac{sgn(r-m)}{\sqrt{(2n+1)(2j+1)}} \tag{2-47}$$

for $r + m$ odd, $j \neq n \pm 1$,

$$\Gamma_{jn}^{rm} = 0 \tag{2-48}$$

V_n^m is related to the airflow. It represents the energy that the rotor extracts from the flow. The definition of the flow matrix is given by,

$$[V]^{c,s} = \begin{bmatrix} \ddots & & \\ & V_n^m & \\ & & \ddots \end{bmatrix} \tag{2-49}$$

$$V_T = \sqrt{\mu^2 + \lambda^2} \tag{2-50}$$

$$V = \frac{\mu^2 + (\lambda + \lambda_0)\lambda}{V_T} \tag{2-51}$$

$$\lambda = \lambda_m + \lambda_f \tag{2-52}$$

where λ_m is the mean inflow and when it is taken as $\lambda_m = \sqrt{3\pi}/2\alpha_1^0$ the theory becomes nonlinear due to the coupling of α_1^0 and V_T terms [33].

The terms τ_n^{mc} and τ_n^{ms} in Eqn. (2-42) are pressure coefficients and constitute forcing functions of the induced flow equation. The forcing functions are given by,

$$\tau_n^{m0} = \frac{1}{2\pi} \sum_{q=1}^{Q} \left[\int_0^1 L_q \phi_n^0(\bar{r}) d\bar{r} \right] \tag{2-53}$$

$$\tau_n^{mc} = \frac{1}{\pi} \sum_{q=1}^{Q} \left[\int_0^1 L_q \phi_n^m(\bar{r}) d\bar{r} \right] \cos(m\psi_q) \tag{2-54}$$

$$\tau_n^{ms} = \frac{1}{\pi} \sum_{q=1}^{Q} \left[\int_0^1 L_q \phi_n^m(\bar{r}) d\bar{r} \right] \sin(m\psi_q) \tag{2-55}$$

Here L_q is the normalized sectional blade lift of the qth blade and Q is the number of the blades. τ_n^{mc} and τ_n^{ms} terms provide the connection between the lift and the wake. Therefore, the coupling of the induced flow model with a lift theory requires circulatory portion of the lift.

CHAPTER 3

FIXED WING FLUTTER ANALYSIS

In this section, equations of motion are derived for the fixed wing flutter analysis. First, derivation of the structural equations of motion is given for general forcing functions. Then, the solution methodologies are discussed based on unsteady aerodynamic theories of Theodorsen, Wagner, Pitt-Peters Inflow and Peters-He Inflow. All of the solution methodologies assume that the blade is at zero angle of attack.

In order to keep the equations of fixed wing flutter analysis in the similar form with the rotary wing flutter equations, r is used as the spanwise coordinate and R is chosen to be the length of the fixed wing.

3.1. Structural Formulation

Structural equations of motion are derived from Lagrange equations using the Euler-Bernoulli beam theory. The equations apply for a cantilever beam with torsional and flapping degrees of freedom. Three-dimensional representation of the beam is performed by the Rayleigh-Ritz method. The shape functions of the Rayleigh-Ritz method are chosen as polynomials up to the 5th degree for the pitching motion and up to the 6th degree for the bending motion to justify the convergence of structural equations. Convergence is justified by the comparison of eigenvalues of the analytical model with Dymore [35] model eigenvalue results. Polynomials of the bending motion start from 2nd degree in order to justify the cantilevered boundary condition.

The wing model is rectangular and it is assumed that it does not experience any warping. Bending and pitching deflections are assumed to be small for the application of the beam theory.

The configuration of the structural element is shown in Figure 3.1. The point P is the aerodynamic center, Q is the shear center and R is the center of gravity.
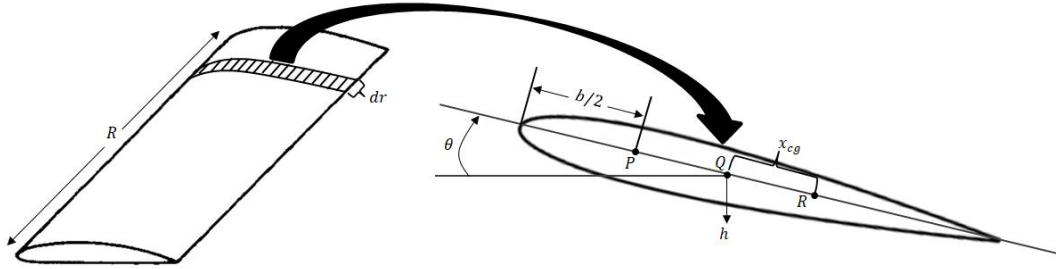
Figure 3.1. Cross-Sectional Element of Fixed Wing

Lagrange's equations of motion require kinetic and potential energy definitions of the system. Kinetic energy dT for the length dr is given by,

$$dT = \frac{1}{2}m\dot{h}^2 dr + mx_{cg}\dot{h}\dot{\theta}dr + \frac{1}{2}I_\theta\dot{\theta}^2 dr \qquad (3\text{-}1)$$

The term m is the mass per length and the term I_θ is the polar moment of inertia for the element dr. The first and last terms of Eqn. (3-1) are related to pure translation and rotation of the section, while the middle term is the coupling term affected by x_{cg} which is the distance between the elastic axis and center of gravity.

The potential energy formulation for an element of length dr is derived utilizing the strain energies as,

$$dU = \frac{1}{2}EI\left(\frac{d^2h}{dr^2}\right)^2 dr + \frac{1}{2}GJ\left(\frac{d\theta}{dr}\right)^2 dr \qquad (3\text{-}2)$$

In Eqn. (3-2) EI and GJ are the bending and the torsional stiffness values per length respectively. One can write the general form of the Lagrange's equation as follows [36],

$$\frac{d}{dt}\left[\frac{\partial T}{\partial \dot{q}_i}\right] - \frac{\partial T}{\partial q_i} + \frac{\partial U}{\partial q_i} + \frac{\partial D}{\partial \dot{q}_i} = F_i \quad i = 1,2,\dots,M \qquad (3\text{-}3)$$

Here D is the dissipation function and it is zero for the particular case of interest. q_i is the generalized coordinate and F_i is the generalized force which consists of aerodynamic forces. Solution of the Lagrange equations with the Rayleigh-Ritz method requires the definition of the bending and pitching degrees of freedoms as follows,

$$h(r,t) = \sum_{j=1}^{n} q_{h_j}(t) W_j(r) \tag{3-4}$$

$$\theta(r,t) = \sum_{j=1}^{n} q_{\theta_j}(t) \Theta_j(r) \tag{3-5}$$

where W is the shape function for the bending motion and Θ is the shape function for the pitching motion. The expansion of the bending and the pitching motions can be written in a more generalized form as,

$$h(r,t) = q_h W, \qquad \theta(r,t) = q_\theta \Theta \tag{3-6}$$

Since it is explained that for the fixed wing analysis, polynomial shape functions up to the 5th degree and up to the 6th degree are used for the pitching and bending motions respectively, the state and shape function vectors in Eqn. (3-6) can be written explicitly as,

$$q_h = [q_{h_1} \quad q_{h_2} \quad q_{h_3} \quad q_{h_4} \quad q_{h_5}]$$
$$q_\theta = [q_{\theta_1} \quad q_{\theta_2} \quad q_{\theta_3} \quad q_{\theta_4} \quad q_{\theta_5}] \tag{3-7}$$

$$W = \begin{bmatrix} r^2 \\ r^3 \\ r^4 \\ r^5 \\ r^6 \end{bmatrix}, \Theta = \begin{bmatrix} r \\ r^2 \\ r^3 \\ r^4 \\ r^5 \end{bmatrix} \tag{3-8}$$

The kinetic and potential energy equations for the system can be written with the separated spatial and time dependent degrees of freedoms as follows,

$$T = \int_0^R \left[\frac{1}{2} m W^2 \dot{q}_h^2 + m x_{cg} W \Theta \dot{q}_h \dot{q}_\theta + \frac{1}{2} I_\theta \Theta^2 \dot{q}_\theta^2 \right] dr \tag{3-9}$$

33

$$U = \int_0^R \left[\frac{1}{2} EI \left(\frac{d^2 W}{dr^2} \right)^2 q_h^2 + \frac{1}{2} GJ \left(\frac{d\Theta}{dr} \right)^2 q_\theta^2 \right] dr \qquad \text{(3-10)}$$

In order to derive the bending and the pitching equations, the Lagrange equation (Eqn. (3-3)) is solved with the kinetic and potential energy equations (3-9) and (3-10) separately for the generalized coordinates of q_h and q_θ. The equations of motion for the fixed are obtained in the form of,

$$\int_0^R \left[mW^2 \ddot{q}_h + mx_{cg} W\Theta \ddot{q}_\theta + EI \left(\frac{d^2 W}{dr^2} \right)^2 q_h \right] dr = L_T \qquad \text{(3-11)}$$

$$\int_0^R \left[I_\theta \Theta^2 \ddot{q}_\theta + mx_{cg} W\Theta \ddot{q}_h + GJ \left(\frac{d\Theta}{dr} \right)^2 q_\theta \right] dr = M_T \qquad \text{(3-12)}$$

On the right hand side of the equations, there are forcing functions. L_T is the total lift of the blade and M_T is the total pitching moment of the blade. The lift and moment terms are derived for each unsteady aerodynamic theory. L_T and M_T are written in general form in Eqns. (3-13) and (3-14).

$$L_T = \int_0^R L_h W dr \qquad \text{(3-13)}$$

$$M_T = \int_0^R M_\theta \Theta dr \qquad \text{(3-14)}$$

Equations (3-11) and (3-12) are the basis for the flutter analyses using different types of aerodynamic models. In the fixed wing flutter analysis, structural part of the equations is kept the same, while the aerodynamic content is changed.

3.2. Flutter Analysis Based on Theodorsen's Theory

Theodorsen's unsteady aerodynamic theory is explained in detail in section 2.3.1. Lift and moment equations of the theory are given by,

$$L_h = 2\pi\rho UbC(k) \left[\dot{h} + U\theta + b \left(\frac{1}{2} - a \right) \dot{\theta} \right] + \pi\rho b^2 (\ddot{h} + U\dot{\theta} - ba\ddot{\theta}) \qquad \text{(3-15)}$$

$$M_{1/4c} = -\pi\rho b^3 \left[\frac{1}{2} \ddot{h} + U\dot{\theta} + b \left(\frac{1}{8} - \frac{a}{2} \right) \ddot{\theta} \right] \qquad \text{(3-16)}$$

The general motion of the system is represented as,

$$q = \bar{q}e^{i\omega t}$$
$$\dot{q} = i\omega\bar{q}e^{i\omega t} = i\omega q \tag{3-17}$$
$$\ddot{q} = -\omega^2\bar{q}e^{i\omega t} = -\omega^2 q$$

Bending and pitching motions are represented as shown in Eqns. (3-4) and (3-5) and the velocity is taken as $U = \frac{b\omega}{k}$ [23]. Since the direction of the bending motion is reversed in aerodynamic equations, it is multiplied by (-1) in order to be correlated with the structural equations. This comes from the definition of the bending motion and lift equation. From Figure 2.5, it can be seen that the directions of the lift and the bending motion are opposite. The lift and moment equations are obtained by the implementation of $U = \frac{b\omega}{k}$ and changing the sign of the bending motion in the Eqns. (3-15) and (3-16). The Eqn. (3-16) gives the pitching moment around the quarter chord point. The overall pitching moment including the effect of lift is obtained as,

$$M_\theta = M_{1/4c} + L_h b\left(\frac{1}{2} + a\right) \tag{3-18}$$

The lift and moment equations can be written as,

$$L_h = \pi\rho b^3\omega^2\left[\left(\frac{1}{b} - \frac{2iC(k)}{kb}\right)\bar{h}\right.$$
$$\left. + \left(\frac{i}{k} + a + \frac{2C(k)}{k^2} + \frac{2iC(k)}{k}\left(\frac{1}{2} - a\right)\right)\bar{\theta}\right] \tag{3-19}$$

$$M_\theta = \pi\rho b^3\omega^2\left[\left(a - \frac{2iC(k)}{k}\left(a + \frac{1}{2}\right)\right)\bar{h}\right.$$
$$+ \left(b\left(\frac{1}{8} + a^2\right) - \frac{ib}{k}\left(\frac{1}{2} - a\right) + \frac{2C(k)b}{k^2}\left(a + \frac{1}{2}\right)\right. \tag{3-20}$$
$$\left.\left. + \frac{2ibC(k)}{k}\left(\frac{1}{2} + a\right)\left(\frac{1}{2} - a\right)\right)\bar{\theta}\right]$$

Now that the aerodynamic equations are obtained, they can be inserted into structural Eqns. (3-11) and (3-12). After the insertion of the aerodynamic forces and the artificial structural damping (g) proportional with the displacement, the final form of the flutter equations are given as,

$$-\omega^2[M]\left\{\begin{matrix}\bar{q}_h\\\bar{q}_\theta\end{matrix}\right\} + (1+ig)[K]\left\{\begin{matrix}\bar{q}_h\\\bar{q}_\theta\end{matrix}\right\} - \pi\rho b^3\omega^2[A]\left\{\begin{matrix}\bar{q}_h\\\bar{q}_\theta\end{matrix}\right\} = \left\{\begin{matrix}0\\0\end{matrix}\right\} \qquad (3\text{-}21)$$

where elements of mass, stiffness and aerodynamic matrices are defined as,

$$[M_{11}] = \int_0^R mWW^T dr \qquad (3\text{-}22)$$

$$[M_{12}] = \int_0^R mx_{cg}\Theta W^T dr \qquad (3\text{-}23)$$

$$[M_{21}] = \int_0^R mx_{cg}W\Theta^T dr \qquad (3\text{-}24)$$

$$[M_{22}] = \int_0^R I_\theta\Theta\Theta^T dr \qquad (3\text{-}25)$$

$$[K_{11}] = \int_0^R EI\left(\frac{d^2W}{dr^2}\right)\left(\frac{d^2W^T}{dr^2}\right) dr \qquad (3\text{-}26)$$

$$[K_{12}] = [K_{21}] = 0 \qquad (3\text{-}27)$$

$$[K_{22}] = \int_0^R GJ\left(\frac{d\Theta}{dr}\right)\left(\frac{d\Theta^T}{dr}\right) dr \qquad (3\text{-}28)$$

$$[A_{11}] = \int_0^R \left(\frac{1}{b} - \frac{2iC(k)}{kb}\right)WW^T dr \qquad (3\text{-}29)$$

$$[A_{12}] = \int_0^R \left(\frac{i}{k} + a + \frac{2C(k)}{k^2} + \frac{2iC(k)}{k}\left(\frac{1}{2} - a\right)\right)\Theta W^T dr \qquad (3\text{-}30)$$

$$[A_{21}] = \int_0^R \left(a - \frac{2iC(k)}{k}\left(a + \frac{1}{2}\right)\right)W\Theta^T dr \qquad (3\text{-}31)$$

$$[A_{22}] = \int_0^R \Bigg(b\left(\frac{1}{8} + a^2\right) - \frac{ib}{k}\left(\frac{1}{2} - a\right) + \frac{2C(k)b}{k^2}\left(a + \frac{1}{2}\right)$$

$$+ \frac{2ibC(k)}{k}\left(\frac{1}{4} - a^2\right)\Bigg)\Theta\Theta^T dr \qquad (3\text{-}32)$$

The shape functions W and Θ are given in Eqn. (3-8). Dividing Eqn. (3-21) by $"-\omega^2"$ one gets Eqn. (3-33).

$$\left[[M] + \pi\rho b^3[A] - \left(\frac{1+ig}{\omega^2}\right)[K]\right]\left\{\begin{matrix}\bar{q}_h\\\bar{q}_\theta\end{matrix}\right\} = \left\{\begin{matrix}0\\0\end{matrix}\right\} \qquad (3\text{-}33)$$

Eqn. (3-33) is a linear algebraic equation set and the determinant of the terms in the brackets has to be equal to zero for a non-trivial solution. If we call the eigenvalue as

$\lambda = \frac{1+ig}{\omega^2}$, solution of the flutter determinant will give the result for a chosen reduced frequency, k.

$$|[M] + \pi\rho b^3[A] - \lambda[K]| = 0 \qquad (3\text{-}34)$$

The frequency and damping information is obtained from the roots as,

$$\omega = \frac{1}{\sqrt{Re(\lambda)}}, \qquad g = \frac{Im(\lambda)}{Re(\lambda)} \qquad (3\text{-}35)$$

The analysis is performed for a varying range of k values. The results are observed by (ω vs k) and (g vs k) plots. The point where the damping curve crosses the zero line is accepted as the flutter point where the damping is zero. From that k value and the corresponding flutter frequency ω, the flutter speed is calculated by using the $U = \frac{b\omega}{k}$ formula.

3.3. Flutter Analysis Based on Wagner's Theory

Wagner's aerodynamic model is explained in section 2.3.3. The lift and moment equations are given by,

$$\begin{aligned}
L_h = {}& \pi\rho b^2\left(\ddot{h} + U\dot{\theta} - ba\ddot{\theta}\right) \\
& + 2\pi\rho Ub\left\{w_{0.75c}(0)\phi(t)\right. \\
& \left. + \int_0^t \phi(\tau - \sigma)\frac{dw_{0.75c}(\sigma)}{d\sigma}d\sigma\right\}
\end{aligned} \qquad (3\text{-}36)$$

$$M_{1/4c} = -\pi\rho b^3\left[\frac{1}{2}\ddot{h} + U\dot{\theta} + b\left(\frac{1}{8} - \frac{a}{2}\right)\ddot{\theta}\right] \qquad (3\text{-}37)$$

For the simplicity of the flutter equations, the wing is assumed to be initially at rest ($w_{0.75c}(0) = 0$) and the lift curve slope correction of Eqn. (2-15) is applied to both lift and moment equations.

The lifting equations can be written with the above approximations as follows. Note that the sign of bending motion in lifting equations is multiplied by (-1) to be

consistent with the axis system of the derived structural equations. This is explained in section 3.2.

$$L_h = \pi\rho b^2\left(-\ddot{h} + U\dot{\theta} - ba\ddot{\theta}\right)$$
$$+ C_{L\phi}\rho U b\left\{-\dot{h} + U\theta + b\left(\frac{1}{2}\left(\frac{C_{L\phi}}{\pi} - 1\right) - a\right)\dot{\theta}\right. \qquad (3\text{-}38)$$
$$\left. - C_1 B_1(t) - C_2 B_2(t)\right\}$$

$$M_\theta = -\pi\rho b^3\left[-\frac{1}{2}\ddot{h} + U\dot{\theta} + b\left(\frac{1}{8} - \frac{a}{2}\right)\ddot{\theta}\right] \qquad (3\text{-}39)$$

The terms B_1 and B_2 in Eqn. (3-38) are the aerodynamic lag states. For the flutter solution, the lift and moment equations are implemented to the Eqns. (3-11) and (3-12). Solution of these governing equations with the aerodynamic lag state Eqns. (2-23) and (2-24) yields the general solution in the form of,

$$[M]\{\ddot{q}_s\} + [C]\{\dot{q}\} + [K]\{q\} = 0 \qquad (3\text{-}40)$$

Here the unknown states are given by Eqn. (3-41). Note that the lag states B_1 and B_2 are also treated as unknowns of the system.

$$q = \begin{Bmatrix} h \\ \theta \\ B_1 \\ B_2 \end{Bmatrix} = \begin{Bmatrix} q_s \\ q_a \end{Bmatrix} \ where \ q_s = \begin{Bmatrix} h \\ \theta \end{Bmatrix} \ and \ q_a = \begin{Bmatrix} B_1 \\ B_2 \end{Bmatrix} \qquad (3\text{-}41)$$

The expansion of the aerodynamic lag states can be written in a generalized form as,

$$B_1(r,t) = q_{B1}\beta_1, \qquad B_2(r,t) = q_{B2}\beta_2 \qquad (3\text{-}42)$$

In Eqn. (3-42) q_{B1} and q_{B2} are time dependent state vectors of the aerodynamic lag state functions. The shape functions of the lag states are defined in Eqn. (3-43) in the similar form of the bending and pitching motion shape functions.

$$\beta_1 = \beta_2 = [r \quad r^2 \quad r^3 \quad r^4 \quad r^5]^T \qquad (3\text{-}43)$$

Elements of the mass, damping and stiffness matrices of the coupled system are defined as,

$$[M_{11}] = \int_0^R (m + \pi\rho b^2) W W^T \, dr \tag{3-44}$$

$$[M_{12}] = \int_0^R (m x_{cg} + \pi\rho a b^3) \Theta W^T \, dr \tag{3-45}$$

$$[M_{21}] = \int_0^R (m x_{cg} + \pi\rho a b^3) W \Theta^T \, dr \tag{3-46}$$

$$[M_{22}] = \int_0^R \left(I_\theta + \pi\rho b^4 \left(\frac{1}{8} + a^2 \right) \right) \Theta \Theta^T \, dr \tag{3-47}$$

$$[M_{31}] = \int_0^R W \beta_1^T \, dr \tag{3-48}$$

$$[M_{32}] = \int_0^R -b \left(\frac{1}{2} \left(\frac{C_{L\phi}}{\pi} - 1 \right) - a \right) \Theta \beta_1^T \, dr \tag{3-49}$$

$$[M_{41}] = \int_0^R W \beta_2^T \, dr \tag{3-50}$$

$$[M_{42}] = \int_0^R -b \left(\frac{1}{2} \left(\frac{C_{L\phi}}{\pi} - 1 \right) - a \right) \Theta \beta_2^T \, dr \tag{3-51}$$

$$[C_{11}] = \int_0^R C_{L\phi} \rho U b W W^T \, dr \tag{3-52}$$

$$[C_{12}] = \int_0^R \left(-\pi\rho U b^2 - C_{L\phi} \rho U b^2 \left(\frac{1}{2} \left(\frac{C_{L\phi}}{\pi} - 1 \right) - a \right) \right) \Theta W^T \, dr \tag{3-53}$$

$$[C_{21}] = \int_0^R C_{L\phi} \rho U b^2 \left(\frac{1}{2} + a \right) W \Theta^T \, dr \tag{3-54}$$

$$[C_{22}] = \int_0^R \left(\pi\rho U b^3 \left(\frac{1}{2} \left(\frac{C_{L\phi}}{\pi} - 1 \right) - a \right) \right.$$
$$\left. - C_{L\phi} \rho U b^3 \left(\frac{1}{2} \left(\frac{C_{L\phi}}{\pi} - 1 \right) - a \right) \left(\frac{1}{2} + a \right) \right) \Theta \Theta^T \, dr \tag{3-55}$$

$$[C_{32}] = \int_0^R -U \Theta \beta_1^T \, dr \tag{3-56}$$

$$[C_{33}] = \int_0^R \beta_1 \beta_1^T \, dr \tag{3-57}$$

$$[C_{42}] = \int_0^R -U \Theta \beta_2^T \, dr \tag{3-58}$$

$$[C_{44}] = \int_0^R \beta_2 \beta_2^T \, dr \tag{3-59}$$

$$[C_{13}] = [C_{14}] = [C_{23}] = [C_{24}] = [C_{31}] = [C_{34}] = [C_{41}] = [C_{43}] = 0 \tag{3-60}$$

$$[K_{11}] = \int_0^R EI \left(\frac{d^2 W}{dr^2} \right) \left(\frac{d^2 W^T}{dr^2} \right) \, dr \tag{3-61}$$

$$[K_{12}] = \int_0^R -C_{L\phi}\rho U^2 b\Theta W^T dr \tag{3-62}$$

$$[K_{13}] = \int_0^R C_{L\phi}\rho U b C_1 \beta_1 W^T dr \tag{3-63}$$

$$[K_{14}] = \int_0^R C_{L\phi}\rho U b C_2 \beta_2 W^T dr \tag{3-64}$$

$$[K_{22}] = \int_0^R GJ\left(\frac{d\Theta}{dr}\right)\left(\frac{d\Theta^T}{dr}\right) dr - \int_0^R C_{L\phi}\rho U^2 b^2\left(a + \frac{1}{2}\right)\Theta\Theta^T dr \tag{3-65}$$

$$[K_{23}] = \int_0^R C_{L\phi}\rho U b^2\left(a + \frac{1}{2}\right)C_1\beta_1\Theta^T dr \tag{3-66}$$

$$[K_{24}] = \int_0^R C_{L\phi}\rho U b^2\left(a + \frac{1}{2}\right)C_2\beta_2\Theta^T dr \tag{3-67}$$

$$[K_{33}] = \int_0^R \varepsilon_1 \frac{U}{b}\beta_1\beta_1^T dr \tag{3-68}$$

$$[K_{44}] = \int_0^R \varepsilon_2 \frac{U}{b}\beta_2\beta_2^T dr \tag{3-69}$$

$$[K_{21}] = [K_{31}] = [K_{32}] = [K_{34}] = [K_{41}] = [K_{42}] = [K_{43}] = 0 \tag{3-70}$$

The shape functions W and Θ are given in Eqn. (3-8). The general governing equation can be expressed in the state space form as shown in Eqn. (3-71).

$$\begin{bmatrix} [C]_{4x4} & [M]_{4x2} \\ [I]_{2x4} & [0]_{2x2} \end{bmatrix}\begin{Bmatrix} \{\dot{q}\}_{4x1} \\ \{\ddot{q}_s\}_{2x1} \end{Bmatrix} + \begin{bmatrix} [K]_{4x4} & [0]_{4x2} \\ [0]_{2x4} & -[I]_{2x2} \end{bmatrix}\begin{Bmatrix} \{q\}_{4x1} \\ \{\dot{q}_s\}_{2x1} \end{Bmatrix} = 0 \tag{3-71}$$

Equation (3-71) can then be expressed as,

$$[A]\{\dot{x}\} + [B]\{x\} = 0 \tag{3-72}$$

The flutter determinant is obtained as follows,

$$\{\dot{x}\} = -[A]^{-1}[B]\{x\} \tag{3-73}$$
$$\{-[A]^{-1}[B] - \lambda[I]\}\{x_0\} = 0 \tag{3-74}$$

where,

$$\{x\} = \{x_0\}e^{\lambda t} \tag{3-75}$$

The determinant solution of the first term of Eqn. (3-74) in the brackets gives the roots of the system. This procedure is performed for varying airspeeds and the results will

be observed in terms of (ω vs U) and (g vs U) plots for each of the roots. The point where the damping curve crosses zero line is accepted as the flutter point where the damping is zero.

3.4. Flutter Analysis Based on Pitt-Peters Inflow Theory

Pitt-Peters inflow theory is explained in detail in section 2.3.4.1. The theory is derived for normalized equations. Therefore structural and aerodynamic equations of flutter analysis should also be normalized to be compatible with the inflow theory. The distance is normalized as $\bar{r} = r/R$ and the time is normalized as $\bar{t} = Ut/R$. The time derivatives are with respect to the normalized time. With these normalizations applied, the bending equation defined in Eqn. (3-11) is normalized with mU^2/R to yield,

$$
\int_0^1 WW^T \ddot{q}_h d\bar{r} + \int_0^1 \bar{x}_{cg} \Theta W^T \ddot{q}_\theta d\bar{r}
$$
$$
+ \int_0^1 \frac{EI}{mU^2R^2} \left(\frac{d^2W}{dr^2}\right)\left(\frac{d^2W^T}{dr^2}\right) q_h d\bar{r} \tag{3-76}
$$
$$
= \int_0^1 \bar{L}_h \left(\frac{\rho R^2}{m}\right) W d\bar{r}
$$

Similarly, the pitching equation defined in Eqn. (3-12) is normalized with mU^2 to yield,

$$
\int_0^1 \bar{x}_{cg} W \Theta^T \ddot{q}_h d\bar{r} + \int_0^1 \bar{k}_m^2 \Theta \Theta^T \ddot{q}_\theta d\bar{r}
$$
$$
+ \int_0^1 \frac{GJ}{mU^2R^2} \left(\frac{d\Theta}{dr}\right)\left(\frac{d\Theta^T}{dr}\right) q_\theta d\bar{r} = \int_0^1 \left[\bar{M}_{1/4c} \right. \tag{3-77}
$$
$$
\left. + \bar{L}_h \left(\frac{1}{2} + a\right) \bar{b}\right] \left(\frac{\rho R^2}{m}\right) \Theta d\bar{r}
$$

Now that we have the normalized structural equations, the next step is to define the normalized aerodynamic terms $\bar{L}_h$ and $\bar{M}_{1/4c}$. The aerodynamic functions for the Pitt-Peters flutter analysis can be defined based on Theodorsen's unsteady aerodynamics. Induced flow term is added to the circulatory part of the lift expression eliminating the

Theodorsen's lift deficiency function $C(k)$. The resulting lift and moment expressions are given by [23],

$$L_h = 2\pi\rho U b\left[\dot{h} + U\theta + b\left(\frac{1}{2} - a\right)\dot{\theta} - \lambda\right] \qquad (3\text{-}78)$$

$$M_{1/4c} = -\pi\rho b^3\left[\frac{1}{2}\ddot{h} + U\dot{\theta} + b\left(\frac{1}{8} - \frac{a}{2}\right)\ddot{\theta}\right] \qquad (3\text{-}79)$$

The lift expression includes only the circulatory part [32]. The induced flow term λ in the lift equation provides coupling with the induced flow theory. The normalization of Eqn. (3-78) is done with $\rho U^2 R$ as,

$$\bar{L}_h = 2\pi\bar{b}\left[\dot{\bar{h}} + \theta + \bar{b}\left(\frac{1}{2} - a\right)\dot{\theta} - \lambda\right] \qquad (3\text{-}80)$$

The moment equation is not affected by the shed wake. Similarly, the moment equation is normalized with $\rho U^2 R^2$ to yield,

$$\bar{M}_{1/4c} = -\pi\bar{b}^3\left[\frac{1}{2}\ddot{\bar{h}} + \dot{\theta} + \bar{b}\left(\frac{1}{8} - \frac{a}{2}\right)\ddot{\theta}\right] \qquad (3\text{-}81)$$

The induced flow is defined with the mean (λ_0), lateral (λ_s) and longitudinal (λ_c) variations of the flow as,

$$\lambda = \lambda_0 + \lambda_s r\sin\psi + \lambda_c r\cos\psi \qquad (3\text{-}82)$$

For the flutter solution, the structural equations of motion and the induced flow equations must be solved together. This solution is a p-type solution because it requires no iteration over the reduced frequency. In general form, the structural equation set is obtained by addition of normalized lift and moment expression Eqns. (3-80) and (3-81) into the normalized structural Eqns. (3-76) and (3-77) with the application of the induced flow given in Eqn. (3-82) as,

$$[M]\begin{Bmatrix}\ddot{q}_h \\ \ddot{q}_\theta\end{Bmatrix} + [C]\begin{Bmatrix}\dot{q}_h \\ \dot{q}_\theta\end{Bmatrix} + [K]\begin{Bmatrix}q_h \\ q_\theta\end{Bmatrix} + [D]\begin{Bmatrix}\lambda_0 \\ \lambda_s \\ \lambda_c\end{Bmatrix} = 0 \qquad (3\text{-}83)$$

42

where mass, damping, stiffness and inflow coefficient matrices are defined in Eqns. (3-84)-(3-101). Note that the bending motion in the lift and moment equations is multiplied with (-1) to be consistent with the axis system of the derived structural equations. The bending motion direction being opposite to the lift direction is explained in Section 3.2.

$$[M_{11}] = \int_0^1 WW^T d\bar{r} \tag{3-84}$$

$$[M_{12}] = \int_0^1 \bar{x}_{cg} \Theta W^T d\bar{r} \tag{3-85}$$

$$[M_{21}] = \int_0^1 \left(\bar{x}_{cg} - \frac{1}{2}\pi\bar{b}^3 \left(\frac{\rho R^2}{m} \right) \right) W\Theta^T d\bar{r} \tag{3-86}$$

$$[M_{22}] = \int_0^1 \left(\bar{k}_m^2 + \pi\bar{b}^4 \left(\frac{1}{8} - \frac{a}{2} \right) \left(\frac{\rho R^2}{m} \right) \right) \Theta\Theta^T d\bar{r} \tag{3-87}$$

$$[C_{11}] = \int_0^1 2\pi\bar{b} \left(\frac{\rho R^2}{m} \right) WW^T d\bar{r} \tag{3-88}$$

$$[C_{12}] = \int_0^1 -2\pi\bar{b}^2 \left(\frac{1}{2} - a \right) \left(\frac{\rho R^2}{m} \right) \Theta W^T d\bar{r} \tag{3-89}$$

$$[C_{21}] = \int_0^1 2\pi\bar{b}^2 \left(\frac{1}{2} + a \right) \left(\frac{\rho R^2}{m} \right) W\Theta^T d\bar{r} \tag{3-90}$$

$$[C_{22}] = \int_0^1 \pi\bar{b}^3 \left(\frac{1}{2} + 2a^2 \right) \left(\frac{\rho R^2}{m} \right) \Theta\Theta^T d\bar{r} \tag{3-91}$$

$$[K_{11}] = \int_0^1 \frac{EI}{mU^2R^2} \left(\frac{d^2 W}{dr^2} \right) \left(\frac{d^2 W^T}{dr^2} \right) d\bar{r} \tag{3-92}$$

$$[K_{12}] = \int_0^1 -2\pi\bar{b} \left(\frac{\rho R^2}{m} \right) \Theta W^T d\bar{r} \tag{3-93}$$

$$[K_{21}] = 0 \tag{3-94}$$

$$[K_{22}] = \int_0^1 \frac{GJ}{mU^2R^2} \left(\frac{d\Theta}{dr} \right) \left(\frac{d\Theta^T}{dr} \right) d\bar{r}$$
$$+ \int_0^1 -2\pi\bar{b}^2 \left(\frac{1}{2} + a \right) \left(\frac{\rho R^2}{m} \right) \Theta\Theta^T d\bar{r} \tag{3-95}$$

$$[D_{11}] = \int_0^1 2\pi\bar{b} \left(\frac{\rho R^2}{m} \right) W d\bar{r} \tag{3-96}$$

$$[D_{12}] = \int_0^1 2\pi\bar{b} \left(\frac{\rho R^2}{m} \right) \bar{r} \sin(\psi) W d\bar{r} \tag{3-97}$$

$$[D_{13}] = \int_0^1 2\pi\bar{b}\left(\frac{\rho R^2}{m}\right)\bar{r}\cos(\psi)W d\bar{r} \tag{3-98}$$

$$[D_{21}] = \int_0^1 2\pi\bar{b}^2\left(\frac{1}{2}+a\right)\left(\frac{\rho R^2}{m}\right)\Theta d\bar{r} \tag{3-99}$$

$$[D_{22}] = \int_0^1 2\pi\bar{b}^2\left(\frac{1}{2}+a\right)\left(\frac{\rho R^2}{m}\right)\bar{r}\sin(\psi)\,\Theta d\bar{r} \tag{3-100}$$

$$[D_{23}] = \int_0^1 2\pi\bar{b}^2\left(\frac{1}{2}+a\right)\left(\frac{\rho R^2}{m}\right)\bar{r}\cos(\psi)\Theta d\bar{r} \tag{3-101}$$

The shape functions W and Θ are given in Eqn. (3-8). The next step is the derivation of inflow equations. As mentioned before the Pitt-Peters inflow theory is a solution of a first order differential equation. The theory is in the form of,

$$[\widetilde{M}]\begin{Bmatrix}\dot{\lambda}_0 \\ \dot{\lambda}_s \\ \dot{\lambda}_c\end{Bmatrix} + [V][L]^{-1}\begin{Bmatrix}\lambda_0 \\ \lambda_s \\ \lambda_c\end{Bmatrix} = \begin{Bmatrix}C_T \\ -C_L \\ -C_M\end{Bmatrix} \tag{3-102}$$

The matrices $[\widetilde{M}]$, $[L]$ and $[V]$ are given in section 2.3.4.1. The induced flow is coupled with the structural equations via the aerodynamic coefficients C_T, C_L and C_M. For the fixed wing equations, these terms are defined as,

$$C_T = \frac{1}{\rho\pi R^2 U^2}\int_0^1 2\pi\bar{b}\left[-\dot{\bar{h}} + \theta + \bar{b}\left(\frac{1}{2}-a\right)\dot{\theta} - \lambda\right]d\bar{r} \tag{3-103}$$

$$C_L = -\frac{1}{\rho\pi R^3 U^2}\int_0^1 2\pi\bar{b}\left[-\dot{\bar{h}} + \theta + \bar{b}\left(\frac{1}{2}-a\right)\dot{\theta} - \lambda\right]\bar{r}sin\psi d\bar{r} \tag{3-104}$$

$$C_M = -\frac{1}{\rho\pi R^3 U^2}\int_0^1 2\pi\bar{b}\left[-\dot{\bar{h}} + \theta + \bar{b}\left(\frac{1}{2}-a\right)\dot{\theta} - \lambda\right]\bar{r}cos\psi d\bar{r} \tag{3-105}$$

These definitions differ from the Eqns. (3-35), (3-36) and (3-37) described in the Pitt-Peters inflow theory part. The theory, in general, is derived for the rotating blades. Hence, the term "ΩR" is replaced with "U" for the fixed wing analysis. In addition, the disk integration is eliminated, since the fixed wing solution is performed for a single blade at a fixed azimuth. The fixed azimuth is selected as $90°$ which makes the C_M term of Eqn. (3-105) zero. For the normalized lift terms in the aerodynamic coefficient equations, the circulatory lift definition of Eqn. (3-80) is used.

After the derivation of the aerodynamic coefficients for the fixed wing, these equations should be implemented to the general form of the inflow Eqn. (3-102). As a result of this implementation, the induced flow equation with the explicit lift definition is given by,

$$[\tilde{M}]\begin{Bmatrix}\dot{\lambda}_0\\\dot{\lambda}_s\\\dot{\lambda}_c\end{Bmatrix} + [[V][L]^{-1} - [G]]\begin{Bmatrix}\lambda_0\\\lambda_s\\\lambda_c\end{Bmatrix} - \frac{1}{\rho\pi R^3 U^2}[E]\begin{Bmatrix}\dot{q}_h\\\dot{q}_\theta\end{Bmatrix}$$
$$- \frac{1}{\rho\pi R^3 U^2}[F]\begin{Bmatrix}q_h\\q_\theta\end{Bmatrix} = 0 \tag{3-106}$$

In Eqn. (3-106) the matrices $[E]$, $[F]$ and $[G]$ comes from the circulatory lift equation. These terms bring the structural degrees of freedom into the inflow equation and hence provide coupling. The elements of the matrices $[E]$, $[F]$ and $[G]$ are given below.

$$[E_{11}] = \int_0^1 -2\pi\bar{b}W^T d\bar{r} \tag{3-107}$$

$$[E_{12}] = \int_0^1 2\pi\bar{b}^2\left(\frac{1}{2} - a\right)\Theta^T d\bar{r} \tag{3-108}$$

$$[E_{21}] = \int_0^1 -2\pi\bar{b}\bar{r}\sin(\psi)\,W^T d\bar{r} \tag{3-109}$$

$$[E_{22}] = \int_0^1 2\pi\bar{b}^2\left(\frac{1}{2} - a\right)\bar{r}\sin(\psi)\,\Theta^T d\bar{r} \tag{3-110}$$

$$[E_{31}] = \int_0^1 -2\pi\bar{b}\bar{r}\cos(\psi)\,W^T d\bar{r} \tag{3-111}$$

$$[E_{32}] = \int_0^1 2\pi\bar{b}^2\left(\frac{1}{2} - a\right)\bar{r}\cos(\psi)\,\Theta^T d\bar{r} \tag{3-112}$$

$$[F_{12}] = \int_0^1 2\pi\bar{b}\Theta^T d\bar{r} \tag{3-113}$$

$$[F_{22}] = \int_0^1 2\pi\bar{b}\bar{r}\sin(\psi)\,\Theta^T d\bar{r} \tag{3-114}$$

$$[F_{32}] = \int_0^1 2\pi\bar{b}\bar{r}\cos(\psi)\,\Theta^T d\bar{r} \tag{3-115}$$

$$[F_{11}] = [F_{21}] = [F_{31}] = 0 \tag{3-116}$$

$$[G_{11}] = \int_0^1 -2\pi\bar{b}d\bar{r} \tag{3-117}$$

$$[G_{12}] = \int_0^1 -2\pi \bar{b}\bar{r}\sin(\psi)\,d\bar{r} \tag{3-118}$$

$$[G_{13}] = \int_0^1 -2\pi \bar{b}\bar{r}\cos(\psi)\,d\bar{r} \tag{3-119}$$

$$[G_{21}] = \int_0^1 -2\pi \bar{b}\bar{r}\sin(\psi)d\bar{r} \tag{3-120}$$

$$[G_{22}] = \int_0^1 -2\pi \bar{b}\bar{r}^2(\sin(\psi))^2 d\bar{r} \tag{3-121}$$

$$[G_{23}] = \int_0^1 -2\pi \bar{b}\bar{r}^2(\cos(\psi))^2 d\bar{r} \tag{3-122}$$

$$[G_{31}] = \int_0^1 -2\pi \bar{b}\bar{r}\cos(\psi)d\bar{r} \tag{3-123}$$

$$[G_{32}] = \int_0^1 -2\pi \bar{b}\bar{r}^2\cos(\psi)\sin(\psi)\,d\bar{r} \tag{3-124}$$

$$[G_{33}] = \int_0^1 -2\pi \bar{b}\bar{r}^2\cos(\psi)\cos(\psi)d\bar{r} \tag{3-125}$$

The coupling of structural and inflow equations require the definition of a general state vector such as,

$$q = \begin{Bmatrix} q_h \\ q_\theta \\ \dot{q}_h \\ \dot{q}_\theta \\ \lambda \end{Bmatrix} \tag{3-126}$$

The general motion of the state vector q is represented as,

$$q = \bar{q}e^{pt} \tag{3-127}$$

With the definition of the general state vector, the two systems can be coupled in one equation as given by,

$$\{\dot{q}\} + [A]\{q\} = 0 \tag{3-128}$$

where,

$$[A] = \begin{bmatrix} [0]_{2x2} & -[I]_{2x2} & [0]_{2x3} \\ [M]^{-1}[K] & [M]^{-1}[C] & [M]^{-1}[D] \\ -[\tilde{M}]^{-1}[F] & -[\tilde{M}]^{-1}[E] & [\tilde{M}]^{-1}\{[V][L]^{-1} - [G]\} \end{bmatrix} \tag{3-129}$$

46

The definition given in Eqn. (3-127) helps to write Eqn. (3-128) in the form of,

$$\{[A] + p[I]\}\{q\} = 0 \tag{3-130}$$

In Eqn. (3-130) p represents the roots of the system. The determinant solution of the $\{[A] + p[I]\}$ will result in 7 roots. Two of the roots are structural states, two of the roots are derivatives of the structural states and three of the roots are the inflow states λ_0, λ_s and λ_c.

The determinant solution will be repeated for a range of airspeed values and the results will be observed in terms of $(\omega \ vs \ U)$ and $(g \ vs \ U)$ plots for the structural states especially. The point where the damping curve crosses zero line is accepted as the flutter point where the damping is zero.

3.5. Flutter Analysis Based on Peters-He Inflow Theory

Peters-He inflow theory is explained in detail in section 2.3.4.2. In this section, Peters-He theory is also derived for normalized equations. Hence, normalized structural and aerodynamic equations of section 3.4 are used here to be compatible with the inflow theory. The distance is normalized as $\bar{r} = r/R$ and the time is normalized as $\bar{t} = Ut/R$. As structural system equations, normalized Eqns. (3-76) and (3-77) are used. The aerodynamic equations of the system should be normalized also. Theodorsen based normalized aerodynamic equations are given by Eqns. (3-80) and (3-81).

Peters-He inflow theory differs from the Pitt-Peters theory basically in the definition of the induced flow. As mentioned in the theory part, the induced flow definition of Peters-He theory is given by,

$$\lambda(\bar{r}, \psi, \bar{t}) = \sum_{r=0}^{\infty} \sum_{j=r+1, r+3, \ldots}^{\infty} \phi_j^r(\bar{r})\left[\alpha_j^r(\bar{t})\cos(r\psi) + \beta_j^r(\bar{t})\sin(r\psi)\right] \tag{3-131}$$

Unlike the Pitt-Peters theory, here it is possible to define the induced flow for an infinite number of states. Peters-He inflow theory flutter solution is also a p-type

solution because the solution does not require any iteration on the reduced frequency. Therefore, general p-type structural and aerodynamic motions are assumed in the equations.

The general form of the structural equations is given by,

$$[M]\begin{Bmatrix}\ddot{q}_h\\\ddot{q}_\theta\end{Bmatrix} + [C]\begin{Bmatrix}\dot{q}_h\\\dot{q}_\theta\end{Bmatrix} + [K]\begin{Bmatrix}q_h\\q_\theta\end{Bmatrix} + [D]\begin{Bmatrix}\alpha_j^r\\\beta_j^r\end{Bmatrix} = 0 \qquad (3\text{-}132)$$

where the elements of the mass, damping, stiffness and inflow coefficient matrix are defined in Eqns. (3-133)-(3-148). Note that the bending motion in lifting equations is multiplied with (-1) to be consistent with the axis system of the derived structural equations. The α_j^r and β_j^r terms are the states of the induced flow defined in Eqn. (3-131).

$$[M_{11}] = \int_0^1 WW^T d\bar{r} \qquad (3\text{-}133)$$

$$[M_{12}] = \int_0^1 \bar{x}_{cg}\Theta W^T d\bar{r} \qquad (3\text{-}134)$$

$$[M_{21}] = \int_0^1 \left(\bar{x}_{cg} - \frac{1}{2}\pi\bar{b}^3\left(\frac{\rho R^2}{m}\right)\right) W\Theta^T d\bar{r} \qquad (3\text{-}135)$$

$$[M_{22}] = \int_0^1 \left(\bar{k}_m^2 + \pi\bar{b}^4\left(\frac{1}{8} - \frac{a}{2}\right)\left(\frac{\rho R^2}{m}\right)\right)\Theta\Theta^T d\bar{r} \qquad (3\text{-}136)$$

$$[C_{11}] = \int_0^1 2\pi\bar{b}\left(\frac{\rho R^2}{m}\right) WW^T d\bar{r} \qquad (3\text{-}137)$$

$$[C_{12}] = \int_0^1 -2\pi\bar{b}^2\left(\frac{1}{2} - a\right)\left(\frac{\rho R^2}{m}\right)\Theta W^T d\bar{r} \qquad (3\text{-}138)$$

$$[C_{21}] = \int_0^1 2\pi\bar{b}^2\left(\frac{1}{2} + a\right)\left(\frac{\rho R^2}{m}\right) W\Theta^T d\bar{r} \qquad (3\text{-}139)$$

$$[C_{22}] = \int_0^1 \pi\bar{b}^3\left(\frac{1}{2} + 2a^2\right)\left(\frac{\rho R^2}{m}\right)\Theta\Theta^T d\bar{r} \qquad (3\text{-}140)$$

$$[K_{11}] = \int_0^1 \frac{EI}{mU^2R^2}\left(\frac{d^2W}{dr^2}\right)\left(\frac{d^2W^T}{dr^2}\right) d\bar{r} \qquad (3\text{-}141)$$

$$[K_{12}] = \int_0^1 -2\pi\bar{b}\left(\frac{\rho R^2}{m}\right)\Theta W^T d\bar{r} \qquad (3\text{-}142)$$

$$[K_{21}] = 0 \qquad (3\text{-}143)$$

$$[K_{22}] = \int_0^1 \frac{GJ}{mU^2R^2} \left(\frac{d\Theta}{dr}\right)\left(\frac{d\Theta^T}{dr}\right) d\bar{r}$$
$$+ \int_0^1 -2\pi\bar{b}^2 \left(\frac{1}{2} + a\right)\left(\frac{\rho R^2}{m}\right) \Theta\Theta^T d\bar{r} \tag{3-144}$$

$$[D_{11}] = \int_0^1 2\pi\bar{b}\left(\frac{\rho R^2}{m}\right) \bar{\phi}_j^r \cos(r\psi) W d\bar{r} \tag{3-145}$$

$$[D_{12}] = \int_0^1 2\pi\bar{b}\left(\frac{\rho R^2}{m}\right) \bar{\phi}_j^r \sin(r\psi) W d\bar{r} \tag{3-146}$$

$$[D_{21}] = \int_0^1 2\pi\bar{b}^2 \left(\frac{1}{2} + a\right)\left(\frac{\rho R^2}{m}\right) \bar{\phi}_j^r \cos(r\psi)\, \Theta d\bar{r} \tag{3-147}$$

$$[D_{22}] = \int_0^1 2\pi\bar{b}^2 \left(\frac{1}{2} + a\right)\left(\frac{\rho R^2}{m}\right) \bar{\phi}_j^r \sin(r\psi)\, \Theta d\bar{r} \tag{3-148}$$

The shape functions W and Θ are given in Eqn. (3-8). The size of the $[D]$ matrix depends on the number of states. Equations (3-145)-(3-148) show the general representation of the matrix. The term $\bar{\phi}_j^r$ is the shape function and it is defined in Eqn. (2-39). The size of the shape function changes for a given harmonic number r and a polynomial order j. For instance, if the harmonic number and the polynomial order are selected as 2, the α_j^r inflow state of Eqn. (3-132) is sized as $[4x1]$ and the β_j^r state of Eqn. (3-132) is sized as $[2x1]$. In this case, the size of the $[D]$ matrix is $[2x6]$.

The second governing equation of the system is the inflow equation. This first order differential equation is given in section 2.3.4.2 as,

$$\{\alpha_n^m\}^* + [\bar{L}^c]^{-1}[V_n^m]\{\alpha_n^m\} = \{\tau_n^{mc}\}$$
$$\{\beta_n^m\}^* + [\bar{L}^s]^{-1}[V_n^m]\{\beta_n^m\} = \{\tau_n^{ms}\} \tag{3-149}$$

The superscript $\{\}^*$ means differentiation with respect to time. Derivations of $[\bar{L}^c]$, $[\bar{L}^s]$ and $[V_n^m]$ matrices are given in section 2.3.4.2 in detail. Repetition of those equations is not done here. However, the construction of $[\bar{L}^c]$ and $[\bar{L}^s]$ matrices is explained for a number of harmonics and polynomial order selection. Selection of the number of harmonics and polynomial order should be performed according to Table 3.1.

Table 3.1. *Harmonics and Polynomial Order Selection*

		Number of Harmonics (r)											Total State #
		0	1	2	3	4	5	6	7	8	9	10	
Polynomial Order (j)	0	1											1
	1	1	1										3
	2	2	1	1									6
	3	2	2	1	1								10
	4	3	2	2	1	1							15
	5	3	3	2	2	1	1						21
	6	4	3	3	2	2	1	1					28
	7	4	4	3	3	2	2	1	1				36
	8	5	4	4	3	3	2	2	1	1			45
	9	5	5	4	4	3	3	2	2	1	1		55
	10	6	5	5	4	4	3	3	2	2	1	1	66

Selected number of harmonics and polynomial order do not have to be equal. The only restriction is that the number of harmonics cannot be bigger than the polynomial order. After the selection of r and j, the format vector is obtained according to the table. For instance, for a selection of 3x3 from the table, the format vector S can be written as,

$$S = [S_0 \quad S_1 \quad S_2 \quad S_3] = [2 \quad 2 \quad 1 \quad 1] \qquad (3\text{-}150)$$

This format vector shows how many times each harmonic is expanded as shown in Table 3.2. The expansion of each harmonic is done with increments of two. The elements of $[\bar{L}^c] = [\bar{L}_{jn}^{rm}]^c$ and $[\bar{L}^s] = [\bar{L}_{jn}^{rm}]^s$ matrices are defined according to the methodology example given in Table 3.2.

Table 3.2. *Harmonic Expansion Example for 3x3*

r=m=0	j=1, j=3 and n=1, n=3
r=m=1	j=2, j=4 and n=2, n=4
r=m=2	j=3 and n=3
r=m=3	j=4 and n=4

According to Table 3.1, selection of 3x3 gives 10 states for the solution. Total state number can be calculated with the following formula.

$$N_s = S_0 + 2[S_1 + S_2 + \cdots + S_{max}] \tag{3-151}$$

N_s is the total number of states. Note that, S_0 expansion exists only in the cosine terms. According to the given information about the expansion of harmonics, an example construction of the influence coefficient matrices can be written as in Eqns. (3-152) and (3-153).

$$[\bar{L}_{jn}^{rm}]^c = \begin{bmatrix} \bar{L}_{11}^{00} & \bar{L}_{13}^{00} & \bar{L}_{12}^{01} & \bar{L}_{14}^{01} & \bar{L}_{13}^{02} & \bar{L}_{14}^{03} \\ \bar{L}_{31}^{00} & \bar{L}_{33}^{00} & \bar{L}_{32}^{01} & \bar{L}_{34}^{01} & \bar{L}_{33}^{02} & \bar{L}_{34}^{03} \\ \bar{L}_{21}^{10} & \bar{L}_{23}^{10} & \bar{L}_{22}^{11} & \bar{L}_{24}^{11} & \bar{L}_{23}^{12} & \bar{L}_{24}^{13} \\ \bar{L}_{41}^{10} & \bar{L}_{43}^{10} & \bar{L}_{42}^{11} & \bar{L}_{44}^{11} & \bar{L}_{43}^{12} & \bar{L}_{44}^{13} \\ \bar{L}_{31}^{20} & \bar{L}_{33}^{20} & \bar{L}_{32}^{21} & \bar{L}_{34}^{21} & \bar{L}_{33}^{22} & \bar{L}_{34}^{23} \\ \bar{L}_{41}^{30} & \bar{L}_{43}^{30} & \bar{L}_{42}^{31} & \bar{L}_{44}^{31} & \bar{L}_{43}^{32} & \bar{L}_{44}^{33} \end{bmatrix} \tag{3-152}$$

$$[\bar{L}_{jn}^{rm}]^s = \begin{bmatrix} \bar{L}_{22}^{11} & \bar{L}_{24}^{11} & \bar{L}_{23}^{12} & \bar{L}_{24}^{13} \\ \bar{L}_{42}^{11} & \bar{L}_{44}^{11} & \bar{L}_{43}^{12} & \bar{L}_{44}^{13} \\ \bar{L}_{32}^{21} & \bar{L}_{34}^{21} & \bar{L}_{33}^{22} & \bar{L}_{34}^{23} \\ \bar{L}_{42}^{31} & \bar{L}_{44}^{31} & \bar{L}_{43}^{32} & \bar{L}_{44}^{33} \end{bmatrix} \tag{3-153}$$

Now that the construction of the influence coefficient matrices is explained, the next critical part of the solution is the composition of the forcing vectors $\{\tau_n^{mc}\}$ and $\{\tau_n^{ms}\}$. As mentioned in the theory part, these forcing vectors are defined as follows. The lift definition $\bar{L}_h$ is obtained from Eqn. (3-80) with the bending motion multiplied by (-1) to be consistent with the axis system of the structural equation of motions.

$$\tau_n^{m0} = \frac{1}{2\pi} \int_0^1 2\pi\bar{b} \left[-\dot{\bar{h}} + \theta + \bar{b}\left(\frac{1}{2} - a\right)\dot{\theta} - \lambda \right] \phi_n^0(\bar{r}) d\bar{r} \tag{3-154}$$

$$\tau_n^{mc} = \frac{1}{\pi} \int_0^1 2\pi\bar{b} \left[-\dot{\bar{h}} + \theta + \bar{b}\left(\frac{1}{2} - a\right)\dot{\theta} - \lambda \right] \phi_n^m(\bar{r}) d\bar{r} \cos(m\psi) \tag{3-155}$$

$$\tau_n^{ms} = \frac{1}{\pi} \int_0^1 2\pi\bar{b} \left[-\dot{\bar{h}} + \theta + \bar{b}\left(\frac{1}{2} - a\right)\dot{\theta} - \lambda \right] \phi_n^m(\bar{r}) d\bar{r} \sin(m\psi) \tag{3-156}$$

The fixed wing flutter problem is solved for one blade at a fixed azimuth. Therefore, the summation terms in the forcing functions disappear. The fixed azimuth (ψ) is selected as 90° which makes τ_n^{mc} equal to zero. After the implementation of the aerodynamic theory into the forcing functions, the governing Eqn. (3-149) is obtained in the following form,

$$\begin{Bmatrix} \{\alpha_n^m\}^* \\ \{\beta_n^m\}^* \end{Bmatrix} + \left[\begin{bmatrix} [\bar{L}^c]^{-1}[V_n^m] & 0 \\ 0 & [\bar{L}^s]^{-1}[V_n^m] \end{bmatrix} - [G] \right] \begin{Bmatrix} \{\alpha_n^m\} \\ \{\beta_n^m\} \end{Bmatrix}$$
$$- [E]\begin{Bmatrix} \dot{q}_h \\ \dot{q}_\theta \end{Bmatrix} - [F]\begin{Bmatrix} q_h \\ q_\theta \end{Bmatrix} = 0 \tag{3-157}$$

where the elements of the matrices $[E]$, $[F]$ and $[G]$ are defined in general form of harmonics and polynomial order as,

$$[E_{11}] = \int_0^1 -2\bar{b}\phi_n^m(\bar{r})W^T\cos(m\psi)d\bar{r} \tag{3-158}$$

$$[E_{12}] = \int_0^1 2\bar{b}^2\left(\frac{1}{2} - a\right)\phi_n^m(\bar{r})\Theta^T\cos(m\psi)d\bar{r} \tag{3-159}$$

$$[E_{21}] = \int_0^1 -2\bar{b}\phi_n^m(\bar{r})W^T\sin(m\psi)d\bar{r} \tag{3-160}$$

$$[E_{22}] = \int_0^1 2\bar{b}^2\left(\frac{1}{2} - a\right)\phi_n^m(\bar{r})\Theta^T\sin(m\psi)d\bar{r} \tag{3-161}$$

$$[F_{12}] = \int_0^1 2\bar{b}\phi_n^m(\bar{r})\Theta^T\cos(m\psi)d\bar{r} \tag{3-162}$$

$$[F_{22}] = \int_0^1 2\bar{b}\phi_n^m(\bar{r})\Theta^T\sin(m\psi)d\bar{r} \tag{3-163}$$

$$[F_{11}] = [F_{21}] = 0 \tag{3-164}$$

$$[G_{11}] = \int_0^1 -2\bar{b}\phi_n^m(\bar{r})\phi_j^r(\bar{r})\cos(r\psi)\cos(m\psi)\,d\bar{r} \tag{3-165}$$

$$[G_{12}] = \int_0^1 -2\bar{b}\phi_n^m(\bar{r})\phi_j^r(\bar{r})\sin(r\psi)\cos(m\psi)\,d\bar{r} \tag{3-166}$$

$$[G_{21}] = \int_0^1 -2\bar{b}\phi_n^m(\bar{r})\phi_j^r(\bar{r})\cos(r\psi)\sin(m\psi)\,d\bar{r} \tag{3-167}$$

$$[G_{22}] = \int_0^1 -2\bar{b}\phi_n^m(\bar{r})\phi_j^r(\bar{r})\sin(r\psi)\sin(m\psi)d\bar{r} \tag{3-168}$$

The coupling of the structural and the inflow equations require the definition of a general state vector such as,

$$q = \begin{Bmatrix} q_h \\ q_\theta \\ \dot{q}_h \\ \dot{q}_\theta \\ \alpha_n^m \\ \beta_n^m \end{Bmatrix} \tag{3-169}$$

The general motion of the state vector q is represented as,

$$q = \bar{q}e^{pt} \tag{3-170}$$

With the definition of the general state vector, the two systems can be coupled in one equation as given by,

$$\{\dot{q}\} + [A]\{q\} = 0 \tag{3-171}$$

where,

$$[A] = \begin{bmatrix} [0]_{2x2} & -[I]_{2x2} & [0]_{2xN_s} \\ [M]^{-1}[K] & [M]^{-1}[C] & [M]^{-1}[D] \\ -[F] & -[E] & \{[V][L]^{-1} - [G]\} \end{bmatrix} \tag{3-172}$$

With the definition given in Eqn. (3-170) and (3-171) can be re-expressed as,

$$\{[A] + p[I]\}\{q\} = 0 \tag{3-173}$$

where p is the root of the system. The determinant solution of the $\{[A] + p[I]\}$ gives the roots. The roots include inflow modes and the derivatives of the structural degrees of freedom also.

The determinant solution is repeated for a range of airspeed values and the results are observed in terms of ($\omega \ vs \ U$) and ($g \ vs \ U$) plots for the structural states especially. The point where the damping curve crosses zero line is accepted as the flutter point where the damping is zero.

CHAPTER 4

ROTARY WING FLUTTER ANALYSIS

In this section, equations of motion are derived for the rotary wing flutter analysis. First, derivation of the structural equations of motion is given for general forcing functions including the rotational effect. Then the solution methodologies are discussed based on unsteady aerodynamic theories of Loewy, Wagner, Pitt-Peters Inflow and Peters-He Inflow. All of the solution methodologies assume that the blade is at zero angle of attack.

4.1. Structural Formulation

Structural equations of motion are derived from Lagrange equations using Euler-Bernoulli beam theory. The equations apply for a beam having rigid flapping motion and cantilevered torsional degree of freedom. Three-dimensional representation of the beam is performed by the Rayleigh-Ritz method similar to the fixed wing equations. The shape functions of the Rayleigh-Ritz method are chosen as polynomials to the 10th degree to justify the convergence of structural equations. Convergence is justified by the comparison of eigenvalues of the analytical model with Dymore [35] model eigenvalue results.

The blade is fully articulated with no control system flexibility at the hinge point. Bending and pitching motions are assumed to be linear and warping of the beam is ignored. Since the flutter problem analyzed in this thesis is based on bending and pitching degrees of freedom, lead-lag motion of the blade is not considered.

The configuration of the structural element is shown in Figure 3.1. Kinetic energy dT for the length dr is given by [37],

$$dT = \frac{1}{2}m\dot{h}^2 dr + mx_{cg}\dot{h}\dot{\theta}dr + \frac{1}{2}I_\theta\dot{\theta}^2 dr - \frac{1}{2}I_\theta\Omega^2\theta^2 dr$$
$$- mx_{cg}\Omega^2 r\theta\frac{dh}{dr}dr - \frac{1}{2}\bar{T}\left(\frac{dh}{dr}\right)^2 dr \qquad (4\text{-}1)$$
$$- \frac{1}{2}k_m^2\bar{T}\left(\frac{d\theta}{dr}\right)^2 dr$$

where,

$$\bar{T} = m\Omega^2 \int_r^R r_1 dr_1 = \frac{m\Omega^2}{2}(R^2 - r^2) \qquad (4\text{-}2)$$

The term m is the mass per length, I_θ is the polar moment of inertia, k_m is the radius of gyration, Ω is the rotational speed of the blade and x_{cg} is the distance between the elastic axis and center of gravity point for the element dr.

The first three terms are the same as the fixed wing kinetic energy terms. The fourth term stands for the propeller moment torsional stiffening caused by the centrifugal force. The fifth term is related to the motion of the center of gravity when the elastic axis and the center of gravity of the beam section are not coincident. The last two terms are the flatwise stiffening terms as a result of the centrifugal force.

The potential energy formulation for an element dr is driven by strain energies and it is the same as the fixed wing.

$$dU = \frac{1}{2}EI\left(\frac{d^2h}{dr^2}\right)^2 dr + \frac{1}{2}GJ\left(\frac{d\theta}{dr}\right)^2 dr \qquad (4\text{-}3)$$

In Eqn. (4-3) EI is the flapwise bending stiffness per unit length and GJ is the torsional stiffness per unit length. The same Rayleigh-Ritz expansion given by Eqn. (3-6) is applied here for the rotating beam equation. The bending and pitching motions of the rotating beam equations are explicitly given as,

$$\begin{aligned}
q_h &= [q_{h_1} \quad q_{h_2} \quad q_{h_3} \quad q_{h_4} \quad q_{h_5} \quad q_{h_6} \quad q_{h_7} \quad q_{h_8} \quad q_{h_9} \quad q_{h_{10}}] \\
q_\theta &= [q_{\theta_1} \quad q_{\theta_2} \quad q_{\theta_3} \quad q_{\theta_4} \quad q_{\theta_5} \quad q_{\theta_6} \quad q_{\theta_7} \quad q_{\theta_8} \quad q_{\theta_9} \quad q_{\theta_{10}}]
\end{aligned} \qquad (4\text{-}4)$$

$$W = \begin{bmatrix} r \\ r^2 \\ r^3 \\ r^4 \\ r^5 \\ r^6 \\ r^7 \\ r^8 \\ r^9 \\ r^{10} \end{bmatrix}, \Theta = \begin{bmatrix} r \\ r^2 \\ r^3 \\ r^4 \\ r^5 \\ r^6 \\ r^7 \\ r^8 \\ r^9 \\ r^{10} \end{bmatrix} \tag{4-5}$$

With these definitions of the motions, the kinetic and potential energy equations can be rewritten as,

$$T = \int_0^R \left[\frac{1}{2} m W^2 \dot{q}_h^2 + m x_{cg} W \Theta \dot{q}_h \dot{q}_\theta + \frac{1}{2} I_\theta \Theta^2 \dot{q}_\theta^2 - \frac{1}{2} I_\theta \Omega^2 \Theta^2 q_\theta^2 \right.$$
$$- m x_{cg} \Omega^2 r \Theta \frac{dW}{dr} q_\theta q_h - \frac{1}{2} \bar{T} \left(\frac{dW}{dr} \right)^2 q_h^2 \tag{4-6}$$
$$\left. - \frac{1}{2} k_m^2 \bar{T} \left(\frac{d\Theta}{dr} \right)^2 q_\theta^2 \right] dr$$

$$U = \int_0^R \left[\frac{1}{2} EI \left(\frac{d^2 W}{dr^2} \right)^2 q_h^2 + \frac{1}{2} GJ \left(\frac{d\Theta}{dr} \right)^2 q_\theta^2 \right] dr \tag{4-7}$$

Derivation of the Lagrange's equation of motion is performed as described in Eqn. (3-3). The bending and pitching equations of motion are obtained as,

$$\int_0^R \left[m W^2 \ddot{q}_h + m x_{cg} W \Theta \ddot{q}_\theta + m x_{cg} \Omega^2 r \Theta \frac{dW}{dr} q_\theta \right.$$
$$\left. + \bar{T} \left(\frac{dW}{dr} \right)^2 q_h + EI \left(\frac{d^2 W}{dr^2} \right)^2 q_h \right] dr = L_T \tag{4-8}$$

$$\int_0^R \left[I_\theta \Theta^2 \ddot{q}_\theta + m x_{cg} W \Theta \ddot{q}_h + I_\theta \Omega^2 \Theta^2 q_\theta + m x_{cg} \Omega^2 r \Theta \frac{dW}{dr} q_h \right.$$
$$\left. + k_m^2 \bar{T} \left(\frac{d\Theta}{dr} \right)^2 q_\theta + GJ \left(\frac{d\Theta}{dr} \right)^2 q_\theta \right] dr = M_T \tag{4-9}$$

Equations (4-8) and (4-9) are the basis for the flutter analysis with different types of aerodynamic models. In the rotary wing flutter analysis, structural part of the equations is kept the same, while the aerodynamic content is changed.

4.2. Flutter Analysis Based on Loewy's Theory

Aerodynamic equations of Loewy's theory are given in section 2.3.2. It should be noted that the flutter analysis based on Loewy's theory is applicable only for the hover condition of the rotating blades. Forward flight dynamics is not considered in the derivations.

The lift and moment equations are the same as the Theodorsen based aerodynamic theory given in Eqns. (3-15) and (3-16). Loewy's theory also assumes simple harmonic motion for the equations. The only difference with the Theodorsen theory comes from the definition of the lift deficiency function $C(k)$ as explained in Eqns. (2-9) and (2-10).

The flutter solution is performed with the modified k method. Modified k method is explained in the Introduction part. Due to the variation of airspeed at each radial station of the rotating blade which is calculated as $U = \Omega r$, the reduced frequency as $k = \frac{b\omega}{U}$ is not constant along the span of the blade.

The lift and moment equations can be simplified as the equations given by Eqns. (3-19) and (3-20) with the assumption of simple harmonic motion. Substituting Eqns. (3-19) and (3-20) into Eqns. (4-8) and (4-9) results in the form given by Eqn. (4-10).

$$-\omega^2[M]\begin{Bmatrix}\bar{q}_h\\\bar{q}_\theta\end{Bmatrix} + (1+ig)[K]\begin{Bmatrix}\bar{q}_h\\\bar{q}_\theta\end{Bmatrix} - \pi\rho b^3\omega^2[A]\begin{Bmatrix}\bar{q}_h\\\bar{q}_\theta\end{Bmatrix} = \begin{Bmatrix}0\\0\end{Bmatrix} \qquad (4\text{-}10)$$

where elements of the mass, stiffness and the aerodynamic matrices are defined as,

$$[M_{11}] = \int_0^R mWW^T dr \qquad (4\text{-}11)$$

$$[M_{12}] = \int_0^R mx_{cg}\Theta W^T dr \qquad (4\text{-}12)$$

$$[M_{21}] = \int_0^R mx_{cg}W\Theta^T dr \qquad (4\text{-}13)$$

$$[M_{22}] = \int_0^R I_\theta\Theta\Theta^T dr \qquad (4\text{-}14)$$

$$[K_{11}] = \int_0^R EI \left(\frac{d^2W}{dr^2}\right)\left(\frac{d^2W^T}{dr^2}\right) dr$$
$$- \frac{m\Omega^2}{2} \int_0^R (R^2 - r^2) \left(\frac{dW}{dr}\right)\left(\frac{dW^T}{dr}\right) dr \qquad (4\text{-}15)$$

$$[K_{12}] = \int_0^R \left(mx_{cg}\Omega^2 r \frac{dW}{dr}\right) \Theta^T dr \qquad (4\text{-}16)$$

$$[K_{12}] = \int_0^R \left(mx_{cg}\Omega^2 r \frac{dW}{dr}\right) \Theta^T dr \qquad (4\text{-}17)$$

$$[K_{22}] \int_0^R \left(GJ \left(\frac{d\Theta}{dr}\right)\left(\frac{d\Theta^T}{dr}\right) + \frac{m\Omega^2 k_m^2}{2} (R^2 - r^2) \left(\frac{d\Theta}{dr}\right)\left(\frac{d\Theta^T}{dr}\right) \right.$$
$$\left. + I_\theta \Omega^2 \Theta\Theta^T \right) dr \qquad (4\text{-}18)$$

$$[A_{11}] = \int_0^R \left(\frac{1}{b} - \frac{2iC(k)}{kb}\right) WW^T dr \qquad (4\text{-}19)$$

$$[A_{12}] = \int_0^R \left(\frac{i}{k} + a + \frac{2C(k)}{k^2} + \frac{2iC(k)}{k}\left(\frac{1}{2} - a\right)\right) \Theta W^T dr \qquad (4\text{-}20)$$

$$[A_{21}] = \int_0^R \left(a - \frac{2iC(k)}{k}\left(a + \frac{1}{2}\right)\right) W\Theta^T dr \qquad (4\text{-}21)$$

$$[A_{22}] = \int_0^R \left(b\left(\frac{1}{8} + a^2\right) - \frac{ib}{k}\left(\frac{1}{2} - a\right) + \frac{2C(k)b}{k^2}\left(a + \frac{1}{2}\right) \right.$$
$$\left. + \frac{2ibC(k)}{k}\left(\frac{1}{4} - a^2\right)\right) \Theta\Theta^T dr \qquad (4\text{-}22)$$

The shape functions W and Θ are given in Eqn. (4-5). In the elements of aerodynamic matrix A, lift deficiency function $C(k)$ is used as Loewy's derivation given in Eqn. (2-9). Dividing Eqn. (4-10) by $" - \omega^2"$ one gets Eqn. (4-23),

$$\left[[M] + \pi\rho b^3 [A] - \left(\frac{1 + ig}{\omega^2}\right) [K] \right] \begin{Bmatrix} \bar{q}_h \\ \bar{q}_\theta \end{Bmatrix} = \begin{Bmatrix} 0 \\ 0 \end{Bmatrix} \qquad (4\text{-}23)$$

For a non-trivial solution of the algebraic system of equations given by Eqn. (4-23), the determinant of the terms in brackets should be equal to zero. If we call the eigenvalue $\lambda = \frac{1+ig}{\omega^2}$, solution of the determinant given by Eqn. (4-24) gives the eigenvalue λ for a chosen reduced frequency, k.

$$|[M] + \pi\rho b^3[A] - \lambda[K]| = 0 \qquad (4\text{-}24)$$

The frequency and damping information is obtained from the roots utilizing the relations given by Eqn. (4-25).

$$\omega = \frac{1}{\sqrt{Re(\lambda)}}, \qquad g = \frac{Im(\lambda)}{Re(\lambda)} \qquad (4\text{-}25)$$

For the hover condition, the analysis is performed for a varying range of rotational speeds of the blade. The results are observed in terms of (ω vs Ω) and (g vs Ω) plots. The point where the damping curve crosses zero line is accepted as the flutter point where the damping is zero.

4.3. Flutter Analysis Based on Wagner's Theory

The detailed derivation of unsteady aerodynamics based on approximate Wagner function is explained in section 2.3.3. In this approach the main assumption is the airfoil being at rest at the beginning of the analysis ($w_{0.75c}(0) = 0$). The lifting functions obtained in section 3.3 and aerodynamic lag state equations derived with the use of the Leibniz rule are given by,

$$
\begin{aligned}
L_h = {}& \pi\rho b^2\left(-\ddot{h} + U\dot{\theta} - ba\ddot{\theta}\right) \\
& + C_{L\phi}\rho Ub\left\{-\dot{h} + U\theta + b\left(\frac{1}{2}\left(\frac{C_{L\phi}}{\pi} - 1\right) - a\right)\dot{\theta}\right. \\
& \left. - C_1 B_1(t) - C_2 B_2(t)\right\}
\end{aligned}
\qquad (4\text{-}26)
$$

$$M_{1/4c} = -\pi\rho b^3\left[-\frac{1}{2}\ddot{h} + U\dot{\theta} + b\left(\frac{1}{8} - \frac{a}{2}\right)\ddot{\theta}\right] \qquad (4\text{-}27)$$

$$\dot{B}_1(t) + \varepsilon_1\frac{U}{b}B_1(t) = \dot{w}_{0.75c}(t) \qquad (4\text{-}28)$$

$$\dot{B}_2(t) + \varepsilon_2\frac{U}{b}B_2(t) = \dot{w}_{0.75c}(t) \qquad (4\text{-}29)$$

The difference of the rotating blade lifting functions and fixed blade lifting functions is in terms of the velocity, U. The velocity is constant for each spanwise station of the fixed blade, while for the rotating blade, the velocity varies along the span due to the

rotational velocity of the blade. This variation is effective in flutter solutions. Therefore, the velocity term in the rotary wing lifting functions is applied as,

$$U = \Omega r + U_\infty \tag{4-30}$$

where U_∞ is the free stream forward speed of the blade. It should be noted that Eqn. (4-30) changes for each azimuthal position of the blade. In the rotating blade flutter analysis of this thesis, flutter of the rotating blade at the most critical instant of the rotation is analyzed, which is the 90° azimuth of the rotor. At this instant position, the blade experiences maximum velocity compared to other azimuthal positions of the rotor. This is schematically shown in Figure 4.1.
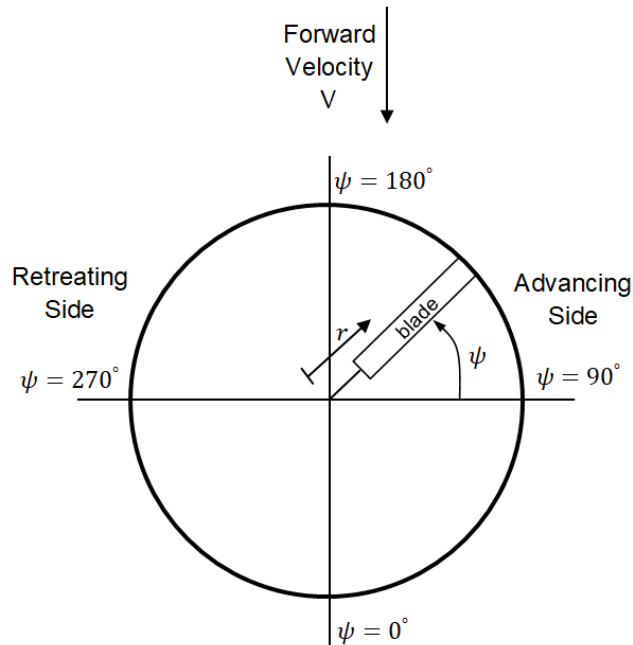

Figure 4.1. Rotating Blade Azimuth Definition

Combination of the structural, aerodynamic and lag state equations results in Eqn. (4-31).

$$[M]\{\ddot{q}_s\} + [C]\{\dot{q}\} + [K]\{q\} = 0 \tag{4-31}$$

The unknown states of in Eqn. (4-31) are defined by Eqn. (4-32).

61

$$q = \begin{Bmatrix} h \\ \theta \\ B_1 \\ B_2 \end{Bmatrix} = \begin{Bmatrix} q_s \\ q_a \end{Bmatrix} \quad where \; q_s = \begin{Bmatrix} h \\ \theta \end{Bmatrix} \; and \; q_a = \begin{Bmatrix} B_1 \\ B_2 \end{Bmatrix} \tag{4-32}$$

The expansion of the aerodynamic lag states can be written in a generalized form as,

$$B_1(r,t) = q_{B1}\beta_1, \qquad B_2(r,t) = q_{B2}\beta_2 \tag{4-33}$$

In Eqn. (4-33) q_{B1} and q_{B2} are time dependent state vectors of the aerodynamic lag state functions. The shape functions of the lag states are defined in Eqn. (4-34) in the similar form of the bending and pitching motion shape functions.

$$\beta_1 = \beta_2 = [r \quad r^2 \quad r^3 \quad r^4 \quad r^5 \quad r^6 \quad r^7 \quad r^8 \quad r^9 \quad r^{10}]^T \tag{4-34}$$

The elements of the mass, damping and stiffness matrices of the coupled system are defined as,

$$[M_{11}] = \int_0^R (m + \pi\rho b^2) W W^T dr \tag{4-35}$$

$$[M_{12}] = \int_0^R (m x_{cg} + \pi\rho a b^3) \Theta W^T dr \tag{4-36}$$

$$[M_{21}] = \int_0^R (m x_{cg} + \pi\rho a b^3) W \Theta^T dr \tag{4-37}$$

$$[M_{22}] = \int_0^R \left(I_\theta + \pi\rho b^4 \left(\frac{1}{8} + a^2 \right) \right) \Theta \Theta^T dr \tag{4-38}$$

$$[M_{31}] = \int_0^R W \beta_1^T dr \tag{4-39}$$

$$[M_{32}] = \int_0^R -b \left(\frac{1}{2} \left(\frac{C_{L\phi}}{\pi} - 1 \right) - a \right) \Theta \beta_1^T dr \tag{4-40}$$

$$[M_{41}] = \int_0^R W \beta_2^T dr \tag{4-41}$$

$$[M_{42}] = \int_0^R -b \left(\frac{1}{2} \left(\frac{C_{L\phi}}{\pi} - 1 \right) - a \right) \Theta \beta_2^T dr \tag{4-42}$$

$$[C_{11}] = \int_0^R C_{L\phi} \rho U b W W^T dr \tag{4-43}$$

$$[C_{12}] = \int_0^R \left(-\pi\rho U b^2 - C_{L\phi} \rho U b^2 \left(\frac{1}{2} \left(\frac{C_{L\phi}}{\pi} - 1 \right) - a \right) \right) \Theta W^T dr \tag{4-44}$$

$$[C_{21}] = \int_0^R C_{L\phi}\rho U b^2 \left(\frac{1}{2} + a\right) W \Theta^T dr \tag{4-45}$$

$$[C_{22}] = \int_0^R \left(\pi\rho U b^3 \left(\frac{1}{2}\left(\frac{C_{L\phi}}{\pi} - 1\right) - a\right) \right.$$
$$\left. - C_{L\phi}\rho U b^3 \left(\frac{1}{2}\left(\frac{C_{L\phi}}{\pi} - 1\right) - a\right)\left(\frac{1}{2} + a\right) \right) \Theta \Theta^T dr \tag{4-46}$$

$$[C_{32}] = \int_0^R -U\Theta \beta_1^T dr \tag{4-47}$$

$$[C_{33}] = \int_0^R \beta_1 \beta_1^T dr \tag{4-48}$$

$$[C_{42}] = \int_0^R -U\Theta \beta_2^T dr \tag{4-49}$$

$$[C_{44}] = \int_0^R \beta_2 \beta_2^T dr \tag{4-50}$$

$$[C_{13}] = [C_{14}] = [C_{23}] = [C_{24}] = [C_{31}] = [C_{34}] = [C_{41}] = [C_{43}] = 0 \tag{4-51}$$

$$[K_{11}] = \int_0^R EI \left(\frac{d^2W}{dr^2}\right)\left(\frac{d^2W^T}{dr^2}\right) dr$$
$$- \frac{m\Omega^2}{2} \int_0^R (R^2 - r^2)\left(\frac{dW}{dr}\right)\left(\frac{dW^T}{dr}\right) dr \tag{4-52}$$

$$[K_{12}] = \int_0^R \left(mx_{cg}\Omega^2 r \frac{dW}{dr}\Theta^T - C_{L\phi}\rho U^2 b\Theta W^T \right) dr \tag{4-53}$$

$$[K_{13}] = \int_0^R C_{L\phi}\rho U b C_1 \beta_1 W^T dr \tag{4-54}$$

$$[K_{14}] = \int_0^R C_{L\phi}\rho U b C_2 \beta_2 W^T dr \tag{4-55}$$

$$[K_{21}] = \int_0^R \left(mx_{cg}\Omega^2 r \frac{dW}{dr} \right)\Theta^T dr \tag{4-56}$$

$$[K_{22}] = \int_0^R \left(GJ\left(\frac{d\Theta}{dr}\right)\left(\frac{d\Theta^T}{dr}\right) + \frac{m\Omega^2 k_m^2}{2}(R^2 - r^2)\left(\frac{d\Theta}{dr}\right)\left(\frac{d\Theta^T}{dr}\right) \right.$$
$$\left. + I_\theta\Omega^2\Theta\Theta^T - C_{L\phi}\rho U^2 b^2 \left(a + \frac{1}{2}\right)\Theta\Theta^T \right) dr \tag{4-57}$$

$$[K_{23}] = \int_0^R C_{L\phi}\rho U b^2 \left(a + \frac{1}{2}\right) C_1 \beta_1 \Theta^T dr \tag{4-58}$$

$$[K_{24}] = \int_0^R C_{L\phi}\rho U b^2 \left(a + \frac{1}{2}\right) C_2 \beta_2 \Theta^T dr \tag{4-59}$$

$$[K_{33}] = \int_0^R \varepsilon_1 \frac{U}{b} \beta_1 \beta_1^T dr \tag{4-60}$$

$$[K_{44}] = \int_0^R \varepsilon_2 \frac{U}{b} \beta_2 \beta_2^T \, dr \qquad (4\text{-}61)$$

$$[K_{31}] = [K_{32}] = [K_{34}] = [K_{41}] = [K_{42}] = [K_{43}] = 0 \qquad (4\text{-}62)$$

The shape functions W and Θ are given in Eqn. (4-5). Similar to the fixed wing case, the general governing equation can be expressed in state space form as shown in Eqn. (4-63).

$$\begin{bmatrix} [C]_{4x4} & [M]_{4x2} \\ [I]_{2x4} & [0]_{2x2} \end{bmatrix} \begin{Bmatrix} \{\dot{q}\}_{4x1} \\ \{\ddot{q}_s\}_{2x1} \end{Bmatrix} + \begin{bmatrix} [K]_{4x4} & [0]_{4x2} \\ [0]_{2x4} & -[I]_{2x2} \end{bmatrix} \begin{Bmatrix} \{q\}_{4x1} \\ \{\dot{q}_s\}_{2x1} \end{Bmatrix} = 0 \qquad (4\text{-}63)$$

Equation (4-63) can be written in a simpler format as,

$$[A]\{\dot{x}\} + [B]\{x\} = 0 \qquad (4\text{-}64)$$

where,

$$[A] = \begin{bmatrix} [C]_{4x4} & [M]_{4x2} \\ [I]_{2x4} & [0]_{2x2} \end{bmatrix}, [B] = \begin{bmatrix} [K]_{4x4} & [0]_{4x2} \\ [0]_{2x4} & -[I]_{2x2} \end{bmatrix} \qquad (4\text{-}65)$$

The final solution is obtained as follows,

$$\{\dot{x}\} = -[A]^{-1}[B]\{x\} \qquad (4\text{-}66)$$
$$\{-[A]^{-1}[B] - \lambda[I]\}\{x_0\} = 0 \qquad (4\text{-}67)$$

where,

$$\{x\} = \{x_0\}e^{\lambda t} \qquad (4\text{-}68)$$

The determinant of the Eqn. (4-67) in the brackets gives the roots of the system. This procedure is performed for varying airspeeds for forward flight analysis and for varying rotational speeds for hover analysis. The results are observed in terms of frequency and damping plots for varying speed parameter for each of the roots. The point where the damping curve crosses zero line is accepted as the flutter point where the damping is zero.

4.4. Flutter Analysis Based on Pitt-Peters Inflow Theory

Rotating blade flutter analysis based on Pitt-Peters induced flow is very similar to the fixed wing analysis. The main difference is in the structural equations. As explained in section 4.1, structural equations of the rotary wings include extra terms related to the rotational velocity of the blade. There are also slight differences in the definition of the induced flow equations as a result of the rotational velocity.

Pitt-Peters inflow theory equations are derived for the normalized induced flow and lifting functions. For that reason, the structural equations of motion should be normalized in order to be coupled with the induced flow theory.

With the distance normalized as $\bar{r} = r/R$ and the time normalized as $\bar{t} = \Omega t$, the bending Eqn. (4-8) is normalized by $m\Omega^2 R$ to obtain,

$$
\int_0^1 WW^T \ddot{q}_h d\bar{r} + \int_0^1 \bar{x}_{cg} \Theta W^T \ddot{q}_\theta d\bar{r} - \int_0^1 \bar{x}_{cg} \left(\bar{r} \frac{dW}{d\bar{r}} \right) \Theta^T q_\theta d\bar{r}
$$
$$
+ \int_0^1 \frac{EI}{m\Omega^2 R^4} \left(\frac{d^2 W}{d\bar{r}^2} \right) \left(\frac{d^2 W^T}{d\bar{r}^2} \right) q_h d\bar{r} \qquad (4\text{-}69)
$$
$$
- \int_0^1 \frac{1}{2} (1 - \bar{r}^2) \frac{dW}{d\bar{r}} \frac{dW^T}{d\bar{r}} q_h d\bar{r} = \int_0^1 \bar{L}_h \left(\frac{\rho R^2}{m} \right) W d\bar{r}
$$

Similarly, the pitching equation is normalized by $m\Omega^2 R^2$ to obtain,

$$
\int_0^1 \bar{x}_{cg} W \Theta^T \ddot{q}_h d\bar{r} + \int_0^1 \frac{I_\theta}{mR^2} \Theta \Theta^T \ddot{q}_\theta d\bar{r} + \int_0^1 \frac{I_\theta}{mR^2} \Theta \Theta^T q_\theta d\bar{r}
$$
$$
+ \int_0^1 \bar{x}_{cg} \left(\bar{r} \frac{dW}{d\bar{r}} \right) \Theta^T q_h d\bar{r}
$$
$$
+ \int_0^1 \frac{GJ}{m\Omega^2 R^4} \left(\frac{d\Theta}{d\bar{r}} \right) \left(\frac{d\Theta^T}{d\bar{r}} \right) q_\theta d\bar{r} \qquad (4\text{-}70)
$$
$$
- \int_0^1 \frac{k_m^2}{2} (1 - \bar{r}^2) \frac{d\Theta}{d\bar{r}} \frac{d\Theta^T}{d\bar{r}} q_\theta d\bar{r} = \int_0^1 \left[\bar{M}_{1/4c} \right.
$$
$$
\left. + \bar{L}_h \left(\frac{1}{2} + a \right) b \right] \left(\frac{\rho R^2}{m} \right) \Theta d\bar{r}
$$

In the normalized structural equations implementation of the normalized lifting functions is required. As mentioned in the fixed wing analysis, the circulatory part of

the lifting functions should be used for the flutter analysis modified by the inflow term λ. The general form of the lift and moment expressions are given by,

$$L_h = 2\pi\rho U b \left[\dot{h} + U\theta + b\left(\frac{1}{2} - a\right)\dot{\theta} - \lambda\right] \qquad (4\text{-}71)$$

$$M_{1/4c} = -\pi\rho b^3 \left[\frac{1}{2}\ddot{h} + U\dot{\theta} + b\left(\frac{1}{8} - \frac{a}{2}\right)\ddot{\theta}\right] \qquad (4\text{-}72)$$

The lift term L_h is normalized by $\rho\Omega^2 R^3$ to yield,

$$\bar{L}_h = 2\pi\bar{b}\left[\frac{U}{\Omega R}\dot{\bar{h}} + \frac{U^2}{(\Omega R)^2}\theta + \bar{b}\left(\frac{1}{2} - a\right)\frac{U}{\Omega R}\dot{\theta} - \frac{U}{\Omega R}\lambda\right] \qquad (4\text{-}73)$$

The moment term M_θ is normalized by $\rho\Omega^2 R^4$ to obtain,

$$\bar{M}_\theta = -\pi\bar{b}^3\left[\frac{1}{2}\ddot{\bar{h}} + \frac{U}{\Omega R}\dot{\theta} + \bar{b}\left(\frac{1}{8} - \frac{a}{2}\right)\ddot{\theta}\right] \qquad (4\text{-}74)$$

where,

$$U = \Omega\bar{r}R + U_\infty \qquad (4\text{-}75)$$

The next step is the coupling of the induced flow and the structural equations. After the normalization of the structural and the lift and moment equations, the structural set of the solution is obtained as given by Eqn. (4-76). As before, induced flow consists of three states; λ_0, λ_s and λ_c.

$$[M]\begin{Bmatrix}\ddot{q}_h \\ \ddot{q}_\theta\end{Bmatrix} + [C]\begin{Bmatrix}\dot{q}_h \\ \dot{q}_\theta\end{Bmatrix} + [K]\begin{Bmatrix}q_h \\ q_\theta\end{Bmatrix} + [D]\begin{Bmatrix}\lambda_0 \\ \lambda_s \\ \lambda_c\end{Bmatrix} = 0 \qquad (4\text{-}76)$$

In Eqn. (4-76), elements of the mass, damping, stiffness and the inflow coefficient matrices are defined in Eqns. (4-77)-(4-94). Note that the bending motion in lifting equations is multiplied with (-1) to be consistent with the axis system of the derived structural equations.

$$[M_{11}] = \int_0^1 WW^T d\bar{r} \qquad (4\text{-}77)$$

$$[M_{12}] = \int_0^1 \bar{x}_{cg} \Theta W^T d\bar{r} \tag{4-78}$$

$$[M_{21}] = \int_0^1 \left(\bar{x}_{cg} - \frac{1}{2} \pi \bar{b}^3 \left(\frac{\rho R^2}{m} \right) \right) W \Theta^T d\bar{r} \tag{4-79}$$

$$[M_{22}] = \int_0^1 \left(\frac{I_\theta}{mR^2} + \pi \bar{b}^4 \left(\frac{1}{8} - \frac{a}{2} \right) \left(\frac{\rho R^2}{m} \right) \right) \Theta \Theta^T d\bar{r} \tag{4-80}$$

$$[C_{11}] = \int_0^1 2\pi \bar{b} \frac{U}{\Omega R} \left(\frac{\rho R^2}{m} \right) W W^T d\bar{r} \tag{4-81}$$

$$[C_{12}] = \int_0^1 -2\pi \bar{b}^2 \left(\frac{1}{2} - a \right) \frac{U}{\Omega R} \left(\frac{\rho R^2}{m} \right) \Theta W^T d\bar{r} \tag{4-82}$$

$$[C_{21}] = \int_0^1 2\pi \bar{b}^2 \left(\frac{1}{2} + a \right) \frac{U}{\Omega R} \left(\frac{\rho R^2}{m} \right) W \Theta^T d\bar{r} \tag{4-83}$$

$$[C_{22}] = \int_0^1 \pi \bar{b}^3 \left(\frac{1}{2} + 2a^2 \right) \frac{U}{\Omega R} \left(\frac{\rho R^2}{m} \right) \Theta \Theta^T d\bar{r} \tag{4-84}$$

$$[K_{11}] = \int_0^1 \frac{EI}{m\Omega^2 R^4} \left(\frac{d^2 W}{d\bar{r}^2} \right) \left(\frac{d^2 W^T}{d\bar{r}^2} \right) d\bar{r}$$
$$- \int_0^1 \frac{1}{2} (1 - \bar{r}^2) \frac{dW}{d\bar{r}} \frac{dW^T}{d\bar{r}} d\bar{r} \tag{4-85}$$

$$[K_{12}] = \int_0^1 -2\pi \bar{b} \frac{U^2}{(\Omega R)^2} \left(\frac{\rho R^2}{m} \right) \Theta W^T d\bar{r} - \int_0^1 \bar{x}_{cg} \left(\bar{r} \frac{dW}{d\bar{r}} \right) \Theta^T d\bar{r} \tag{4-86}$$

$$[K_{21}] = \int_0^1 \bar{x}_{cg} \bar{r} \frac{dW}{d\bar{r}} \Theta^T d\bar{r} \tag{4-87}$$

$$[K_{22}] = \int_0^1 \left(\frac{GJ}{m\Omega^2 R^4} \left(\frac{d\Theta}{d\bar{r}} \right) \left(\frac{d\Theta^T}{d\bar{r}} \right) - \frac{\bar{k}_m^2}{2} (1 - \bar{r}^2) \frac{d\Theta}{d\bar{r}} \frac{d\Theta^T}{d\bar{r}} \right.$$
$$+ \frac{I_\theta}{mR^2} \Theta \Theta^T \tag{4-88}$$
$$\left. - 2\pi \bar{b}^2 \left(\frac{1}{2} + a \right) \frac{U^2}{(\Omega R)^2} \left(\frac{\rho R^2}{m} \right) \Theta \Theta^T \right) d\bar{r}$$

$$[D_{11}] = \int_0^1 2\pi \bar{b} \frac{U}{\Omega R} \left(\frac{\rho R^2}{m} \right) W d\bar{r} \tag{4-89}$$

$$[D_{12}] = \int_0^1 2\pi \bar{b} \frac{U}{\Omega R} \left(\frac{\rho R^2}{m} \right) \bar{r} \sin(\psi) W d\bar{r} \tag{4-90}$$

$$[D_{13}] = \int_0^1 2\pi \bar{b} \frac{U}{\Omega R} \left(\frac{\rho R^2}{m} \right) \bar{r} \cos(\psi) W d\bar{r} \tag{4-91}$$

$$[D_{21}] = \int_0^1 2\pi \bar{b}^2 \left(\frac{1}{2} + a \right) \frac{U}{\Omega R} \left(\frac{\rho R^2}{m} \right) \Theta d\bar{r} \tag{4-92}$$

$$[D_{22}] = \int_0^1 2\pi\bar{b}^2 \left(\frac{1}{2} + a\right) \frac{U}{\Omega R} \left(\frac{\rho R^2}{m}\right) \bar{r}\sin(\psi)\,\Theta\,d\bar{r} \tag{4-93}$$

$$[D_{23}] = \int_0^1 2\pi\bar{b}^2 \left(\frac{1}{2} + a\right) \frac{U}{\Omega R} \left(\frac{\rho R^2}{m}\right) \bar{r}\cos(\psi)\,\Theta\,d\bar{r} \tag{4-94}$$

The shape functions W and Θ are given in Eqn. (4-5). The second equation for the flutter analysis is the induced flow equation given in the form of,

$$[\widetilde{M}]\begin{Bmatrix} \dot{\lambda}_0 \\ \dot{\lambda}_s \\ \dot{\lambda}_c \end{Bmatrix} + [V][L]^{-1}\begin{Bmatrix} \lambda_0 \\ \lambda_s \\ \lambda_c \end{Bmatrix} = \begin{Bmatrix} C_T \\ -C_L \\ -C_M \end{Bmatrix} \tag{4-95}$$

where the matrices $[\widetilde{M}]$, $[L]$ and $[V]$ are given in section 2.3.4.1. The induced flow is coupled with the structural equations via the aerodynamic coefficients C_T, C_L and C_M. For the rotary wing equations, these terms are derived from Eqns. (2-35)-(2-37) using the lift definition in Eqn. (4-73).

$$
\begin{aligned}
C_T = {}& \frac{1}{\rho\pi\Omega^2 R^4} \int_0^1 2\pi\bar{b} \left[-\frac{U}{\Omega R}\dot{\bar{h}} + \frac{U^2}{(\Omega R)^2}\theta \right. \\
& \left. + \bar{b}\left(\frac{1}{2} - a\right)\frac{U}{\Omega R}\dot{\theta} - \frac{U}{\Omega R}\lambda \right] d\bar{r}
\end{aligned}
\tag{4-96}
$$

$$
\begin{aligned}
C_L = {}& -\frac{1}{\rho\pi\Omega^2 R^5} \int_0^1 2\pi\bar{b} \left[-\frac{U}{\Omega R}\dot{\bar{h}} + \frac{U^2}{(\Omega R)^2}\theta \right. \\
& \left. + \bar{b}\left(\frac{1}{2} - a\right)\frac{U}{\Omega R}\dot{\theta} - \frac{U}{\Omega R}\lambda \right] \bar{r}\sin\psi\,d\bar{r}
\end{aligned}
\tag{4-97}
$$

$$
\begin{aligned}
C_M = {}& -\frac{1}{\rho\pi\Omega^2 R^5} \int_0^1 2\pi\bar{b} \left[-\frac{U}{\Omega R}\dot{\bar{h}} + \frac{U^2}{(\Omega R)^2}\theta \right. \\
& \left. + \bar{b}\left(\frac{1}{2} - a\right)\frac{U}{\Omega R}\dot{\theta} - \frac{U}{\Omega R}\lambda \right] \bar{r}\cos\psi\,d\bar{r}
\end{aligned}
\tag{4-98}
$$

The disk integration is eliminated for the rotating blade also because the rotating blade solution is performed for a single blade for the 90° azimuth. For the normalized lift terms in aerodynamic coefficients C_T, C_L and C_M, the circulatory lift definition given by Eqn. (4-73) is used.

With the substitution of the aerodynamic coefficients, Eqn. (4-95) is re-written as Eqn. (4-99).

$$[\tilde{M}]\begin{Bmatrix}\dot{\lambda}_0\\\dot{\lambda}_s\\\dot{\lambda}_c\end{Bmatrix} + [[V][L]^{-1} - [G]]\begin{Bmatrix}\lambda_0\\\lambda_s\\\lambda_c\end{Bmatrix} - \frac{1}{\rho\pi R^3 U^2}[E]\begin{Bmatrix}\dot{q}_h\\\dot{q}_\theta\end{Bmatrix}$$
$$- \frac{1}{\rho\pi R^3 U^2}[F]\begin{Bmatrix}q_h\\q_\theta\end{Bmatrix} = 0 \tag{4-99}$$

In Eqn. (4-99) the matrices $[E]$, $[F]$ and $[G]$ involve the terms in the aerodynamic coefficients given by Eqns. (4-96)-(4-98). The elements of the matrices $[E]$, $[F]$ and $[G]$ are given by Eqns. (4-100)-(4-118).

$$[E_{11}] = \int_0^1 -2\pi\bar{b}\frac{U}{\Omega R}W^T d\bar{r} \tag{4-100}$$

$$[E_{12}] = \int_0^1 2\pi\bar{b}^2\frac{U}{\Omega R}\left(\frac{1}{2} - a\right)\Theta^T d\bar{r} \tag{4-101}$$

$$[E_{21}] = \int_0^1 -2\pi\bar{b}\bar{r}\frac{U}{\Omega R}\sin(\psi)W^T d\bar{r} \tag{4-102}$$

$$[E_{22}] = \int_0^1 2\pi\bar{b}^2\frac{U}{\Omega R}\left(\frac{1}{2} - a\right)\bar{r}\sin(\psi)\Theta^T d\bar{r} \tag{4-103}$$

$$[E_{31}] = \int_0^1 -2\pi\bar{b}\bar{r}\frac{U}{\Omega R}\cos(\psi)W^T d\bar{r} \tag{4-104}$$

$$[E_{32}] = \int_0^1 2\pi\bar{b}^2\frac{U}{\Omega R}\left(\frac{1}{2} - a\right)\bar{r}\cos(\psi)\Theta^T d\bar{r} \tag{4-105}$$

$$[F_{12}] = \int_0^1 2\pi\bar{b}\frac{U^2}{(\Omega R)^2}\Theta^T d\bar{r} \tag{4-106}$$

$$[F_{22}] = \int_0^1 2\pi\bar{b}\bar{r}\frac{U^2}{(\Omega R)^2}\sin(\psi)\Theta^T d\bar{r} \tag{4-107}$$

$$[F_{32}] = \int_0^1 2\pi\bar{b}\bar{r}\frac{U^2}{(\Omega R)^2}\cos(\psi)\Theta^T d\bar{r} \tag{4-108}$$

$$[F_{11}] = [F_{21}] = [F_{31}] = 0 \tag{4-109}$$

$$[G_{11}] = \int_0^1 -2\pi\bar{b}\frac{U}{\Omega R}d\bar{r} \tag{4-110}$$

$$[G_{12}] = \int_0^1 -2\pi\bar{b}\bar{r}\frac{U}{\Omega R}\sin(\psi)d\bar{r} \tag{4-111}$$

$$[G_{13}] = \int_0^1 -2\pi\bar{b}\bar{r}\frac{U}{\Omega R}\cos(\psi)d\bar{r} \tag{4-112}$$

$$[G_{21}] = \int_0^1 -2\pi\bar{b}\bar{r}\frac{U}{\Omega R}\sin(\psi)d\bar{r} \tag{4-113}$$

$$[G_{22}] = \int_0^1 -2\pi\bar{b}\bar{r}^2\frac{U}{\Omega R}(\sin(\psi))^2 d\bar{r} \tag{4-114}$$

$$[G_{23}] = \int_0^1 -2\pi\bar{b}\bar{r}^2\frac{U}{\Omega R}(\cos(\psi))^2 d\bar{r} \tag{4-115}$$

$$[G_{31}] = \int_0^1 -2\pi\bar{b}\bar{r}\frac{U}{\Omega R}\cos(\psi)d\bar{r} \tag{4-116}$$

$$[G_{32}] = \int_0^1 -2\pi\bar{b}\bar{r}^2\frac{U}{\Omega R}\cos(\psi)\sin(\psi)\,d\bar{r} \tag{4-117}$$

$$[G_{33}] = \int_0^1 -2\pi\bar{b}\bar{r}^2\frac{U}{\Omega R}\cos(\psi)\cos(\psi)\,d\bar{r} \tag{4-118}$$

The coupling of structural and inflow equations requires the definition of a general state vector such as,

$$q = \begin{Bmatrix} q_h \\ q_\theta \\ \dot{q}_h \\ \dot{q}_\theta \\ \lambda \end{Bmatrix} \tag{4-119}$$

The general motion of the state vector q is represented as,

$$q = \bar{q}e^{pt} \tag{4-120}$$

With the definition of the general state vector, the two systems can be coupled in one equation as given by,

$$\{\dot{q}\} + [A]\{q\} = 0 \tag{4-121}$$

where,

$$
[A] = \begin{bmatrix} [0]_{2x2} & -[I]_{2x2} & [0]_{2x3} \\ [M]_{2x2}^{-1}[K]_{2x2} & [M]_{2x2}^{-1}[C]_{2x2} & [M]_{2x2}^{-1}[D]_{2x3} \\ -[\widetilde{M}]_{3x3}^{-1}[F]_{3x2} & -[\widetilde{M}]_{3x3}^{-1}[E]_{3x2} & [\widetilde{M}]_{3x3}^{-1}\{[V]_{3x3}[L]_{3x3}^{-1} - [G]_{3x3}\} \end{bmatrix} \tag{4-122}
$$

Substituting Eqn. (4-120) into Eqn. (4-121) results in Eqn. (4-123).

$$\{[A] + p[I]\}\{q\} = 0 \tag{4-123}$$

Here p is the roots of the system. The determinant solution of the $\{[A] + p[I]\}$ results in 7 roots. Two of the roots are structural states, two of the roots are derivatives of the structural states and three of the roots are the inflow states λ_0, λ_s and λ_c. This procedure is performed for varying airspeeds for forward flight analysis and for varying rotational speeds for hover analysis. The results are observed in terms of frequency and damping plots for varying speed parameter for each of the roots. The point where the damping curve crosses zero line is accepted as the flutter point where the damping is zero.

4.5. Flutter Analysis Based on Peters-He Inflow Theory

Flutter analysis of the rotating blades based on Peters-He inflow theory is very similar to the fixed wing solution, except the structural equations and induced flow equations include extra terms. These terms exist as a result of the rotational velocity of the blade. Forcing functions of the Peters-He inflow theory is based on normalized lifting equations. Therefore, it is necessary for structural equations to be in the normalized form. The structural equations for the rotating blade are already normalized in section 4.4 and given by Eqns. (4-69) and (4-70).

The normalized lifting functions $\bar{L}_h$ and $\bar{M}_\theta$ are derived in section 4.4 and valid for this section also. The velocity is represented as $U = \Omega \bar{r} R + U_\infty$.

The general form of the structural equations is given by,

$$[M]\begin{Bmatrix} \ddot{q}_h \\ \ddot{q}_\theta \end{Bmatrix} + [C]\begin{Bmatrix} \dot{q}_h \\ \dot{q}_\theta \end{Bmatrix} + [K]\begin{Bmatrix} q_h \\ q_\theta \end{Bmatrix} + [D]\begin{Bmatrix} \alpha_j^r \\ \beta_j^r \end{Bmatrix} = 0 \tag{4-124}$$

where elements of the mass, damping, stiffness and inflow coefficient matrix are defined in Eqns. (4-125)-(4-140). The α_j^r and β_j^r terms are the states of the induced flow defined in Eqn. (2-38).

$$[M_{11}] = \int_0^1 WW^T d\bar{r} \tag{4-125}$$

$$[M_{12}] = \int_0^1 \bar{x}_{cg} \Theta W^T d\bar{r} \tag{4-126}$$

$$[M_{21}] = \int_0^1 \left(\bar{x}_{cg} - \frac{1}{2}\pi\bar{b}^3 \left(\frac{\rho R^2}{m} \right) \right) W\Theta^T d\bar{r} \tag{4-127}$$

$$[M_{22}] = \int_0^1 \left(\frac{I_\theta}{mR^2} + \pi\bar{b}^4 \left(\frac{1}{8} - \frac{a}{2} \right) \left(\frac{\rho R^2}{m} \right) \right) \Theta\Theta^T d\bar{r} \tag{4-128}$$

$$[C_{11}] = \int_0^1 2\pi\bar{b} \frac{U}{\Omega R} \left(\frac{\rho R^2}{m} \right) WW^T d\bar{r} \tag{4-129}$$

$$[C_{12}] = \int_0^1 -2\pi\bar{b}^2 \left(\frac{1}{2} - a \right) \frac{U}{\Omega R} \left(\frac{\rho R^2}{m} \right) \Theta W^T d\bar{r} \tag{4-130}$$

$$[C_{21}] = \int_0^1 2\pi\bar{b}^2 \left(\frac{1}{2} + a \right) \frac{U}{\Omega R} \left(\frac{\rho R^2}{m} \right) W\Theta^T d\bar{r} \tag{4-131}$$

$$[C_{22}] = \int_0^1 \pi\bar{b}^3 \left(\frac{1}{2} + 2a^2 \right) \frac{U}{\Omega R} \left(\frac{\rho R^2}{m} \right) \Theta\Theta^T d\bar{r} \tag{4-132}$$

$$[K_{11}] = \int_0^1 \frac{EI}{m\Omega^2 R^4} \left(\frac{d^2 W}{d\bar{r}^2} \right) \left(\frac{d^2 W^T}{d\bar{r}^2} \right) d\bar{r}$$
$$- \int_0^1 \frac{1}{2}(1 - \bar{r}^2) \frac{dW}{d\bar{r}} \frac{dW^T}{d\bar{r}} d\bar{r} \tag{4-133}$$

$$[K_{12}] = \int_0^1 -2\pi\bar{b} \frac{U^2}{(\Omega R)^2} \left(\frac{\rho R^2}{m} \right) \Theta W^T d\bar{r} - \int_0^1 \bar{x}_{cg} \left(\bar{r} \frac{dW}{d\bar{r}} \right) \Theta^T d\bar{r} \tag{4-134}$$

$$[K_{21}] = \int_0^1 \bar{x}_{cg} \bar{r} \frac{dW}{d\bar{r}} \Theta^T d\bar{r} \tag{4-135}$$

$$[K_{22}] = \int_0^1 \left(\frac{GJ}{m\Omega^2 R^4} \left(\frac{d\Theta}{d\bar{r}} \right) \left(\frac{d\Theta^T}{d\bar{r}} \right) - \frac{\bar{k}_m^2}{2} (1 - \bar{r}^2) \frac{d\Theta}{d\bar{r}} \frac{d\Theta^T}{d\bar{r}} \right.$$
$$+ \frac{I_\theta}{mR^2} \Theta\Theta^T \tag{4-136}$$
$$\left. - 2\pi\bar{b}^2 \left(\frac{1}{2} + a \right) \frac{U^2}{(\Omega R)^2} \left(\frac{\rho R^2}{m} \right) \Theta\Theta^T \right) d\bar{r}$$

$$[D_{11}] = \int_0^1 2\pi\bar{b} \frac{U}{\Omega R} \left(\frac{\rho R^2}{m} \right) \bar{\phi}_j^r \cos(r\psi) W d\bar{r} \tag{4-137}$$

$$[D_{12}] = \int_0^1 2\pi\bar{b} \frac{U}{\Omega R} \left(\frac{\rho R^2}{m} \right) \bar{\phi}_j^r \sin(r\psi) W d\bar{r} \tag{4-138}$$

$$[D_{21}] = \int_0^1 2\pi\bar{b}^2 \frac{U}{\Omega R} \left(\frac{1}{2} + a \right) \left(\frac{\rho R^2}{m} \right) \bar{\phi}_j^r \cos(r\psi) \Theta d\bar{r} \tag{4-139}$$

$$[D_{22}] = \int_0^1 2\pi\bar{b}^2 \frac{U}{\Omega R} \left(\frac{1}{2} + a \right) \left(\frac{\rho R^2}{m} \right) \bar{\phi}_j^r \sin(r\psi) \Theta d\bar{r} \tag{4-140}$$

The shape functions W and Θ are given in Eqn. (4-5). The size of the $[D]$ matrix depends on the number of states and changes for a given polynomial order and number of harmonics. Equations (4-137)-(4-140) show only the general representation of the $[D]$ matrix. It should be noted that the definition of $\bar{\phi}_j^r$ is given by Eqn. (2-39).

The induced flow equation is given in implicit form as,

$$\begin{aligned}
\{\alpha_n^m\}^* + [\bar{L}^c]^{-1}[V_n^m]\{\alpha_n^m\} &= \{\tau_n^{mc}\} \\
\{\beta_n^m\}^* + [\bar{L}^s]^{-1}[V_n^m]\{\beta_n^m\} &= \{\tau_n^{ms}\}
\end{aligned} \tag{4-141}$$

Note that the derivations of the $[\bar{L}^c]$, $[\bar{L}^s]$ and $[V_n^m]$ matrices are given in section 2.3.4.2 in detail. The most critical part of the solution is the composition of the forcing vectors $\{\tau_n^{mc}\}$ and $\{\tau_n^{ms}\}$. They are derived with the given normalized circulatory lifting function as shown in Eqns. (4-142)-(4-144).

$$\begin{aligned}
\tau_n^{m0} = \frac{1}{2\pi}\int_0^1 2\pi\bar{b}\Bigg[-\frac{U}{\Omega R}\dot{\bar{h}} + \frac{U^2}{(\Omega R)^2}\theta \\
+ \bar{b}\left(\frac{1}{2} - a\right)\frac{U}{\Omega R}\dot{\theta} - \frac{U}{\Omega R}\lambda\Bigg]\phi_n^0(\bar{r})d\bar{r}
\end{aligned} \tag{4-142}$$

$$\begin{aligned}
\tau_n^{mc} = \frac{1}{\pi}\int_0^1 2\pi\bar{b}\Bigg[-\frac{U}{\Omega R}\dot{\bar{h}} + \frac{U^2}{(\Omega R)^2}\theta \\
+ \bar{b}\left(\frac{1}{2} - a\right)\frac{U}{\Omega R}\dot{\theta} - \frac{U}{\Omega R}\lambda\Bigg]\phi_n^m(\bar{r})d\bar{r}\cos(m\psi)
\end{aligned} \tag{4-143}$$

$$\begin{aligned}
\tau_n^{ms} = \frac{1}{\pi}\int_0^1 2\pi\bar{b}\Bigg[-\frac{U}{\Omega R}\dot{\bar{h}} + \frac{U^2}{(\Omega R)^2}\theta \\
+ \bar{b}\left(\frac{1}{2} - a\right)\frac{U}{\Omega R}\dot{\theta} - \frac{U}{\Omega R}\lambda\Bigg]\phi_n^m(\bar{r})d\bar{r}\sin(m\psi)
\end{aligned} \tag{4-144}$$

The flutter problem is solved at the 90° azimuth (same as the rotating blade flutter analysis based on Pitt-Peters inflow theory). As a result of this approach, the summation terms in the forcing functions disappear. When the forcing terms are adjusted in the induced flow equation, the explicit form of the equation is obtained as,

$$
\begin{Bmatrix} \{\alpha_n^m\}^* \\ \{\beta_n^m\}^* \end{Bmatrix} + \left[\begin{bmatrix} [\bar{L}^c]^{-1}[V_n^m] & 0 \\ 0 & [\bar{L}^s]^{-1}[V_n^m] \end{bmatrix} - [G] \right] \begin{Bmatrix} \{\alpha_n^m\} \\ \{\beta_n^m\} \end{Bmatrix}
$$
$$
- [E] \begin{Bmatrix} \dot{q}_h \\ \dot{q}_\theta \end{Bmatrix} - [F] \begin{Bmatrix} q_h \\ q_\theta \end{Bmatrix} = 0
$$
(4-145)

where the elements of the matrices $[E]$, $[F]$ and $[G]$ are defined in the general form of harmonics and polynomial order as in Eqns. (4-146)-(4-156).

$$
[E_{11}] = \int_0^1 -2\bar{b}\frac{U}{\Omega R}\,\phi_n^m(\bar{r})W^T\cos(m\psi)\,d\bar{r} \tag{4-146}
$$

$$
[E_{12}] = \int_0^1 2\bar{b}^2\frac{U}{\Omega R}\left(\frac{1}{2}-a\right)\phi_n^m(\bar{r})\Theta^T\cos(m\psi)\,d\bar{r} \tag{4-147}
$$

$$
[E_{21}] = \int_0^1 -2\bar{b}\frac{U}{\Omega R}\,\phi_n^m(\bar{r})W^T\sin(m\psi)\,d\bar{r} \tag{4-148}
$$

$$
[E_{22}] = \int_0^1 2\bar{b}^2\frac{U}{\Omega R}\left(\frac{1}{2}-a\right)\phi_n^m(\bar{r})\Theta^T\sin(m\psi)\,d\bar{r} \tag{4-149}
$$

$$
[F_{12}] = \int_0^1 2\bar{b}\frac{U^2}{(\Omega R)^2}\,\phi_n^m(\bar{r})\Theta^T\cos(m\psi)\,d\bar{r} \tag{4-150}
$$

$$
[F_{22}] = \int_0^1 2\bar{b}\frac{U^2}{(\Omega R)^2}\,\phi_n^m(\bar{r})\Theta^T\sin(m\psi)\,d\bar{r} \tag{4-151}
$$

$$
[F_{11}] = [F_{21}] = 0 \tag{4-152}
$$

$$
[G_{11}] = \int_0^1 -2\bar{b}\frac{U}{\Omega R}\,\phi_n^m(\bar{r})\phi_j^r(\bar{r})\cos(r\psi)\cos(m\psi)\,d\bar{r} \tag{4-153}
$$

$$
[G_{12}] = \int_0^1 -2\bar{b}\frac{U}{\Omega R}\,\phi_n^m(\bar{r})\phi_j^r(\bar{r})\sin(r\psi)\cos(m\psi)\,d\bar{r} \tag{4-154}
$$

$$
[G_{21}] = \int_0^1 -2\bar{b}\frac{U}{\Omega R}\,\phi_n^m(\bar{r})\phi_j^r(\bar{r})\cos(r\psi)\sin(m\psi)\,d\bar{r} \tag{4-155}
$$

$$
[G_{22}] = \int_0^1 -2\bar{b}\frac{U}{\Omega R}\,\phi_n^m(\bar{r})\phi_j^r(\bar{r})\sin(r\psi)\sin(m\psi)\,d\bar{r} \tag{4-156}
$$

The coupling of structural and inflow equations requires the definition of a general state vector such as,

$$
q = \begin{Bmatrix} q_h \\ q_\theta \\ \dot{q}_h \\ \dot{q}_\theta \\ \alpha_n^m \\ \beta_n^m \end{Bmatrix} \tag{4-157}
$$

The general motion of the state vector q is represented as in Eqn. (4-158).

$$q = \bar{q}e^{pt} \qquad (4\text{-}158)$$

With the definition of the general state vector, the two systems can be coupled in one equation as given by,

$$\{\dot{q}\} + [A]\{q\} = 0 \qquad (4\text{-}159)$$

where,

$$[A] = \begin{bmatrix} [0]_{2x2} & -[I]_{2x2} & [0]_{2xN_s} \\ [M]^{-1}[K] & [M]^{-1}[C] & [M]^{-1}[D] \\ -[F] & -[E] & \{[V][L]^{-1} - [G]\} \end{bmatrix} \qquad (4\text{-}160)$$

Substituting Eqn. (4-158) into Eqn. (4-159) one gets,

$$\{[A] + p[I]\}\{q\} = 0 \qquad (4\text{-}161)$$

where p is the roots of the system. The determinant solution of the $\{[A] + p[I]\}$ will give the roots. The roots include inflow modes and the derivatives of the structural degrees of freedom also.

As before, this procedure is performed for varying airspeeds for forward flight analysis and for varying rotational speeds for hover analysis. The results are observed in terms of frequency and damping plots for varying speed parameter for each of the roots. The point where the damping curve crosses zero line is accepted as the flutter point where the damping is zero.

CHAPTER 5

RESULTS AND DISCUSSIONS

In this chapter, the structural equations of the fixed and the rotating blades are validated with the eigenvalue solution of Dymore [35] which is a finite element based multi-body dynamics solver. After the validation of the structural modeling, the flutter solution methodologies of the fixed wing are validated with the Goland wing results in the literature [22]. With the confidence of the matching the fixed wing flutter results, the rotary wing flutter results are compared with the results of the Couch [21] and case studies are performed in order to investigate the effect of cg variation, shear center location variation and forward speed on the flutter results.

5.1. Validation of the Structural Equations

Fixed and rotary wing structural equations are modeled with the properties of Goland wing and compared with the eigenvalue solution of the Dymore wing models. The properties of the Goland wing are given in Table 5.1.

Table 5.1. *Properties of the Goland Wing [22]*

	Unit	Value	Definition
m	kg/m	35.7187	Mass per Length
R	m	6.0960	Radius
c	m	1.8288	Chord
x_{cg}	m	0.1829	CG Distance from EA
I_θ	kgm	8.6429	Polar Moment of Inertia
EI	Nm^2	$9.77 * 10^6$	Bending Stiffness per Length
GJ	Nm^2	$9.88 * 10^5$	Torsion Stiffness per Length
a	-	-0.34	Nondimensional EA Distance Parameter
ρ_{air}	kg/m^3	1.02	Air Density

Although all of the derivations explained in the theory part are given for the Rayleigh-Ritz expansion, the analytical equations are also solved with the Galerkin method to

show that Rayleigh-Ritz method gives better solutions for the higher modes. The natural frequencies of the fixed wing model are compared in Table 5.2.

Table 5.2. *Natural Frequency Comparison of Fixed Wing*

Mode #	Dymore (rad/s)	Analytical Model Rayleigh-Ritz (rad/s)	Analytical Model Galerkin (rad/s)	Mode Definition
1	48.00	48.16	48.30	1st Flap Mode
2	95.64	95.72	95.63	1st Torsion Mode
3	242.71	243.77	251.57	2nd Torsion Mode
4	340.70	347.61	372.47	2nd Flap Mode
5	442.41	444.19	-	3rd Torsion Mode

The Galerkin method gives good results for the first torsion and bending modes, while for the second torsion and bending modes the results do not approach to Dymore's natural frequency results. The fifth mode of the Galerkin method solution is not available due to the assumption of two mode shapes for each motion.

Galerkin method can be used for the flutter analysis of the models that are interested only in the first torsion and bending modes. However, this may not be the case all the time. For the better approximation of higher modes also, the Rayleigh-Ritz method is used as an expansion method in this thesis.

The Goland wing properties are also used for the comparison of the rotary wing structural model with the Dymore model. The rotational speed of the blade is taken as $30\ rad/s$. The natural frequency comparisons are given in Table 5.3.

Table 5.3. *Natural Frequency Comparison of Rotary Wing*

Mode #	Dymore (rad/s)	Analytical Model Rayleigh-Ritz (rad/s)	Mode Definition
1	29.88	29.70	1st Flap Mode
2	118.71	106.42	1st Torsion Mode
3	215.49	210.52	2nd Flap Mode
4	350.73	322.51	2nd Torsion Mode

The natural frequency results of the fixed and rotating blade analytical models show good correlation with the Dymore results and it is decided that the structural model can be used further for the flutter analysis. It should also be noted that the first flapping modes of Table 5.2 and Table 5.3 are not comparable. For the fixed wing analysis, the first flapping mode is an elastic mode due to the cantilevered boundary condition. On the other hand, the first flapping mode of the rotary wing analysis is a rigid mode as a result of the pinned boundary condition.

5.2. Validation of the Fixed Wing Flutter Theories

Validation of the fixed wing flutter theories is performed for the Goland wing [22]. Structural properties of the Goland wing are given in section 5.1. The flutter results are obtained in terms of damping and frequency of each mode. The results are shown from Figure 5.1 to Figure 5.8.
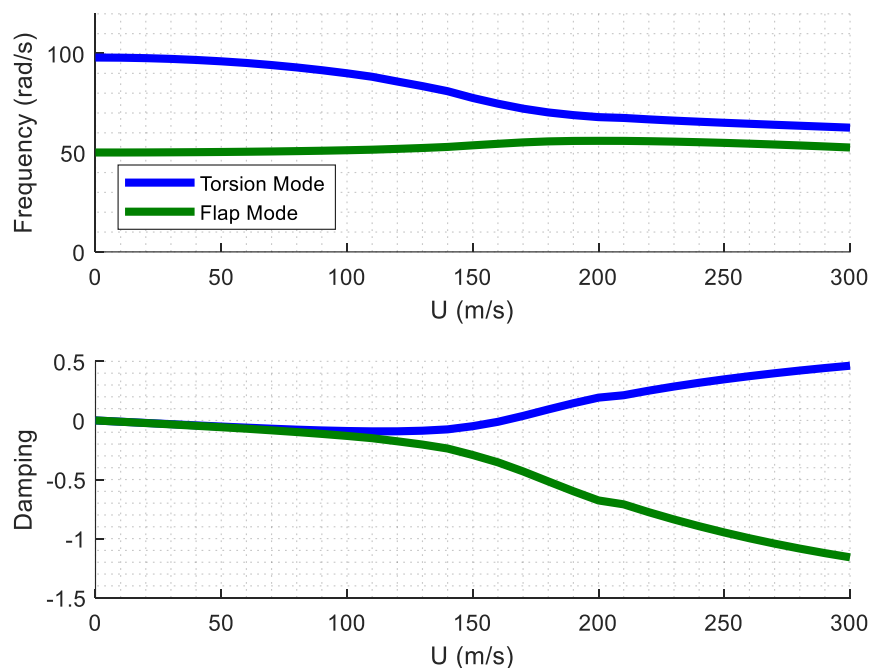

*Figure 5.1.* Fixed Goland Wing Flutter Based on Theodorsen's Theory
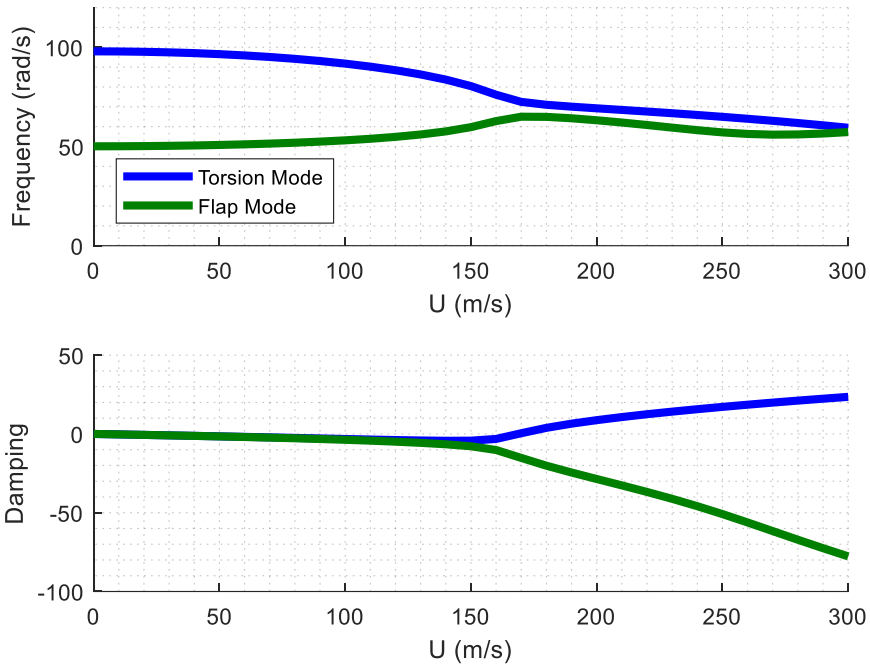
*Figure 5.2.* Fixed Goland Wing Flutter Based on Wagner's Theory
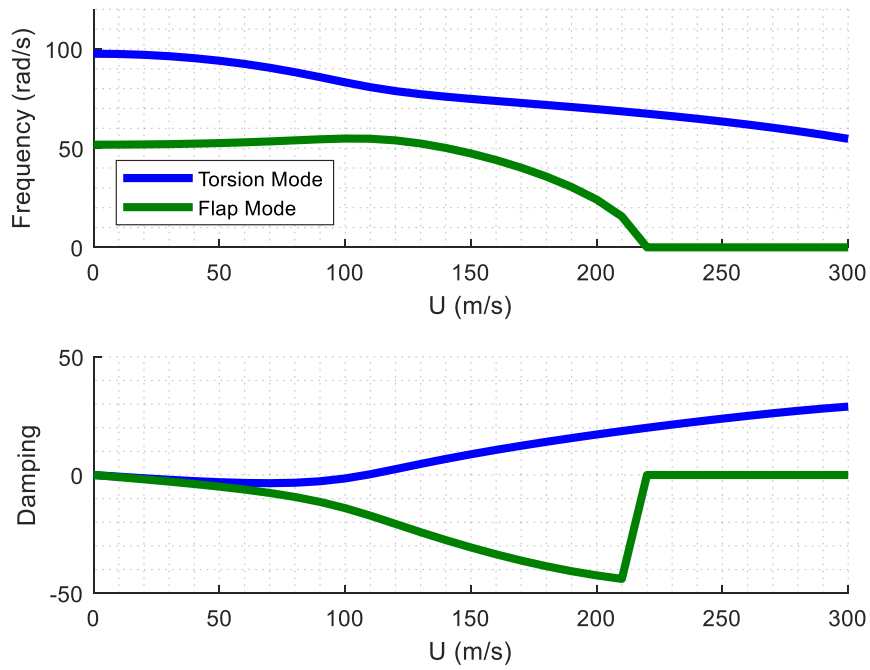
*Figure 5.3.* Fixed Goland Wing Flutter Based on Pitt-Peters Inflow Theory
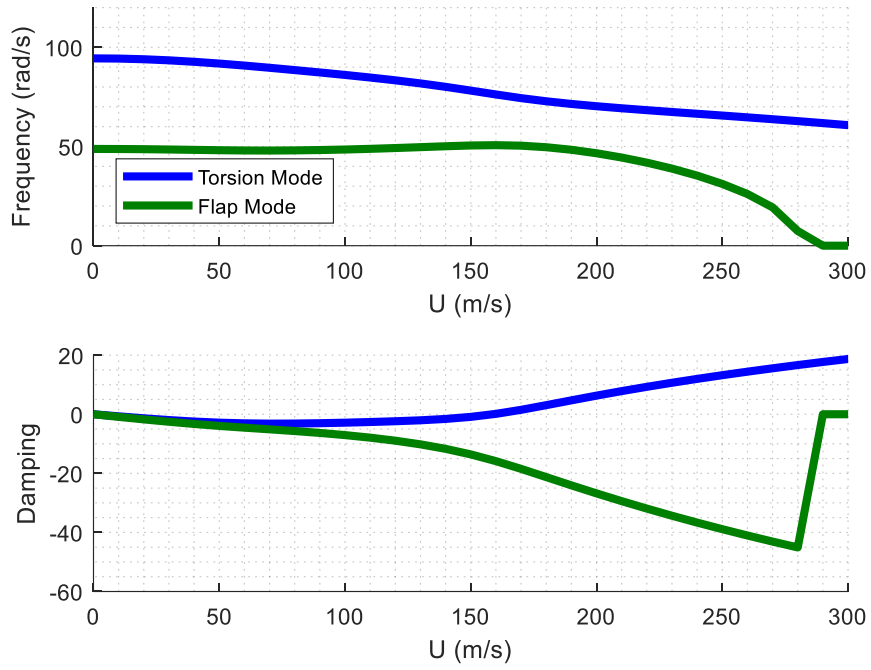
Figure 5.4. Fixed Goland Wing Flutter Based on Peters-He Inflow Theory (6 States)
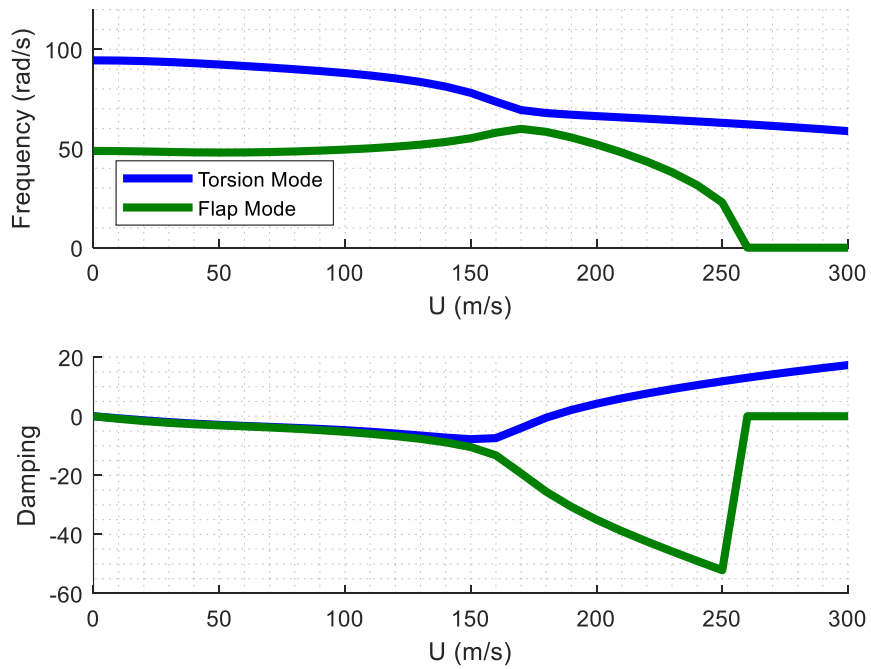
Figure 5.5. Fixed Goland Wing Flutter Based on Peters-He Inflow Theory (10 States)
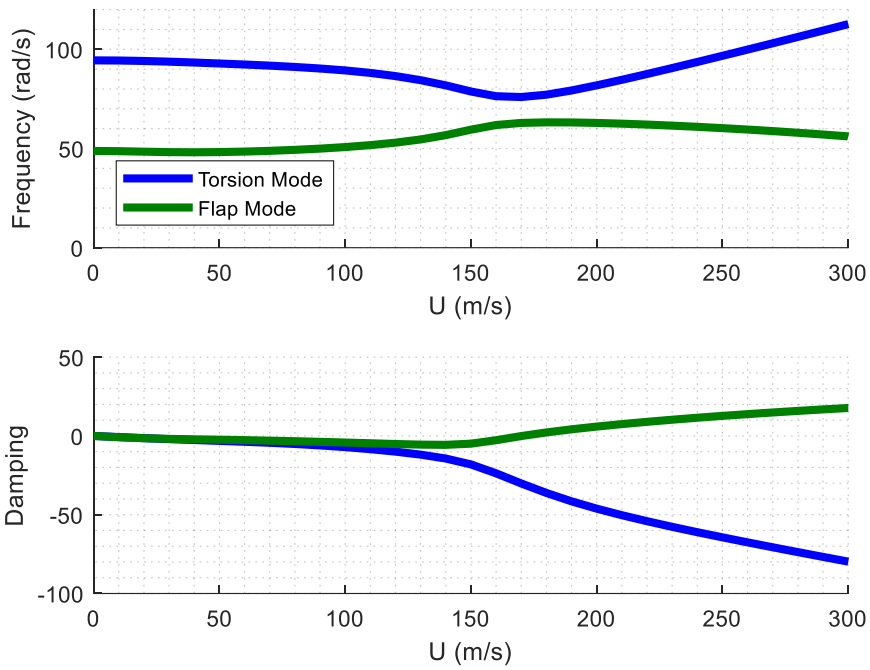
Figure 5.6. Fixed Goland Wing Flutter Based on Peters-He Inflow Theory (15 States)
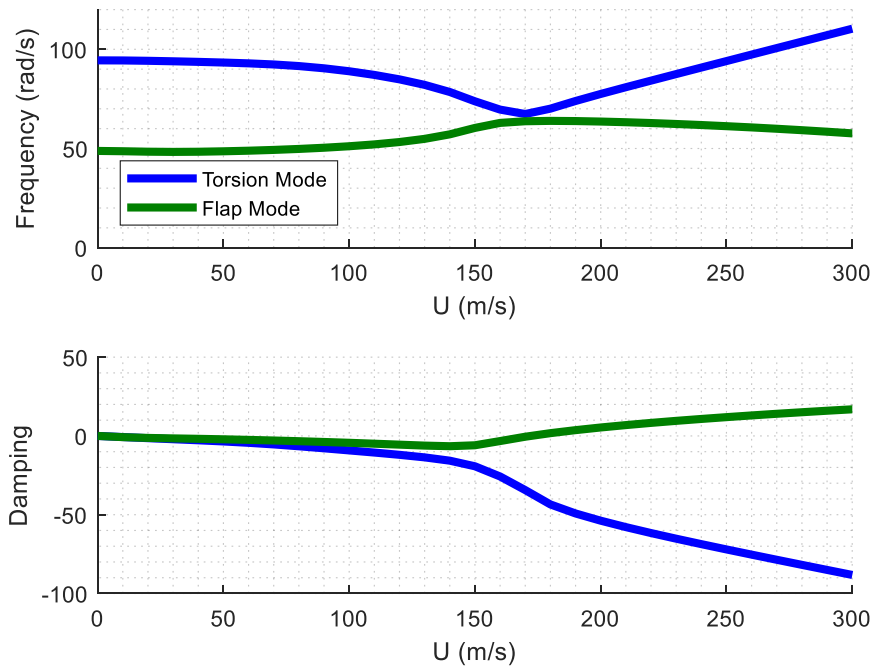

Figure 5.7. Fixed Goland Wing Flutter Based on Peters-He Inflow Theory (21 States)

82
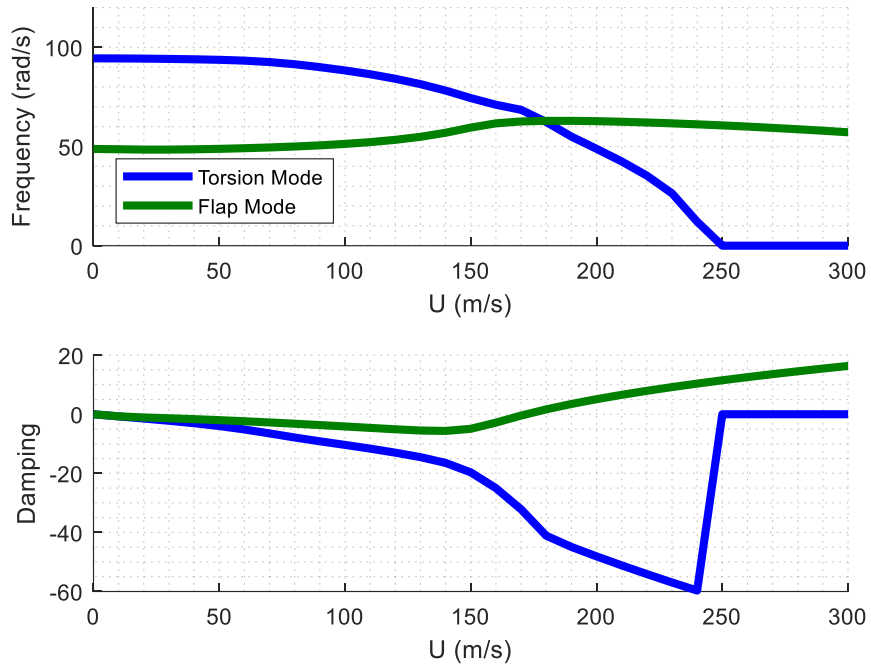
Figure 5.8. Fixed Goland Wing Flutter Based on Peters-He Inflow Theory (28 States)

The flutter velocity and frequency results obtained by using different unsteady aerodynamic methodologies with the flutter results obtained by Goland [22] are given together in Table 5.4. Goland solved the flutter problem with a three-dimensional wing expanded by Rayleigh-Ritz method and Theodorsen's unsteady aerodynamics.

Table 5.4. *Fixed Goland Wing Flutter Results*

Flutter Method	Flutter Velocity (m/s)	Flutter Velocity (% Difference)	Flutter Frequency (rad/s)
Theodorsen	162.3	5.7	74.12
Wagner	168.8	1.9	72.92
Pitt-Peters	108.2	37.1	81.19
Peters-He (6 States)	158.7	7.8	76.47
Peters-He (10 States)	181.8	5.6	67.72
Peters-He (15 States)	170.4	1.0	75.99
Peters-He (21 States)	172.2	0.1	67.97
Peters-He (28 States)	172.1	0.0	67.19
Goland	172.1	-	67.40

The flutter velocity results are compared with Goland's results [22] in terms of percent difference also. It should be noted that the Theodorsen based flutter solution gives good approximations for both flutter velocity and the frequency. It can be chosen as a quick guide of flutter information. However, it gives correct damping only at the flutter point. Therefore, someone who is interested in the damping behavior of the model for varying airspeeds should look for other methods like Wagner based or Inflow based flutter solutions. The results show that Wagner based flutter solution is also a good approximation in terms of both velocity and frequency. Pitt-Peters Inflow based flutter solution is inadequate and is not suggested for the flutter calculations. This is because Pitt-Peters theory includes only three inflow states. This problem is also solved with the Peters-He inflow based flutter solution. Peters-He inflow theory allows for infinite number of inflow states. When the results given in Table 5.4 are analyzed, it is observed that by increasing number of inflow states, the correct flutter solution is approached in terms of flutter speed. The results show that the convergence is obtained at 28 states (6 harmonics). Further increase of the state number only increases the computational time and after some point, there is a risk for the solution to diverge. It should also be noted that for Peters-He dynamic inflow based solutions, increase of the inflow state number has an effect on the flutter mode. As mentioned before, inflow and structural equations are coupled. This coupling explains the influence of induced flow on structural states. Goland [22] did not state flutter mode type which makes it impossible to compare the flutter modes with the analytical results of this study.

5.3. Validation of the Rotary Wing Flutter Theories

5.3.1. Helicopter Blade Model

Validation of the rotary wing flutter methodologies is performed by comparing the flutter analysis results with the results obtained by the rotary wing model of Couch [21]. Couch derived structural equations by Holzer Method for uncoupled torsional natural frequencies and by Myklestad-Prohl Method for uncoupled bending natural

frequencies. For the flutter solution, Couch coupled the structural equations with Loewy's unsteady aerodynamic theory. The structural properties of the studied wing are given in Table 5.5.

Table 5.5. *Structural Properties of the Couch Wing [21]*

STA	m	c	I_{zz}	J	I_θ	e	a
m	kg/m	m	m^4	m^4	kgm	-	-
0.3208	92.5650	0.2057	2.0812E-06	4.1623E-05	2.2241	-0.5	-0.5
0.3966	152.2417	0.2057	2.0812E-06	4.1623E-05	2.2241	-0.5	-0.5
0.7087	92.4640	0.2057	2.0812E-06	3.1217E-05	2.2241	-0.5	-0.5
1.1811	13.5508	0.2057	1.9563E-06	1.6649E-05	1.2677	-0.5	-0.5
1.6535	6.6306	0.2057	1.5484E-06	9.1571E-06	0.3003	-0.5	-0.5
2.1260	9.7488	0.3346	1.2383E-06	4.9740E-06	0.2869	-0.5	-0.5
2.5984	7.6483	0.4636	1.1883E-06	3.9334E-06	0.2825	-0.5	-0.5
3.0709	9.2112	0.4636	1.1467E-06	3.6420E-06	0.2780	-0.5	-0.5
3.5433	9.4725	0.4636	1.1051E-06	3.4755E-06	0.2713	-0.5	-0.5
4.0157	9.7488	0.4636	1.0635E-06	3.3507E-06	0.2624	-0.5	-0.5
4.4882	9.3381	0.4636	1.0323E-06	3.2258E-06	0.2513	-0.5	-0.5
4.9606	9.6912	0.4636	9.9896E-07	3.1009E-06	0.2380	-0.5	-0.5
5.4331	8.3012	0.4636	9.6566E-07	2.9761E-06	0.2246	-0.5	-0.5
5.9055	9.8448	0.4636	9.3236E-07	2.8720E-06	0.2157	-0.5	-0.5
6.3779	7.7059	0.4636	8.9282E-07	2.7888E-06	0.2068	-0.5	-0.5
6.8504	9.6336	0.4636	8.6160E-07	2.6847E-06	0.1979	-0.35	-0.5
7.3228	9.4341	0.4636	8.4079E-07	2.5598E-06	0.1913	-0.2	-0.5
7.7953	9.6528	0.4636	8.3038E-07	2.4766E-06	0.1846	-0.2	-0.5
8.2677	9.4533	0.4636	8.1998E-07	2.4141E-06	0.1802	-0.2	-0.5
8.7401	9.6720	0.4636	8.0749E-07	2.3309E-06	0.1735	-0.35	-0.5
9.2126	9.4533	0.4636	6.0354E-07	1.7274E-06	0.1179	-0.5	-0.5
9.4488	0.3782	0.4636	4.0374E-07	1.1655E-06	0.0667	-0.5	-0.5

The wing model is a cantilevered rotating beam with the nominal rotational velocity (Ω_0) of 203 rpm. The beam is modeled as a rotating cantilevered beam without flapping and pitching hinges. This boundary condition is obtained from Couch's study.

The elastic modulus (E) of the blade is 6.8948×10^{10} Pa and the shear modulus (G) is 2.5924×10^{10} Pa. Couch, in his study, treated the mass of the blade as lumped

masses at each given radial station of the blade. This is because the structural method he used required mass information of the blade to be defined in terms of lumped masses. He evaluated the lumped masses as the summation of the half of the masses of elements that are on the front side and back side of that radial station. The lumped mass information of Couch [21] is inapplicable for the flutter analysis methods used in this thesis because the equations are derived based on the mass per length information of the blade. Therefore, lumped masses are distributed to their nearest stations. The distribution technique is explained in detail in Appendix A. Note that this distribution technique does not exactly represent the same model that Couch used. Distribution of the lumped masses requires the assumption of the mass per length value of the first element. The distribution slightly changes with respect to that assumed value. However, the distribution formulation depends on keeping the total mass of the blade the same for each configuration (lumped and distributed). Therefore, the modal characteristic of the structural model is not affected. In Table 5.5 evaluated distributed mass distribution is given. The fan plot configurations of the two models are given in Figure 5.9 and Figure 5.10 for comparison of the modal behaviors. Fan plots are useful for investigating the variation of the natural frequencies of each mode with increasing rotational speed of the blade. Fan plots are mostly used in the design phase of a blade. It is required that natural frequencies of the blade are not coincident with the per rev lines at the operational rotational speed of the rotor blade to avoid harmonic excitations occurring due to the rotation. In Figure 5.9 and Figure 5.10, per rev lines are shown with dashed lines. They represent multiples of the rotational speed at each point. It is observed from Figure 5.9 that Couch's helicopter blade model is not a good blade design due to the coalescence of second bending and first torsional modes with the per rev lines at the operational rotational speed, but this is not the topic of this thesis study and does not affect the comparison of flutter analyses results.

86
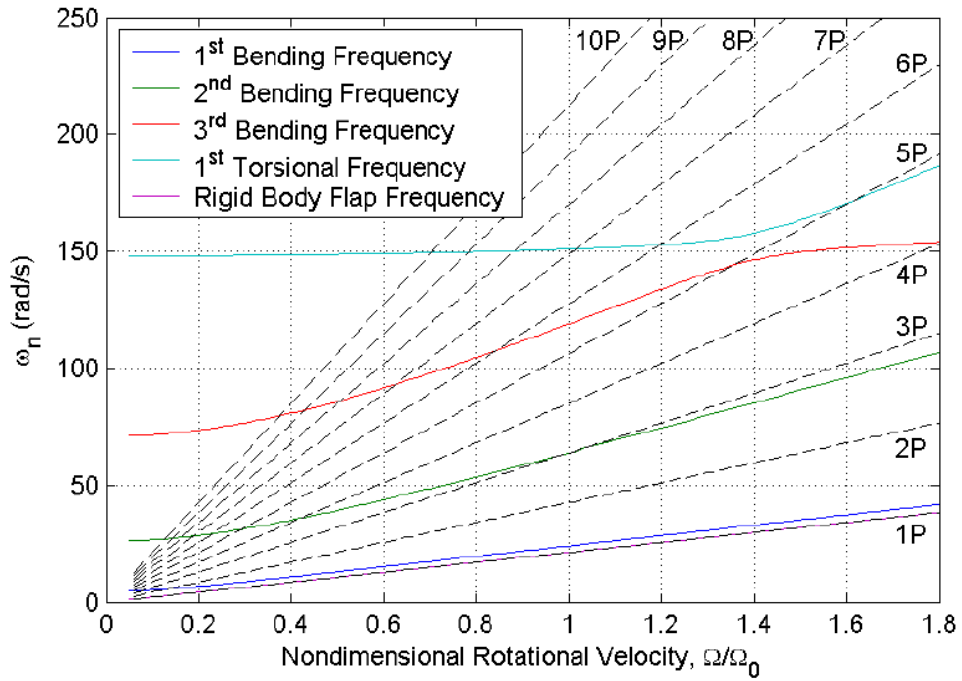
Figure 5.9. Fan Plot of Couch's Model [21]
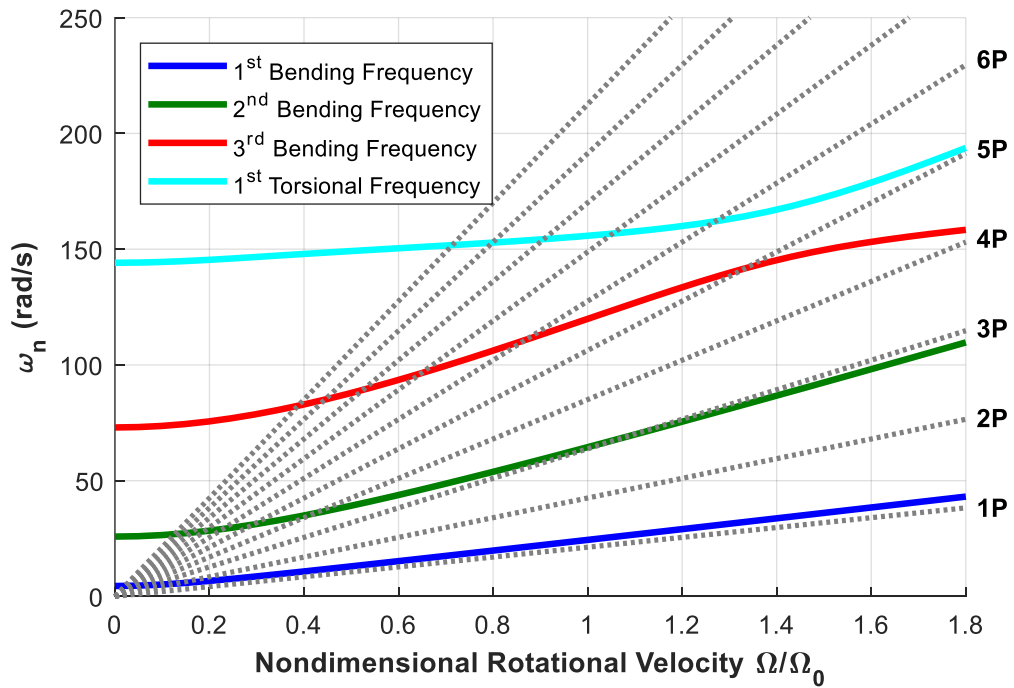
Figure 5.10. Fan Plot of the Analytical Model of the Present Study

87

The fan plots of both configurations are similar. The similarity proves the structural models of Couch's and this study are approximate and the flutter analysis results of Couch's and this study can be compared. The frequency and damping behavior of each flutter analysis of this study based on different aerodynamic models are given from Figure 5.11 to Figure 5.17.
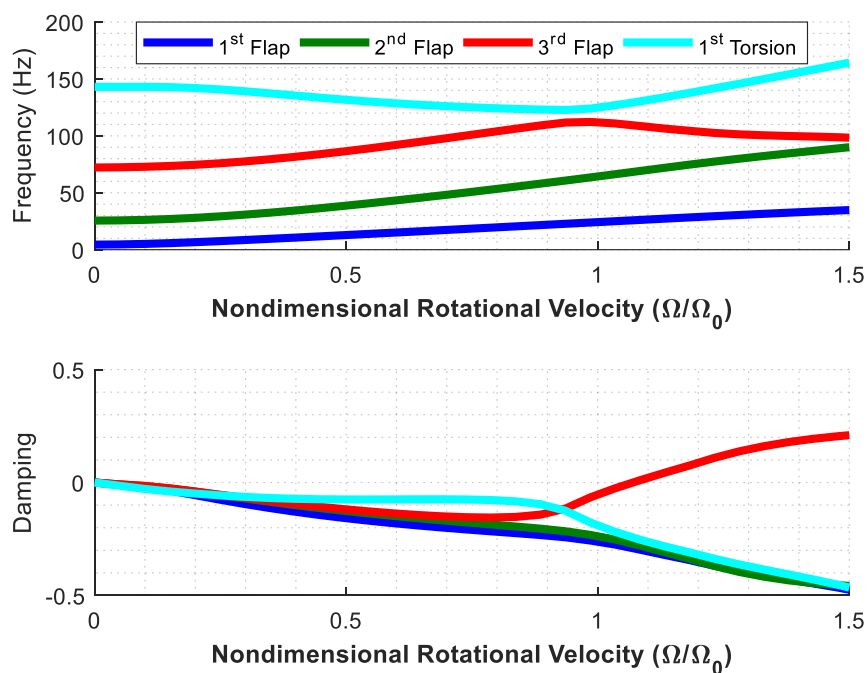

Figure 5.11. Couch's Wing Flutter Analysis Based on Loewy Theory, m=0.25
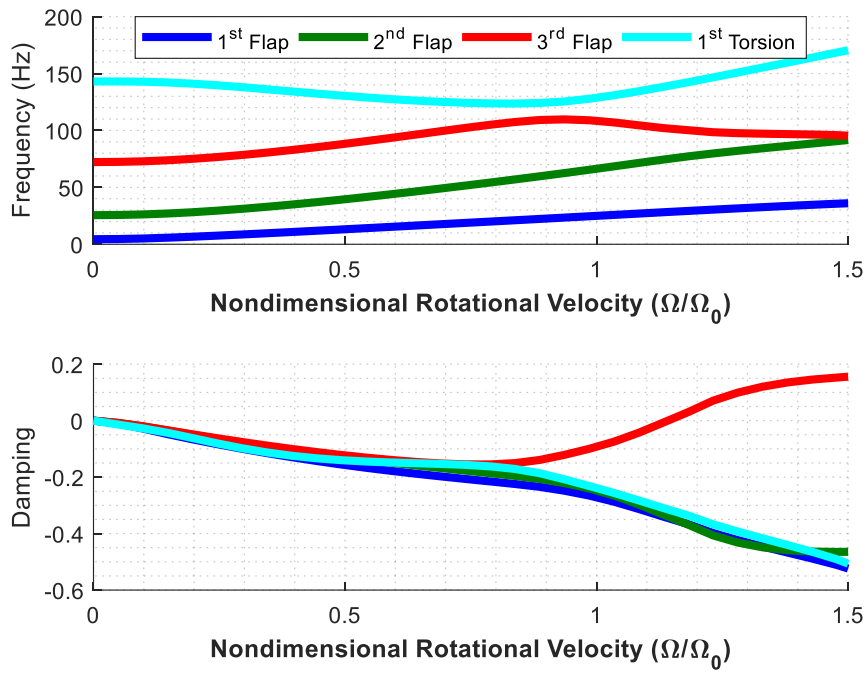
Figure 5.12. Couch's Wing Flutter Analysis Based on Loewy Theory, m=0.50
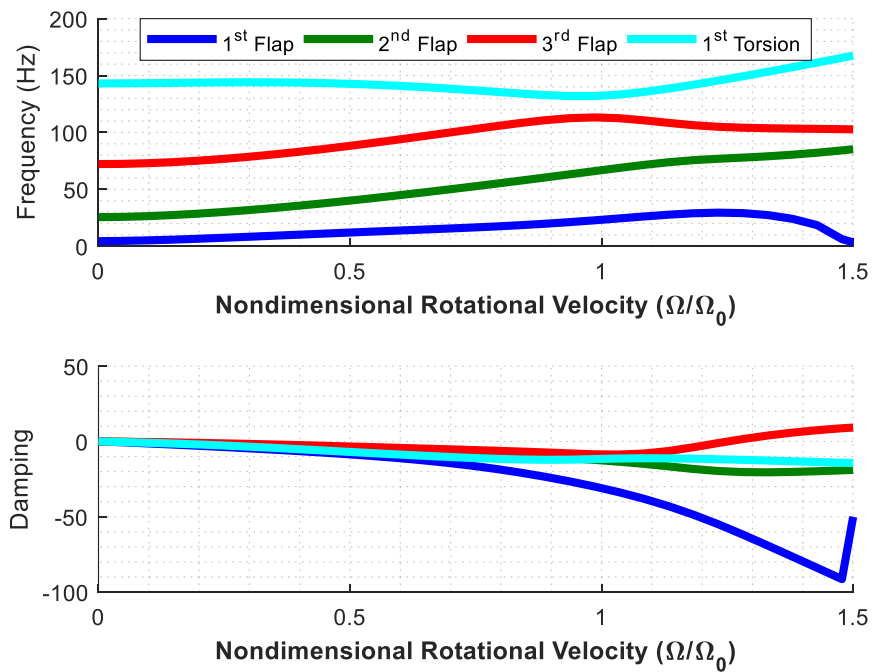
*Figure 5.13.* Couch's Wing Flutter Analysis Based on Wagner Theory

89
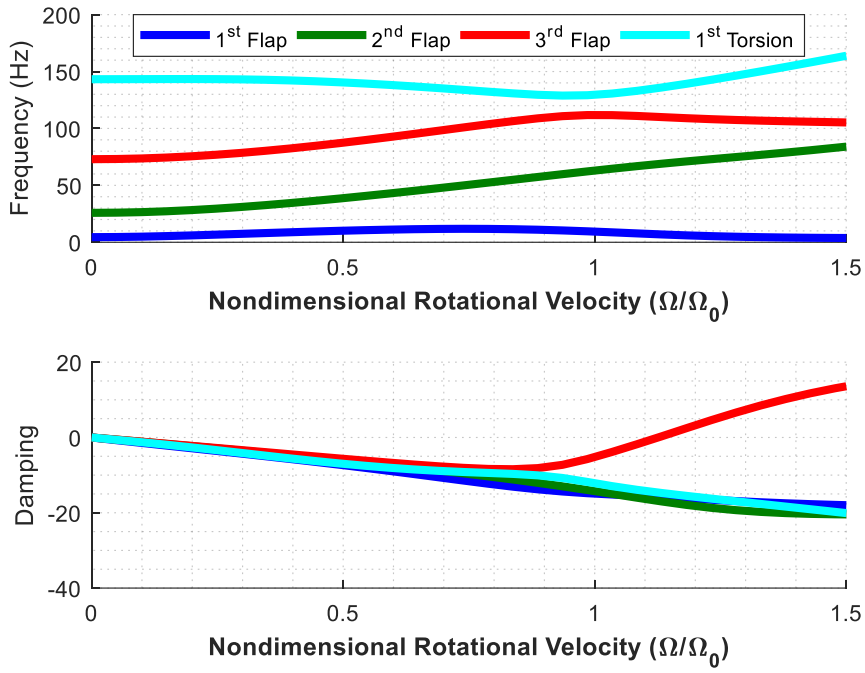
Figure 5.14. Couch's Wing Flutter Analysis Based on Pitt-Peters Inflow Theory
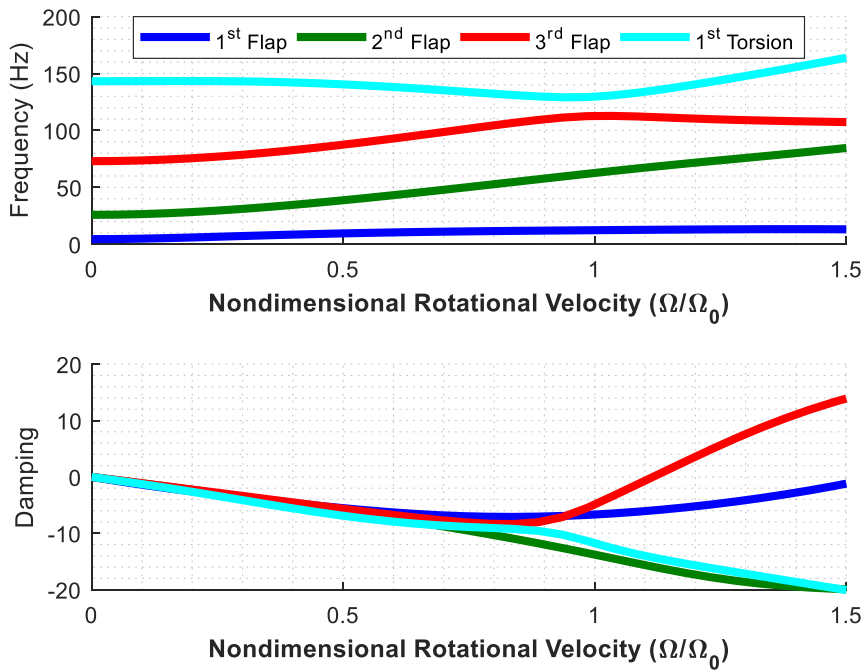

Figure 5.15. Couch's Wing Flutter Analysis Based on Peters-He Inflow Theory (6 States)

90
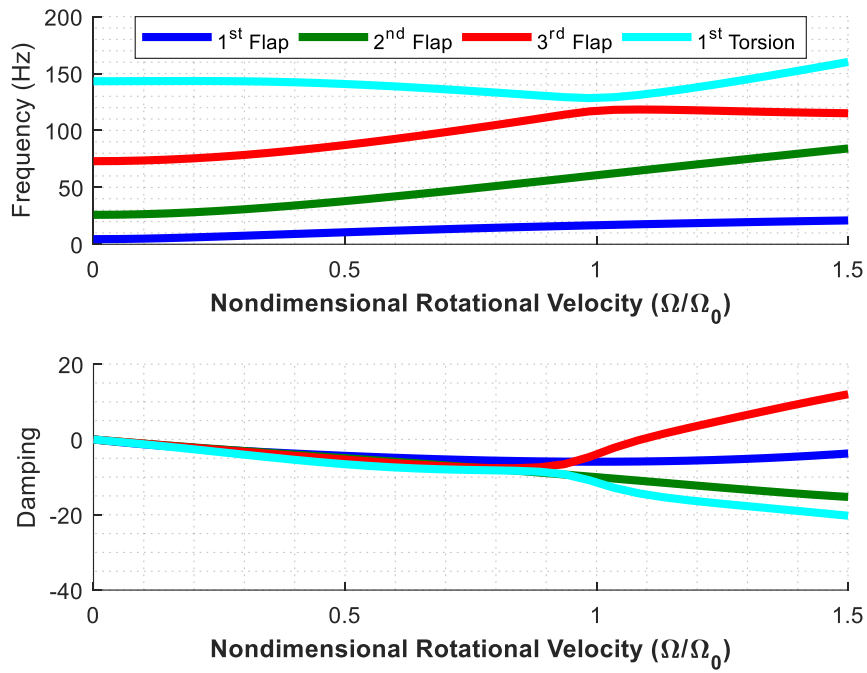
Figure 5.16. Couch's Wing Flutter Based on Peters-He Inflow Theory (21 States)
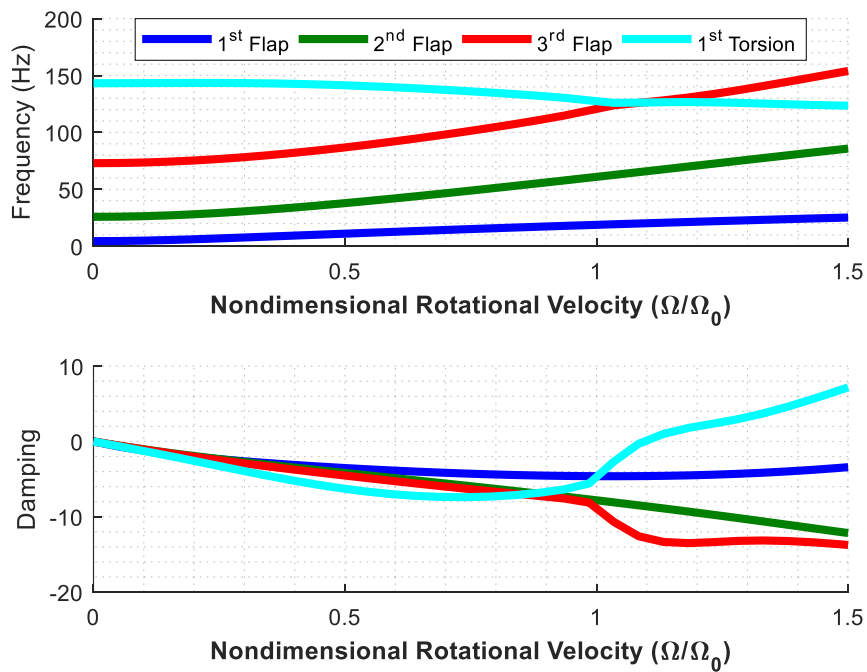

Figure 5.17. Couch's Wing Flutter Analysis Based on Peters-He Inflow Theory (55 States)

The flutter velocity and frequency results of each methodology and with flutter results obtained by Couch are given in Table 5.6. In the Loewy's unsteady aerodynamics based flutter solutions, m is the frequency ratio. As before, if m is not an integer, there exists a phase between the wakes. The phasing influences the real and imaginary parts of the lift deficiency functions which makes the unsteady aerodynamics different. In order to have comparable result cases with Couch's studies, Loewy's unsteady aerodynamics based flutter equations are solved with different frequency ratio values.

Table 5.6. *Couch's Wing Flutter Analysis Results*

Flutter Method	Nondimensional Flutter Velocity (Ω/Ω_0)	Flutter Frequency (rad/s)
Loewy (m=0.25)	1.070	109.3
Loewy (m=0.50)	1.142	101.7
Wagner	1.251	104.6
Pitt-Peters	1.126	110.1
Peters-He (6 States)	1.116	111.8
Peters-He (10 States)	1.109	113.9
Peters-He (15 States)	1.100	116.2
Peters-He (21 States)	1.089	118.4
Peters-He (28 States)	1.079	120.4
Peters-He (36 States)	1.074	122.5
Peters-He (45 States)	1.080	124.5
Peters-He (55 States)	1.095	126.3
Couch Loewy (m=0.25)	1.108	107.2
Couch Loewy (m=0.50)	1.278	98.8

Table 5.6 shows that flutter analysis results obtained by the aeroelastic model based on Loewy's unsteady aerodynamic theory are in good correlation with the Couch's results. Wagner's unsteady aerodynamics based flutter solution gives more flutter rotational speed clearance with respect to other methodologies, while inflow unsteady aerodynamics based flutter analysis gives more conservative result close to the Couch's conservative result of Loewy's model. It should be noted that when the state number is increased in the solution of Peters-He based inflow flutter model, the flutter speed converges to a point after some point. In this problem, solution converged in 55

states. Further increase of the state number increases the computational time of the solution and does not create a considerable influence. As observed before in the fixed wing flutter results, the flutter mode also changed when the inflow state number of the Peters-He inflow based flutter model is increased. This occurrence is due to the coupled relation of the inflow and structural equations.

5.3.2. Flutter Analysis of the Wind Turbine Blade

Flutter analysis of the rotary wing theories is also compared with the modified version of NREL's 5 MW wind turbine blade [38]. The blade model used by Farsadi is very similar to NREL's wind turbine blade in terms of stiffness properties, but there exists a slight difference in terms of inertial properties. The structural properties of Farsadi's blade are given in Table 5.7.

Table 5.7. *Structural Properties of NREL Blade [37]*

STA	m	c	EI	GJ	I_θ	x_{cg}	a
m	kg/m	m	Nm^2	Nm^2	kgm	m	-
0.000 – 2.733	7.59E+02	3.6266	1.64E+10	4.33E+09	1.96E+03	0	-5.41E-03
2.733 – 5.466	6.49E+02	3.8804	1.19E+10	3.66E+09	1.33E+03	0	-2.25E-02
5.466 – 8.200	6.13E+02	4.3033	7.53E+09	2.47E+09	1.02E+03	0	-4.86E-02
8.200 – 12.30	5.46E+02	4.6045	3.95E+09	1.30E+09	7.45E+02	0	-7.86E-02
12.30 – 16.40	4.35E+02	4.5550	2.23E+09	9.90E+08	6.03E+02	0	-6.19E-02
16.40 – 20.50	4.12E+02	4.3535	1.74E+09	7.16E+08	4.98E+02	0	-8.44E-02
20.50 – 24.60	3.55E+02	4.1280	1.05E+09	3.84E+08	3.53E+02	0	-9.13E-02
24.60 – 28.70	2.95E+02	3.8775	6.82E+08	2.21E+08	2.53E+02	0	-9.62E-02
28.70 – 32.80	2.42E+02	3.6250	4.65E+08	1.35E+08	1.77E+02	0	-9.64E-02
32.80 – 36.90	1.58E+02	3.3790	2.61E+08	6.69E+07	9.92E+01	0	-9.57E-02
36.90 – 41.00	1.10E+02	3.1330	1.52E+08	3.76E+07	5.99E+01	0	-9.31E-02
41.00 – 45.10	1.03E+02	2.8870	8.22E+07	2.70E+07	4.90E+01	0	-9.44E-02
45.10 – 49.20	7.90E+01	2.6410	5.13E+07	1.95E+07	3.30E+01	0	-9.78E-02
49.20 – 53.30	5.74E+01	2.4090	2.87E+07	1.33E+07	2.10E+01	0	-9.73E-02
53.30 – 56.03	4.40E+01	2.1930	1.71E+07	8.44E+06	1.38E+01	0	-9.92E-02
56.03 – 58.76	3.08E+01	1.7525	7.83E+06	3.91E+06	7.06E+00	0	-9.45E-02
58.76 – 61.50	1.65E+01	0.9595	1.84E+06	8.41E+05	1.71E+00	0	-8.79E-02

The free vibration analysis is performed with the above structural properties keeping the lift and moment zero for the nonrotating blade configuration. The analysis includes

the torsional and bending degrees of freedoms only. The results are compared in Table 5.8 with the baseline model (no twist) results of Farsadi [38]. The structural frequencies show great correlation within 2% difference.

Table 5.8. *Structural Frequency Comparison of the Wind Turbine Blade Model*

Mode #	Mode Type	Present Study (Hz)	Farsadi (Hz)
1	1st Flap	0.80	0.80
2	2nd Flap	2.06	2.11
3	3rd Flap	4.28	4.31
4	4th Flap	7.44	7.49
5	1st Torsion	9.66	9.54

In his dissertation, Farsadi performed flutter analysis of the baseline wing based on Wagner's aerodynamics. In the present study, flutter analyses are performed with Loewy, Wagner and inflow based aerodynamics models. The results are compared in Table 5.9.

Table 5.9. *Flutter Results Comparison for NREL Blade*

Flutter Method	Flutter Speed (rpm)	Flutter Frequency (Hz)
Present Study - Loewy	25.22	6.95
Present Study - Wagner	25.17	6.64
Present Study - Pitt-Peters	21.57	7.02
Present Study - Peters-He (6 States)	21.55	7.04
Present Study - Peters-He (21 States)	21.53	7.10
Farsadi – Baseline (Incompressible Aerodynamics)	25.12	6.40

The results show that flutter results of Wagner and Loewy unsteady aerodynamics based models are the same as the Farsadi's results in terms of flutter speed and give close results to Farsadi in terms of flutter frequencies. The flutter analysis results obtained by the aeroelastic models utilizing inflow are in good agreement with each other and slightly different than the other methods. This shows that induced flow effect on the unsteady aerodynamic model results in more conservative results. Here the

three stated Pitt-Peters inflow model, highly stated Peters-He inflow models give similar results. Increase in the state number does not create a considerable effect and the convergence is obtained around 21.5 rpm. Ineffectiveness of the state number in this model is a result of the center of gravity being on the elastic axis. This characteristic of the structural model eliminates some terms from the general flutter matrix and reduces the effect of induced flow states.

5.4. Case Studies

The general section representation of the models to be used in Sections 5.4.1, 5.4.2 and 5.4.3 is given in Figure 5.18 where P is the aerodynamic center, Q is the elastic axis point and R is the center of gravity point.
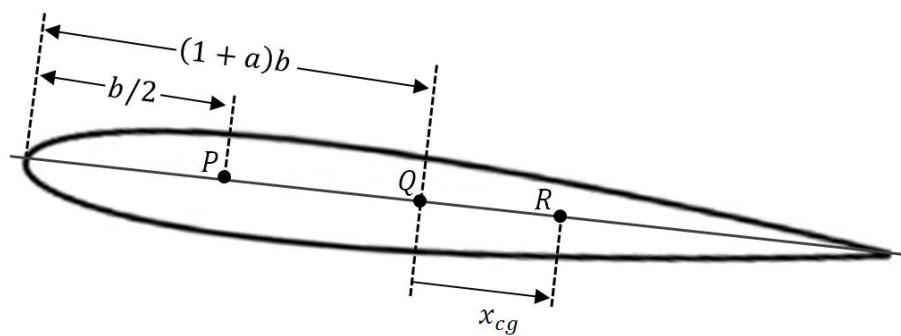

Figure 5.18. Cross-Sectional Representation of the Models Used in the Case Studies

5.4.1. Center of Gravity Effect on the Flutter Results of Rotary Wings

One of the main effective parameters on the flutter characteristics is the distance of the center of gravity from the elastic axis. The increase of this distance towards the trailing edge of the wing has a destabilizing effect on the flutter solutions. This phenomenon is investigated with the rotating blade model of Couch [21]. For the purpose of the investigation, the distance of the center of gravity from the elastic axis is taken same for all stations from root to tip of the blade and this constant distance value is varied step by step in order to find out its effect on the flutter analysis results. The analyses are performed for the constant nominal operating rotational velocity of

203 rpm. Figure 5.19 shows the damping variation obtained from the flutter solution methods utilizing different unsteady aerodynamic theories on the same figure together. The results verify that when the position of the center of gravity point is moved away from the elastic axis towards the trailing edge of the wing, the blade gets closer to the flutter region for the same rotational speed.
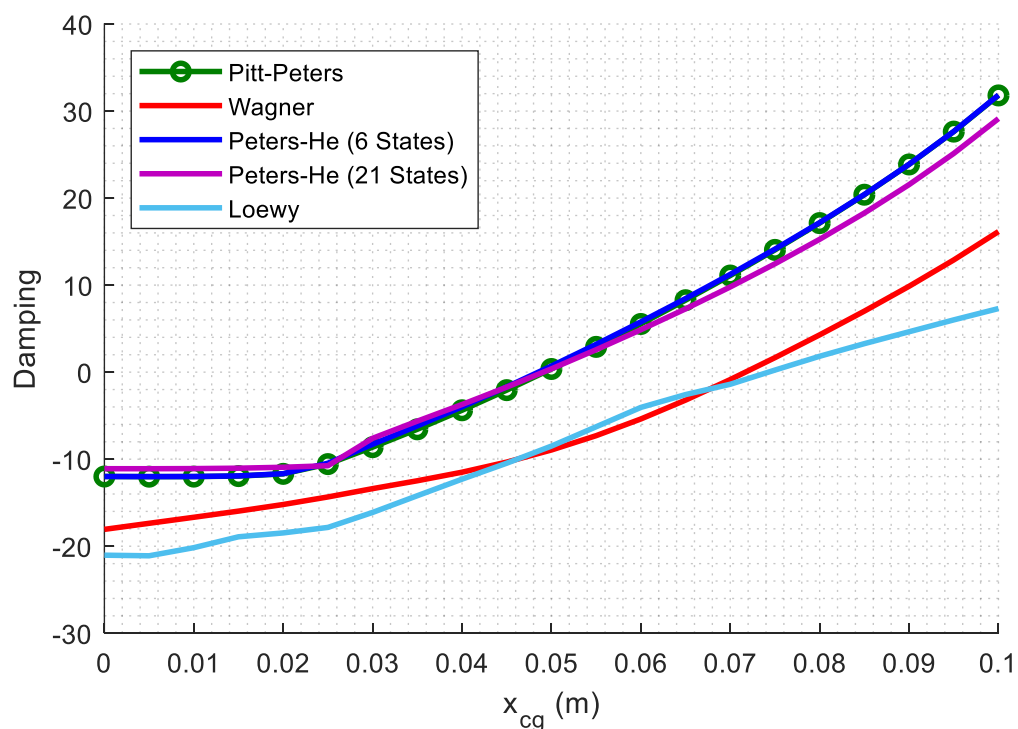

Figure 5.19. Center of Gravity Effect on the Damping

The results clarify that the rotating blade model has no flutter instability when the center of gravity point is coincident with the elastic axis at its nominal rotational speed. When the damping behaviors are analyzed, it is seen that the inflow based solutions are similar and give more conservative results when compared to the damping results obtained by the aeroelastic models involving Loewy's and Wagner's unsteady aerodynamic models. In addition, the increase in the solution state number of Peters-He induced flow does have an impact on the flutter point.

5.4.2. Shear Center Effect on the Flutter Results of Rotary Wings

The chordwise location of the shear center is an effective parameter for flutter solutions. The shear center location defines the boundary condition for the flutter equations. The distance between the shear center and the quarter chord determines the effect of the lift force on the system. Likewise, the distance of the shear center from the center of gravity is also an important parameter as discussed in the previous section.

Investigation of this problem is again performed using the rotating blade model of Couch [21]. All of the parameters given in section 5.3 are used except the parameter "a". The parameter "a" defines the dimensionless position of the shear center in the chordwise direction. Figure 5.18 shows the definition of the parameter "a".
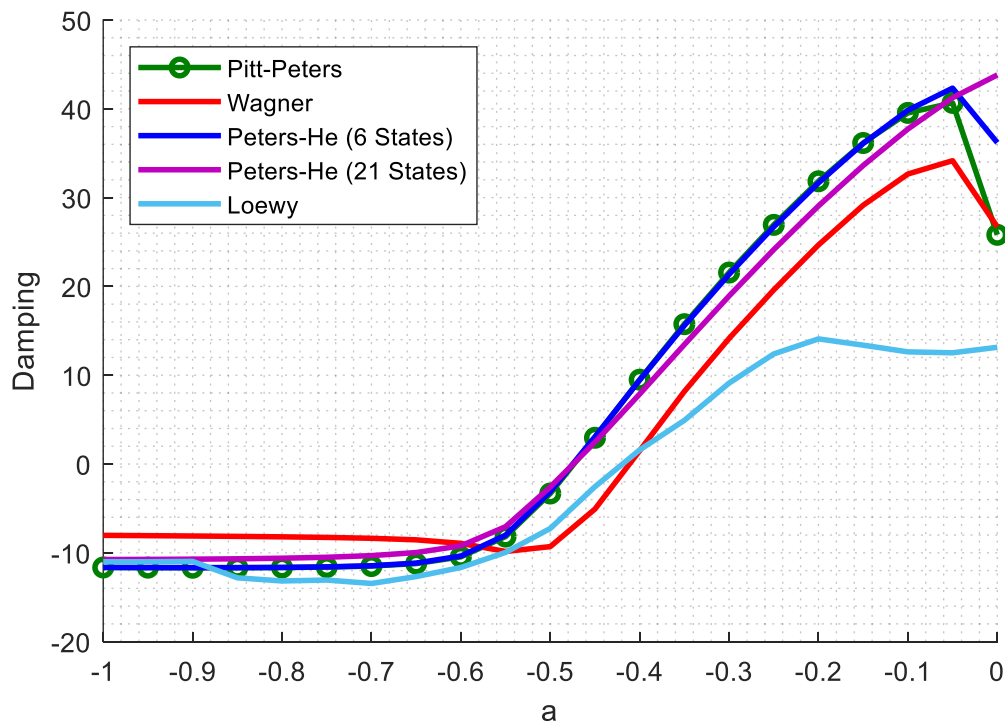

Figure 5.20. Shear Center Position Effect on the Damping

In order to understand the effect of the shear center position, the parameter "a" is kept constant and same for all of the radial stations from root to tip of the blade. The

constant "a" parameter is varied to change the position of the shear center under the condition of the normal operating rotational velocity of 203 rpm. The analyses are performed utilizing different unsteady aerodynamic models in flutter solutions. Damping variation of each method with varying shear center position is given in Figure 5.20.

From Figure 5.20 it is clearly seen that there is almost no effect of the shear center position on the damping until a is "-0.5". At this point, the shear center is at the quarter chord. Beyond this point, the moment created by the lifting force changes direction from being nose down to nose up. This creates a destabilizing effect when we move towards the trailing edge and at some point, damping becomes positive indicating flutter condition. It is seen that there are small differences between the solution methodologies involving different unsteady aerodynamic methods. Again, as seen in the center of gravity position effect, inflow based flutter solutions give more conservative results when compared to the damping results obtained by the aeroelastic models involving Loewy's and Wagner's unsteady aerodynamic models.

5.4.3. Forward Velocity Effect on the Flutter Results of Rotary Wings

Forward velocity effect on the flutter solution is investigated again using the rotating blade model of Couch [21]. In his thesis, Couch only studied the hover condition of the helicopter, because his solution methodology (Loewy) is only applicable to the hover condition.

In this study, Wagner and inflow based aerodynamic methods are used in the aeroelastic models to study the forward velocity effect. For the rotational speed of the Couch's model, the nominal rotational speed of 203 rpm is used. The results are given in Figure 5.21 to Figure 5.24.
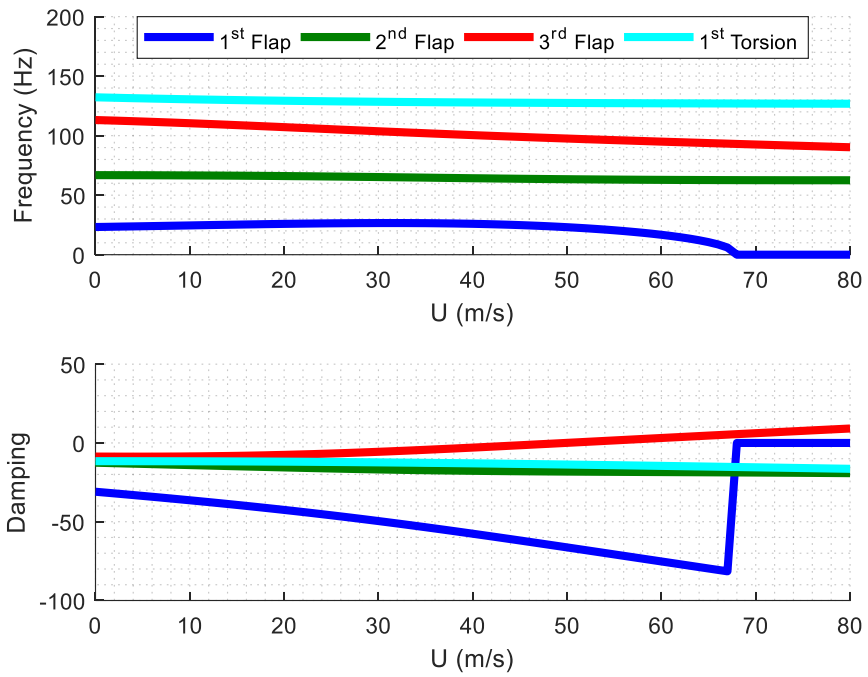
*Figure 5.21.* Forward Flight Flutter Based on Wagner Theory
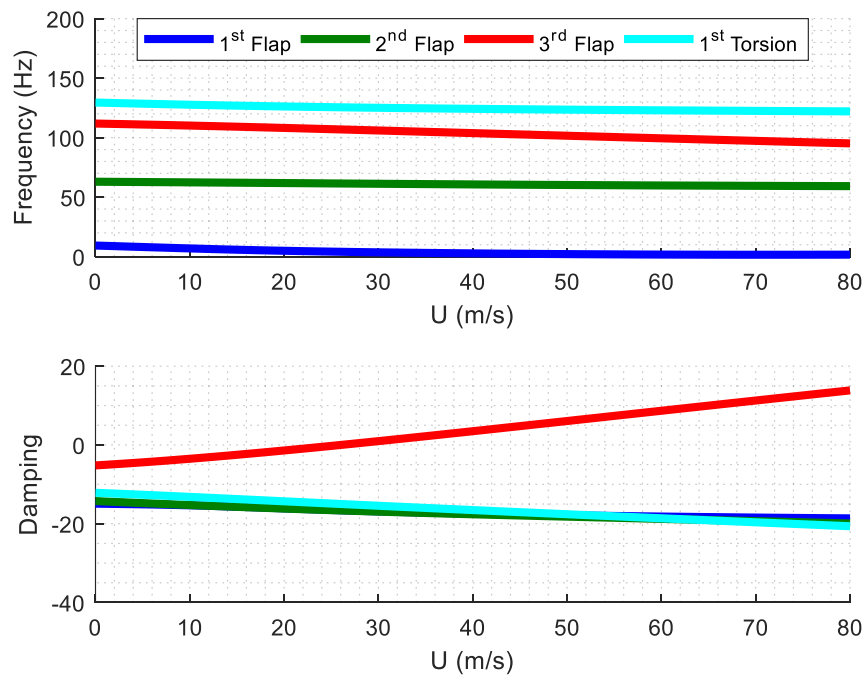
*Figure 5.22.* Forward Flight Flutter Based on Pitt-Peters Inflow Theory
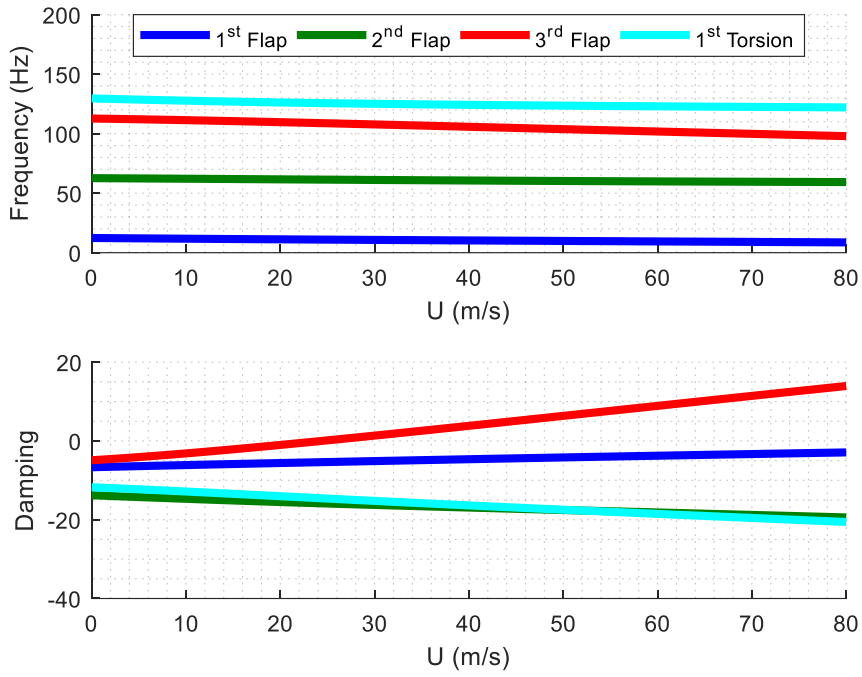
*Figure 5.23.* Forward Flight Flutter Based on Peters-He Inflow Theory (6 States)
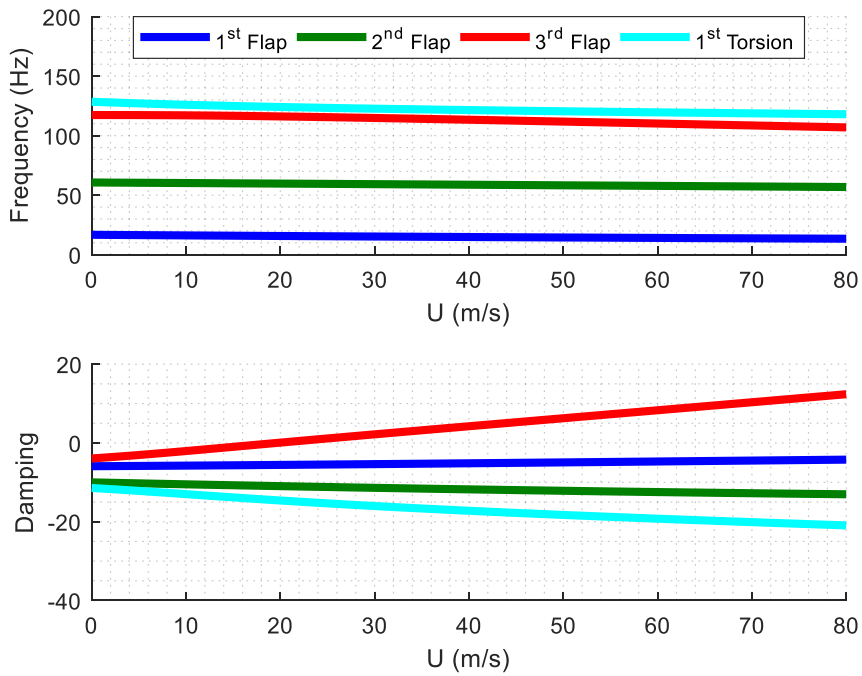
Figure 5.24. Forward Flight Flutter Based on Peters-He Inflow Theory (21 States)

Table 5.10. *Comparison of Forward Velocity Effect on the Flutter Results*

Flutter Method	Flutter Velocity (Blade FWD Velocity) (m/s)	Flutter Velocity (Blade Tip Speed) (m/s)	Flutter Frequency (rad/s)
Wagner	49.81	250.67	97.62
Pitt-Peters	26.03	226.89	106.9
Peters-He (6 States)	24.36	225.22	108.8
Peters-He (21 States)	19.63	220.49	116.2

The results in Table 5.10 show that all of the aeroelastic models give forward velocity flutter speeds that are unrealistically slow for an operational helicopter. This may be the result of Couch's rotating blade model not belonging to a real helicopter rotor model. In his study, Couch states that, for the purpose of flutter analysis investigations, he developed a model based on other helicopters by manipulating the structural properties to obtain a rotor blade that can observe flutter instability. This might have made the developed model more susceptible to the flutter instability in the forward flight analysis conditions. The results in Table 5.10 also show that the flutter analysis solutions including inflow based unsteady aerodynamic models give more conservative results in terms of flutter speed. Although the flutter velocity results of different unsteady aerodynamic models seem diverse in terms of blade forward velocity, when the results are examined in terms of blade relative tip speed considering the rotational speed (ΩR), the diversity disappears.

CHAPTER 6

CONCLUSION AND RECOMMENDATION FOR FUTURE WORK

6.1. Conclusion

In this thesis, flutter analysis of fixed and rotary wings are performed for different types of unsteady aerodynamic models. Euler-Bernoulli beam theory is used as the structural model for the derivation of the equations of motion with the Rayleigh-Ritz assumed mode method for both fixed and rotary wings. The fixed wing equations are also solved with the Galerkin assumed mode method. The accuracy of the structural models is demonstrated by the eigenvalue results of free vibration analysis. The eigenvalue results of the analytical models are shown to have a good correlation with the Dymore [35] solutions. The Galerkin and Rayleigh-Ritz model results are shown to have similar results for the primary modes. The Rayleigh-Ritz assumed modes method is utilized for the aeroelastic models of the flutter solutions of this thesis due to the simplicity of the mode shapes (only geometric boundary conditions should be satisfied) and requirement of less computational time.

The aeroelastic models are created by the coupling of the structural models expanded by Rayleigh-Ritz assumed modes method and the unsteady aerodynamic models. The models are coupled in the frequency domain in order to determine the modal behavior of the roots of the system to check for the flutter stability. The coupling procedure has slight differences depending on the type of the unsteady aerodynamic models. Some of the theories such as Theodorsen and Loewy requires the assumption of the harmonic motion for the airfoil, while Wagner and Inflow based models are formed depending on the general motion of the airfoil. All of the aeroelastic models are simplified to one equation to generate eigenvalue solutions. The frequency and damping results of the aeroelastic models are obtained from the complex roots of the eigenvalue solutions.

The fixed wing flutter analyses are performed utilizing the unsteady aerodynamic models of Theodorsen, Wagner, Pitt-Peters and Peters-He. The analyses are conducted

for the Goland wing [22] found in the literature. The results shows that all unsteady aerodynamic models in the aeroelastic system produces very close results with the Goland wing analysis results. It is observed that when the inflow states of the Peters-He model are increased until the convergence of the modes, flutter speed and frequency results approaches to the flutter speed and frequency results of the Goland's wing.

Since the unsteady aerodynamic model of Theodorsen is applicable for fixed wings only, a modified version of Theodorsen's model for the rotating blades in hover condition (Loewy's unsteady aerodynamic model) is used for the rotating blade flutter analysis to include the wake effect of the rotating blades for low inflow conditions. Considering the replacement of Theodorsen's model with Loewy's model, rotating blade flutter analyses are conducted using the Loewy's, Wagner's unsteady aerodynamic models and Pitt-Peters, Peters-He inflow models. The flutter analysis results are compared with the analytical results of Couch's [21] helicopter blade model and Farsadi's [38] wind turbine blade model. The results show that aeroelastic models utilizing inflow models give more conservative results compared to the aeroelastic models utilizing unsteady aerodynamic models of Loewy and Wagner. The results of aeroelastic models utilizing Peters-He inflow model generally converges around 21 states (5x5) which is computationally fast. Hence it is concluded that Peters-He inflow model can be confidently used in aeroelastic models for the flutter analysis.

The rotary wing flutter analyses are also performed for investigation of some critical parameters affecting the performance of aeroelastic models. One of the critical parameters is the distance of the center of gravity point to the elastic axis. All of the flutter analysis results performed with different unsteady aerodynamic models show that when the center of gravity is coincident with the elastic axis, there is no risk of flutter instability. When the center of gravity is placed away from the elastic axis towards the trailing edge of the cross-section, at some point flutter instability is observed by the aeroelastic models utilizing different unsteady aerodynamic models. Another critical parameter is the chordwise position of the shear center. The analyses show that when the shear center is in front of the quarter-chord point, there is no risk

of flutter. If the shear center is moved away from the quarter-chord towards the trailing edge of the cross-section the flutter susceptibility increases.

6.2. Recommendation for Future Work

For future work, the structural model formulation can be improved to include the effects of twist and the sweep angle. In addition, the effect of lag dynamics can also be studied for the flutter analysis. In terms of aerodynamics, the compressible flow effect can be investigated. Moreover, a finite element based beam structural model can be developed to be used in conjunction with the unsteady aerodynamic models to increase the fidelity of the aeroelastic analysis of rotary wings.

REFERENCES

[1]   G. Politakis, W. Haans, and G. Van Bussel, "Suppression of Classical Flutter Using a 'Smart Blade,'" *Am. Inst. Aeronaut. Astronaut.*, no. January, pp. 1–16, 2008.

[2]   D. H. Hodges and R. Ormiston, "Stability of Elastic Bending and Torsion of Uniform Cantilevered Rotor Blades in Hover," in *14th Structures, Structural Dynamics, and Materials Conference*, American Institute of Aeronautics and Astronautics, 1973.

[3]   M. J. Patil, R. N. Yurkovich, and D. H. Hodges, "Incorrectness of the k Method for Flutter Calculations," *J. Aircr.*, vol. 41, no. 2, pp. 402–405, 2004.

[4]   C. Denegri, Jr. and M. Cutchins, "Evaluation of Classical Flutter Analysis for the Prediction of Limit Cycle Oscillations," *38th Struct. Struct. Dyn. Mater. Conf.*, no. 2, 1997.

[5]   S. P. Viswanathan, "An Analysis of the Flutter and Damping Characteristics of Helicopter Rotors," Georgia Institute of Technology, 1977.

[6]   S. Irani and S. Sazesh, "A New Flutter Speed Analysis Method Using Stochastic Approach," *J. Fluids Struct.*, vol. 40, pp. 105–114, 2013.

[7]   G. A. Pierce and J. R. White W., "Unsteady Rotor Aerodynamics at Low Inflow and Its Effect on Flutter," in *2nd Atmospheric Flight Mechanics Conference*, American Institute of Aeronautics and Astronautics, 1972.

[8]   G. W. Brooks and J. E. Baker, "An Experimental Investigation of the Effect of Various Parameters Including Tip Mach Number on the Flutter of Some Model Helicopter Rotor Blades," 1953.

[9]   M. Dinyavari and P. P. Friedmann, "Unsteady Aerodynamics in Time and Frequency Domains for Finite Time Arbitrary Motion of Rotary Wings in Hover and Forward Flight," in *25th Structures, Structural Dynamics and Materials Conference*, American Institute of Aeronautics and Astronautics, 1984.

[10]   R. T. Jones, "The Unsteady Lift of a Wing of Finite Aspect Ratio," 1940.

[11]   K. W. Shipman, "Helicopter Blade-Tip Stability in Forward Flight," Georgia Institute of Technology, 1971.

[12]   H. Haddadpour and R. D. Firouz-Abadi, "Evaluation of Quasi-Steady Aerodynamic Modeling for Flutter Prediction of Aircraft Wings in Incompressible Flow," *Thin-Walled Struct.*, vol. 44, no. 9, pp. 931–936, 2006.

[13] R. G. Loewy, "A Two-Dimensional Approximation to the Unsteady Aerodynamics of Rotary Wings," *J. Aeronaut. Sci.*, vol. 24, no. 2, pp. 81–92, 1957.

[14] C. E. Hammond, "A Parametric Study of Helicopter Rotor Blade Flutter Under Low Inflow Conditions, Using Incompressible Aerodynamics," *Georg. Inst. Technol. Sch. Aerosp. Eng. AE 60U Spec. Probl. June*, vol. 80, 1968.

[15] K. W. Shipman and E. R. Wood, "A Two-Dimensional Theory for Rotor Blade Flutter in Forward Flight," *J. Aircr.*, vol. 8, no. 12, pp. 1008–1015, 1971.

[16] C. A. Gates, R. A. Piziali, and F. A. DuWaldt, "Comparison of Theoretical and Experimental Flutter Characteristics for a Model Rotor in Translational Flight," *J. Am. Helicopter Soc.*, vol. 8, no. 2, 1963.

[17] C. W. Stammers, *The Flapping Torsion Flutter of a Helicopter Blade in Forward Flight*. University of Southampton, Institute of Sound and Vibration Research, 1968.

[18] I. Tuzcu and N. Nguyen, "Flutter of Maneuvering Aircraft," *J. Aerosp. Eng.*, vol. 28, no. 4, pp. 1–15, 2015.

[19] B. D. Nibbelink, "Finite-State Inflow Applied to Aeroelastic Flutter of Fixed and Rotating Wings," Georgia Institute of Technology, 1992.

[20] W. J. Rauchenstein Jr., "A 3D Theodorsen-Based Rotor Blade Flutter Model Using Normal Modes," Naval Postgraduate School, 2015.

[21] M. A. Couch, "A Three-Dimensional Flutter Theory for Rotor Blades with Trailing-Edge Flaps," Naval Postgraduate School, 2003.

[22] M. Goland, "The Flutter of a Uniform Cantilever Wing," *J. Appl. Mech. Asme*, vol. 12, no. 4, pp. A197--A208, 1945.

[23] D. H. Hodges and G. A. Pierce, *Introduction to Structural Dynamics and Aeroelasticity*. Cambridge University Press, 2011.

[24] S. N. Karunamoorthy, "Use of Hierarchical Elastic Blade Equations and Automatic Trim for Helicopter Vibration Analysis.," Washington University, 1987.

[25] J. Wright and J. Cooper, *Introduction to Aircraft Aeroelasticity and Loads*. 2007.

[26] E. H. Dowell, *A Modern Course in Aeroelasticity*, 5th ed., vol. 217. Springer, 2015.

[27] H. Haddadpour, M. A. Kouchakzadeh, and F. Shadmehri, "Aeroelastic Instability of Aircraft Composite Wings in an Incompressible Flow," *Compos. Struct.*, vol. 83, no. 1, pp. 93–99, 2008.

[28] D. M. Pitt, "Rotor Dynamic Inflow Derivatives and Time Constants from Various Inflow Models," Washington University, 1980.

[29] D. Pitt and D. A. Peters, "Theoretical Prediction of Dynamic-Inflow Derivatives," *Vertica*, vol. 5, pp. 21–34, 1981.

[30] K. R. Krothapalli, J. V. R. Prasad, and D. A. Peters, "Helicopter Rotor Dynamic Inflow Modeling for Maneuvering Flight," *J. Am. Helicopter Soc.*, vol. 46, no. 2, pp. 129–139, 2001.

[31] A. Suzuki, "Application of Dynamic Inflow Theory to Wind Turbine Rotors," The University of Utah, 2000.

[32] D. A. Peters, D. Barwey, and A. Su, "An Integrated Airloads-Inflow Model for Use in Rotor Aeroelasticity and Control Analysis," *Math. Comput. Model.*, vol. 19, no. 3–4, pp. 109–123, 1994.

[33] D. A. Peters and C. J. He, "Finite State Induced Flow Models Part II: Three-Dimensional Rotor Disk," *J. Aircr.*, vol. 32, no. 2, pp. 323–333, 1995.

[34] D. A. Peters and C. J. He, "Correlation of Measured Induced Velocities with a Finite-State Wake Model," *J. Am. Helicopter Soc.*, vol. 36, no. 3, pp. 59–70, 1991.

[35] "Dymore" [Online]. Available: http://www.dymoresolutions.com/.

[36] R. L. Bielawa, *Rotary Wing Structural Dynamics and Aeroelasticity*. American Institute of Aeronautics and Astronautics, 2006.

[37] P. J. Magari, L. A. Shultz, and V. R. Murthy, "Dynamics of Helicopter Rotor Blades," *Comput. Struct.*, vol. 29, no. 5, pp. 763–776, 1988.

[38] T. Farsadi, "Aeroelastic Analysis of Composite Wings and Wind Turbine Blades Including Geometrical Nonlinearity and Compressibility," Middle East Technical University, 2018.

A. Distribution of Lumped Masses

The mass configuration of the Couch's structural model is given in Figure 0.1. Here M is the lumped mass and x is the coordinate of the lumped mass.


Figure 0.1. Lumped Mass Configuration of Couch's Structural Model

For the solution methodologies of this study, the lumped masses shown in Figure 0.1 are distributed to the neighbor stations to obtain a general mass per length distribution shown in Figure 0.2. Here m corresponds to the mass per length of that section.
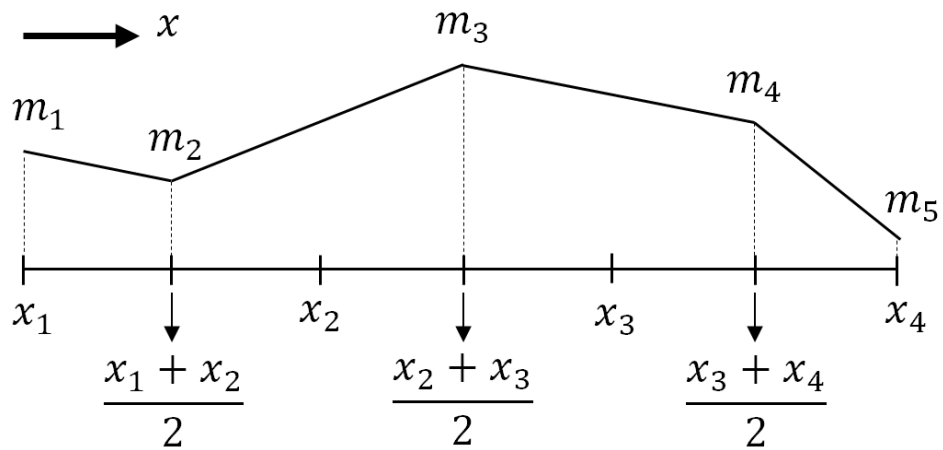

Figure 0.2. Distributed Mass Configuration of the Couch's Model

In his study, Couch starts to build his model from the configuration shown in Figure 0.2. He obtains the lumped mass values according to formulation shown in Eqns. (0-1)-(0-4).

$$\left(\frac{m_1 + m_2}{2}\right)\left(\frac{x_2 - x_1}{2}\right) = M_1 \qquad (0\text{-}1)$$

$$\left(\frac{m_2 + m_3}{2}\right)\left(\frac{x_3 - x_1}{2}\right) = M_2 \qquad (0\text{-}2)$$

$$\left(\frac{m_3 + m_4}{2}\right)\left(\frac{x_4 - x_2}{2}\right) = M_3 \qquad (0\text{-}3)$$

$$\left(\frac{m_4 + m_5}{2}\right)\left(\frac{x_4 - x_3}{2}\right) = M_4 \qquad (0\text{-}4)$$

Equations (0-1)-(0-4) can be written in matrix form as,

$$\begin{bmatrix} \dfrac{x_2 - x_1}{4} & 0 & 0 & 0 \\[2mm] \dfrac{x_3 - x_1}{4} & \dfrac{x_3 - x_1}{4} & 0 & 0 \\[2mm] 0 & \dfrac{x_4 - x_2}{4} & \dfrac{x_4 - x_2}{4} & 0 \\[2mm] 0 & 0 & \dfrac{x_4 - x_3}{4} & \dfrac{x_4 - x_3}{4} \end{bmatrix} \begin{bmatrix} m_2 \\ m_3 \\ m_4 \\ m_5 \end{bmatrix} = \begin{bmatrix} M_1 - m_1\left(\dfrac{x_2 - x_1}{4}\right) \\ M_2 \\ M_3 \\ M_4 \end{bmatrix} \qquad (0\text{-}5)$$

In Eqn. (0-5), there are 5 unknowns to be solved for a system of 4 equations. If m_1 is selected with an initial guess, the rest of the mass per length values can be determined keeping the total mass of the blade the same.